UNIVERSIDADE FEDERAL DE MINAS GERAIS
Graduate Program in Electrical Engineering
and UNIVERSITÉ POLYTECHNIQUE HAUTS-DE-FRANCE
and INSA HAUTS-DE-FRANCE

Rafael Nascimento Silva

Event-triggered control for nonlinear systems: Application to vehicle platoons

Valenciennes
2024

PhD Thesis

Submitted for the degree of Doctor of Philosophy from

UNIVERSIDADE FEDERAL DE MINAS GERAIS Graduate Program in Electrical Engineering and UNIVERSITÉ POLYTECHNIQUE HAUTS-DE-FRANCE and INSA HAUTS-DE-FRANCE

Subject: **Automatic control, Production**

Rafael NASCIMENTO SILVA

Doctoral school:	PPGEE – Programa de Pós-Graduação em Engenharia Elétrica UFMG
	Doctoral School Polytechnique Hauts-de-France (ED PHF n°635)
Research units:	Laboratoire d'Automatique, de Mécanique et d'Informatique Industrielles et Humaines (LAMIH - UMR CNRS 8201)
	Laboratório de Deteção de Falhas, Controle, Otimização e Modelagem (DIFCOM)

Event-triggered control for nonlinear systems: Application to vehicle platoons

Jury:	D'ANDRÉA-NOVEL, Brigitte	Professeure, Universités Mines ParisTech
Reviewers:	ADOUANE, Lounis	Professor, Université de Technologie de Compiègne
	DÓREA, Carlos	Professor, Universidade Federal do Rio Grande do Norte
Examiners:	D'ANDRÉA-NOVEL, Brigitte	Professor, Universités Mines ParisTech
	DEAECTO, Grace	Associate Professor , Universidade Estadual de Campinas
Thesis directors:	FREZZATO, Luciano	Adjunct Professor, Universidade Federal de Minas Gerais
	GUERRA, Thierry Marie	Professor, Université Polytechnique Hauts de France
Thesis co-supervisor:	NGUYEN, Anh-Tu	Associate Professor, Université Polytechnique Hauts de France
	SOUZA, Fernando	Associate Professor, Universidade Federal de Minas Gerais

Valenciennes
2024

Rafael Nascimento Silva

EVENT-TRIGGERED CONTROL FOR NONLINEAR SYSTEMS: Application to vehicle platoons

Thesis submitted to the joint PhD program from the Graduate Program in Electrical Engineering of the Universidade Federal de Minas Gerais, Université Polytechnique Hauts-de-France and INSA Hauts-de-France in partial fulfillment of the requirements for the degree of Doctor in Electrical Engineering.

Supervisor: Prof. Luciano Antonio Frezzatto Santos, PhD (UFMG)
Prof. Thierry-Marie Guerra, PhD (UPHF)

Co-Supervisor: Prof. Fernando de Oliveira Souza, PhD (UFMG)
Prof. Anh-Tu Nguyen, PhD (UPHF)

Valenciennes
2024

Silva, Rafael Nascimento.
S586e Event-triggered control for nonlinear systems [recurso eletrônico] : application to vehicle platoons / Rafael Nascimento Silva. – 2024.
1 recurso online (137 f. : il., color.) : pdf.

Orientadores: Luciano Antonio Frezzatto Santos, Thierry-Marie Guerra.
Coorientadores: Fernando de Oliveira Souza, Anh-Tu Nguyen.

Tese (doutorado) – Universidade Federal de Minas Gerais, Escola de Engenharia.

Bibliografia: f. 129-137.

1. Engenharia elétrica – Teses. 2. Sistemas não lineares – Teses. 3. Veículos a motor – Dispositivos de transmissão – Teses. 4. Controle remoto – Teses. 5. Simuladores (Computadores digitais) – Teses. I. Santos, Luciano Antonio Frezzatto. II. Guerra, Thierry-Marie, 1963-. III. Souza, Fernando de Oliveira. IV. Nguyen, Anh-Tu, 1954-. V. Universidade Federal de Minas Gerais. Escola de Engenharia. VI. Título.

CDU: 621.3(043)

Ficha catalográfica elaborada pelo Bibliotecário Marcio A. A. Gomes CRB/6 2812
Biblioteca Prof. Mário Werneck, Escola de Engenharia da UFMG

UNIVERSIDADE FEDERAL DE MINAS GERAIS

ESCOLA DE ENGENHARIA

PÓS-GRADUAÇÃO EM ENGENHARIA ELÉTRICA

FOLHA DE APROVAÇÃO

"EVENT-TRIGGERED CONTROL FOR NONLINEAR SYSTEMS: APPLICATION TO PLATOONING"

RAFAEL NASCIMENTO SILVA

Tese de Doutorado submetida à Banca Examinadora designada pelo Colegiado do Programa de Pós-Graduação em Engenharia Elétrica da Escola de Engenharia da Universidade Federal de Minas Gerais, como requisito para obtenção do grau de Doutor em Engenharia Elétrica. Aprovada em 05 de julho de 2024. Por:

Prof. Dr. Luciano Antonio Frezzatto Santos
DELT (UFMG)

Prof. Dr. Thierry-Marie Guerra
LAMIH-CNRS (Université Polytechnique Hauts-de-France)

Prof. Dr. Fernando de Oliveira Souza
DELT (UFMG)

Prof. Dr. Anh-Tu Nguyen
LAMIH-CNRS (Université Polytechnique Hauts-de-France)

Profa. Dra. Brigitte D'Andrea-Novel
(Mines ParisTech)

Prof. Dr. Lounis Adouane
LASMEA (Université de Technologie de Compigne)

Profa. Dra. Grace Silva Deaecto
FEM (Universidade Estadual de Campinas)

Prof. Dr. Carlos Eduardo Trabuco Dórea
DCA (Universidade Federal do Rio Grande do Norte)

Documento assinado eletronicamente por **Luciano Antonio Frezzatto Santos**, **Professor do Magistério Superior**, em 05/07/2024, às 11:40, conforme horário oficial de Brasília, com fundamento no art. 5º do Decreto nº 10.543, de 13 de novembro de 2020.

Documento assinado eletronicamente por **Fernando de Oliveira Souza**, **Professor do Magistério Superior**, em 05/07/2024, às 11:42, conforme horário oficial de Brasília, com fundamento no art. 5º do Decreto nº 10.543, de 13 de novembro de 2020.

Documento assinado eletronicamente por **Carlos Eduardo Trabuco Dórea**, **Usuário Externo**, em 05/07/2024, às 16:31, conforme horário oficial de Brasília, com fundamento no art. 5º do Decreto nº 10.543, de 13 de novembro de 2020.

Documento assinado eletronicamente por **Thierry-Marie Guerra**, **Usuário Externo**, em 08/07/2024, às 09:34, conforme horário oficial de Brasília, com fundamento no art. 5º do Decreto nº 10.543, de 13 de novembro de 2020.

Documento assinado eletronicamente por **Anh-Tu Nguyen**, **Usuário Externo**, em 10/07/2024, às 17:43, conforme horário oficial de Brasília, com fundamento no art. 5º do Decreto nº 10.543, de 13 de novembro de 2020.

Documento assinado eletronicamente por **Grace Silva Deaecto**, **Usuária Externa**, em 12/07/2024, às 10:03, conforme horário oficial de Brasília, com fundamento no art. 5º do Decreto nº 10.543, de 13 de novembro de 2020.

Documento assinado eletronicamente por **Brigitte D'Andrea Novel**, **Usuário Externo**, em 16/07/2024, às 05:16, conforme horário oficial de Brasília, com fundamento no art. 5º do Decreto nº 10.543, de 13 de novembro de 2020.

Documento assinado eletronicamente por **Lounis Adouane**, **Usuário Externo**, em 17/07/2024, às 04:00, conforme horário oficial de Brasília, com fundamento no art. 5º do Decreto nº 10.543, de 13 de novembro de 2020.

A autenticidade deste documento pode ser conferida no site https://sei.ufmg.br/sei/controlador_externo.php?acao=documento_conferir&id_orgao_acesso_externo=0, informando o código verificador **3348200** e o código CRC **723F7D6B**.

Referência: Processo nº 23072.235875/2024-68 SEI nº 3348200

Special thanks to my family

Acknowledgements

Firstly, I want to thank my family, especially my parents Jaime Marques and Maria Oliveira, for all opportunities they gave me, for education, trust, and the for always been by my side, regardless of distance.

I thank the professors Fernando, Luciano, Anh-Tu and Guerra for their excellent orientation, for their patience and for knowledge share; These factors helped me on the way to become a better researcher.

I thank all the professors of the Postgraduate Program in Electrical Engineering (PPGEE) whose knowledge contributed to this work, in addition to the aid in the research process that underlies the same. And I thank UPHF for the support.

I thank all my friends and colleagues of D!Fcom and LAMIH, friends and teachers of IFBA Campus Vitória da Conquista. Special thanks to all my friends of many years, who were by my side and supported me in the difficulties that occurred during this time.

This work was supported by the French Ministry of Higher Education and Research, by the CNRS, by the Hauts-de-France region (Allocation de recherche 2020 de la région Hauts-de-France Convention 20003875), by the Coordination for the Improvement of Higher Education Personnel - Brazil (CAPES) through the Academic Excellence Program (PROEX), by the project InSAC (National Institute of Science and Technology for Cooperative Autonomous Systems Applied to Security and Environment) under the grants CNPq (Conselho Nacional de Desenvolvimento Científico e Tecnológico) 465755/2014-3 and 88887.513093/2020-00, Fundação de Amparo à Pesquisa do Estado de Minas Gerais (FAPEMIG), and São Paulo Research Foundation (FAPESP) 2014/50851-0, and also by the grants CNPq: 312034/2020-2, FAPEMIG: APQ-00543-217 and APQ-00630-23, and Universidade Federal de Minas Gerais.

Special thanks to my family

Abstract

In this thesis we address the design of event-triggered control for nonlinear systems focusing on the application of nonhomogeneous vehicle platooning. Due to the presence of parametric uncertainties and unmeasured exogenous disturbances, the classical feedback linearization technique cannot be applied to attain linear and homogeneous platoon. To address this issue, we propose a disturbance observer (DOB) to estimate a lumped disturbance, representing the effects of both the parametric uncertainty and the unmeasured external signals. The estimated disturbance is directly incorporated into the feedback linearization control law for uncertainty compensation. Considering the compensation effects, to assess individual stability and string stability, we formulate an overlapping subsystem representing the interaction between vehicles, which directly exchange information. Through this modeling formulation, individual and string stability of the nonhomogeneous platoon can be studied using $\mathcal{L}_2$ stability analysis of a single overlapping subsystem, ensuring the scalability of the proposed stability conditions. Considering event-based transmission for resource-efficient communication, we derive sufficient design conditions using suitable Lyapunov-Krasovskii functionals and relaxation techniques for dynamic event-triggered control (ETC) methods to ensure individual and string stability in cases with and without communication delays. To ensure Zeno-free behavior, a minimum time between consecutive transmissions is imposed. To account for the enforced time, the overlapping subsystem is rewritten as a switching system based on the intervals during which the triggering mechanism is active. As an extension of ETC methods for platooning applications, we propose a co-design ETC method for nonlinear systems, based on a feedback linearization technique. The co-design conditions for both the controller and the event-triggering mechanism are recast as an optimization problem subject to linear matrix inequality constraints. Extensive simulations and comparisons are presented for each proposed ETC control result to illustrate the advantages of the respective methods over the related literature.

Keywords: Nonlinear Systems; Networked Control; Event-Triggered Control; Vehicle Platoon; Disturbance Observer.

Resumo

Nesta tese abordamos o projeto de controle acionado por eventos para sistemas não lineares, com foco na aplicação em comboio de veículos não homogêneos. Devido à presença de incertezas paramétricas e distúrbios exógenos, a técnica clássica de linearização por realimentação não pode ser aplicada para obter um comboio linear e homogêneo. Para resolver essa questão, propomos um observador de distúrbios (DOB : *Disturbance observer*) para estimar um distúrbio "virtual", representando os efeitos tanto da incerteza paramétrica quanto dos sinais externos não medidos. O distúrbio estimado é incorporado diretamente na lei de controle de linearização por realimentação para compensação das incertezas. Considerando os efeitos da compensação, para avaliar a estabilidade individual e a estabilidade do comboio, formulamos um subsistema sobreposto que representa a interação entre veículos que trocam informações diretamente. Por meio dessa formulação, a estabilidade individual e do comboio não homogêneo pode ser estudada utilizando a análise de estabilidade $\mathcal{L}_2$ de apenas um subsistema sobreposto, garantindo a escalabilidade das condições de estabilidade propostas. Considerando a transmissão baseada em eventos para comunicação eficiente em termos de recursos, derivamos condições suficientes usando funcionais de Lyapunov-Krasovskii adequados e técnicas de relaxamento para métodos de controle acionado por eventos dinâmicos (ETC : *Event-triggered control*) para garantir a estabilidade individual e do comboio nos casos, com e sem atrasos de comunicação. Para garantir um comportamento livre de Zenão, um tempo mínimo entre transmissões consecutivas é imposto. Para incluir esse tempo no modelo do subsistema sobreposto, o mesmo é reescrito como um sistema chaveado baseado nos intervalos durante os quais o mecanismo de disparo está ativo. Como uma extensão das abordagem ETC aplicada ao comboio, propomos um método para co-projeto de ETC aplicado a sistemas não lineares, baseado em uma técnica de linearização por realimentação. As condições de co-projeto para o controlador e o mecanismo de acionamento de eventos são reformuladas como um problema de otimização sujeito a restrições sob a forma de desigualdades matriciais lineares. Simulações extensivas e comparações são apresentadas para cada controlador ETC proposto com intuito de ilustrar as vantagens dos respectivos métodos em relação à literatura relacionada.

Palavras-chave: Sistemas Não Lineares; Controle Em Rede; Controle Acionado Por Evento; Comboio De Veículos; Observador De Distúrbios.

Résumé

Cette thèse aborde la mise en œuvre d'une commande événementielle pour les systèmes non linéaires avec une application au convoi non homogène de véhicules. La commande linéarisante est appliquée pour homogénéiser le convoi. Néanmoins, elle a des limitations en présence d'incertitudes paramétriques et de perturbations exogènes non mesurées. Pour résoudre ce problème, nous proposons d'utiliser un observateur de perturbations (DOB : disturbance observer) qui estime une perturbation "virtuelle", représentant les effets à la fois des incertitudes paramétriques et des signaux externes non mesurés. Cette estimation est directement intégrée dans la loi de commande linéarisante pour compenser les incertitudes. En tenant compte des effets de compensation, la stabilité individuelle de chaque véhicule et la stabilité du convoi de véhicules est formulée à partir d'un sous-système interconnecté. Ce dernier représente l'interaction entre deux véhicules consécutifs qui échangent directement des informations. Grâce à cette formulation, la stabilité individuelle et en convoi non homogène peut être étudiée en utilisant une analyse de stabilité $\mathcal{L}_2$ d'un seul sous-système interconnecté, assurant la scalabilité des conditions de stabilité proposées. En considérant une transmission basée sur les événements pour réduire le taux de communication, des conditions suffisantes de stabilité sont proposées. Elles utilisent la théorie de Lyapunov et dans le cas de retards, des fonctionnelles de Lyapunov-Krasovskii. Pour éviter le phénomène de Zenon, un délai minimum entre les transmissions consécutives est imposé. Pour tenir compte du délai imposé, le sous-système interconnecté est réécrit sous forme d'un système à commutation basé sur les intervalles pendant lesquels le mécanisme de déclenchement est actif. En tant qu'extension des méthodes ETC pour les applications autour des convois de véhicules, une méthode de co-design pour les systèmes non linéaires est également proposée à partir d'une technique de commande linéarisante. Les conditions de synthèse à la fois pour le contrôleur et le mécanisme de déclenchement d'événements sont reformulées sous forme d'un problème d'optimisation écrit à l'aide de contraintes d'inégalité matricielle linéaire. Des simulations et des comparaisons sont présentées pour chaque partie du mémoire.

Mots clés: Systèmes Non Linéaires; Commande En Réseau; Commande Événementielle; Convoi Du Véhicule; Observateur Des Perturbations.

List of figures

List of tables

List of symbols and notations

$\in$	belong to
$\forall$	for all
$\mathbb{R}$, $\mathbb{N}$, $\mathbb{Z}$	set of real, natural and integers numbers
$\mathbb{R}^n$	n dimensional vector space with real entries
$\mathbb{R}^{n\times m}$	$n \times m$ dimensional matrix space with real entries
$a > b$ $(a < b)$	a is greater (less) then b
$a \geq b$ $(a \leq b)$	a is greater (less) or equal to b
$A \succ 0$ $(A \prec 0)$	matrix A is positive (negative) definite
$A \succeq 0$ $(A \preceq 0)$	matrix A is positive (negative) semidefinite
$A \succ B$ $(A \prec B)$	$A - B$ is positive definite (negative definite)
$(\cdot)^T$	transpose
$(\cdot)^{-1}$	matrix inverse
$\mathrm{Tr}(A)$	is the Trace of matrix A
$\mathrm{diag}(A, B, C)$	is a block diagonal matrix with entries A, B, C
$\mathrm{He}\{A\}$	represents $A^T + A$
$\mathrm{col}\{x, y\}$	represents $\begin{bmatrix} x^T & y^T \end{bmatrix}^T$

Summary

1 Introduction

Traffic congestion and accidents have become more frequent as the population grows, resulting in problems such as transportation delays, traffic jams, and increased fuel consumption (GUANETTI *et al.*, 2018; BIAN *et al.*, 2019; CHEN *et al.*, 2023; VILCA *et al.*, 2015). In this context, high-level platoon coordination (JOHANSSON *et al.*, 2023; BAI *et al.*, 2023) together with physical-level platooning control (JIA *et al.*, 2016; FENG *et al.*, 2019) have been considered a promising solution. Through platooning, vehicles can travel in a string-like configuration, maintaining controlled short distances and velocity according to a predefined strategy/policy and safety constraints a feat that is often unattainable by humans alone (MAHFOUZ *et al.*, 2023; JU *et al.*, 2022a; WANG *et al.*, 2018). This shorter distancing facilitates aerodynamic drag reduction, subsequently decreasing fuel consumption (LESCH *et al.*, 2022). Furthermore, with optimized distance spacing, traffic flow improves, thereby avoiding congestion. These aspects motivate the study of vehicles equipped with adaptive cruise control (ACC) systems. In this setup, a leader is followed by N follower vehicles in a string-like formation. The vehicles have sensors that can measure the distance between themselves and the vehicle in front. The measured distances are compared with a pre-defined distance policy to ensure a safe distance between vehicles.

For platooning control, two main properties are of fundamental importance. One is individual stability, which refers to the ability of each vehicle in the platoon to achieve and maintain the desired distance policy. The other property is string stability, which ensures that small disturbances are not amplified throughout the platoon. While individual stability ensures platoon formation, string stability ensures that fast disturbances affecting the leader or other vehicles will not cause excessive changes in the formation, for example, avoiding vehicles suddenly braking.

While individual stability can be defined considering classical control theory or in the Lyapunov sense (KHALIL, 2002), string stability presents many mathematical definitions and has been analyzed under different frameworks in the literature (FENG *et al.*, 2019). Among these approaches, the main ones are frequency-domain analysis (in terms of $\mathcal{H}_\infty$ norm) done in the works of (PLOEG *et al.*, 2011; NUNEN *et al.*, 2019; SAMII; BEKIARIS-LIBERIS, 2024) and time-domain methods (in terms of $\mathcal{L}_p$ norms) used in (DOLK *et al.*, 2017; ZHU *et al.*, 2020; PLOEG *et al.*, 2014). The time-domain approach relies on evaluating the $\mathcal{L}_p$ norm between the leader input or perturbations and the output of the last vehicle in the platoon. This can also be studied by evaluating the $\mathcal{L}_p$ norm between the input and the output of the subsystems that composes the string.

Feedback linearization of vehicle platoons with uncertainties

The homogeneity and linearity of the platoon are common assumptions employed to simplify individual and string stability analysis (DOLK *et al.*, 2017; PLOEG *et al.*, 2011; ZHENG *et al.*, 2016; WANG *et al.*, 2022b; SU *et al.*, 2024). Although this assumption can be achieved through feedback linearization techniques, the procedure requires precise knowledge of the vehicle parameters. Parametric uncertainties and unmeasured external variables can cause mismatches, resulting in nonhomogeneous platooning systems (GUO *et al.*, 2016; GAO *et al.*, 2016; HUANG; KARIMI, 2021; JU *et al.*, 2022b). To overcome these problems, (WANG *et al.*, 2022a) proposes an intermediate-based robust observer to jointly estimate the sensor and actuator faults as well as matched disturbances, whose effects can be compensated via a robust non-fragile fault-tolerant control method. (LUO *et al.*, 2021) utilizes a proportional multiple-integral observer to simultaneously estimate the state and a lumped disturbance, which is compensated via a tube-based model predictive control scheme. Alternatively, the authors in (GAO *et al.*, 2016) consider a filtering technique to attenuate the effects of disturbances, while the works (GUO *et al.*, 2016; HUANG; KARIMI, 2021) explore Lyapunov-like string stability conditions with disturbances. These works evaluate string stability based on the overall platoon dynamics describing the relationship between the input of the leader and the output of the last vehicle. In this case, whenever new vehicles are added to the platoon, the stability analysis conditions must be reevaluated. Moreover, as the number of vehicles in the platoon grows, more decision variables and constraints are involved in the stability analysis, which can increase the problem's solution complexity. These factors may compromise the scalability of the application.

Wireless communication and event-triggered control

Ensuring individual and string stability while minimizing the distance between vehicles can be conflicting objectives, as a shorter distance can compromise stability. As some practical applications have demonstrated, this problem can be relaxed by incorporating communication devices within the vehicles and allowing information to be shared along the platoon, which can enhance platoon performance (DARBHA *et al.*, 2019; MILANES *et al.*, 2014; DEY *et al.*, 2016) and, theoretically, enable shorter distance policies (DARBHA *et al.*, 2019) without compromising safety. This inclusion of communication into ACC is known as cooperative ACC (CACC). In the CACC framework, communication plays an important role, and different flow typologies can be differentiated according to which vehicles are able to share information. Another fundamental component of communication is its quality and mechanism (FENG *et al.*, 2019). Communication quality refers to issues that can occur during communication. Some works in the literature (WU *et al.*, 2022; LINSENMAYER; DIMAROGONAS, 2015; ZHANG *et al.*, 2021; GE *et al.*, 2024) consider

perfect communication; however, phenomena such as packet dropouts, denial of service (PESSIM *et al.*, 2021), attacks (PEIXOTO *et al.*, 2023), and communication delays can compromise individual and, especially, string stability (LIU *et al.*, 2001; ONCU *et al.*, 2014).

The communication mechanism specifies how communication is established between vehicles. Most vehicular platoon control methods rely on periodic communication (FENG *et al.*, 2019), which can be assumed continuous with fast transmission (SWAROOP *et al.*, 1994; WANG *et al.*, 2023), causing high bandwidth and energy consumption. Alternatively, event-triggered control (ETC) makes communication more efficient by transmitting information based on a specified criterion. However, communication efficiency may trade off with performance. In applying ETC to CACC systems, minimizing communication requirements while maintaining stability, even in the presence of delays, is fundamental.

Event-triggered control schemes vary according to their event-triggering mechanisms (ETMs). Static ETMs involve parameters that do not change over time (LI *et al.*, 2021; SU *et al.*, 2024; PEIXOTO *et al.*, 2023; WEI *et al.*, 2017; WU *et al.*, 2022). Adaptive or dynamic ETMs consider parameters that change according to adaptive or dynamic triggering conditions, aiming to reduce the transmitted events (GIRARD, 2015; ZHANG *et al.*, 2021; LI *et al.*, 2019; DOLK *et al.*, 2017; XIAO *et al.*, 2022). In ETC design, two approaches can be distinguished, namely emulation approach and co-design approach (PENG; LI, 2018). The emulation approach consists of a two-step procedure where the controller is first designed assuming continuous communication, and in the second step, the ETM is designed based on the desired controller. In the co-design approach, both the controller and the ETM are jointly designed within the same optimization problem. The co-design approach offers more flexibility since it allows both control performance and communication efficiency to be incorporated as constraints or cost functions. Additionally, both individual and string stability can be evaluated directly from the optimization-based design problem.

When designing event-triggered controllers, it is essential to avoid Zeno behavior, which is the phenomenon of having an infinite number of events (transmissions) in a finite time interval, i.e., the time between events converges to zero. Many works regarding ETC derive their mechanisms from the classical conditions proposed by (TABUADA, 2007), where Zeno-free behavior can be ensured with minor assumptions. However, under uncertainties and disturbances, these ETMs can no longer guarantee a positive lower bound for the inter-event time (IET) to prevent Zeno behavior. Therefore, substantial investigations are required to ensure a minimum time between events in these scenarios (BORGERS; HEEMELS, 2014). To ensure Zeno-free behavior for dynamic systems with disturbances, a minimum waiting time can be enforced, so that the triggering condition is only evaluated after a specified time interval has elapsed (ABDELRAHIM *et al.*, 2016; DOLK *et al.*, 2017; CARNEVALE *et al.*, 2007). Alternatively, the triggering condition

can be verified periodically instead of continuously (HEEMELS *et al.*, 2011; GE *et al.*, 2020). This results in a periodic ETC, where Zeno behavior is avoided, as the inter-event time is limited by the sampling period.

Combining communication quality with communication mechanisms and system uncertainties makes the platooning control problem more challenging. Design conditions must account for both network-induced delays and event-triggered communication while ensuring Zeno-free behavior in the presence of uncertainties and disturbances. Additionally, it is crucial to ensure that information arrives in the correct sequence, avoiding packet reordering. This imposes further constraints on time delays and the minimum time between transmissions (WU *et al.*, 2022; WEI *et al.*, 2017).

In the literature, (LINSENMAYER; DIMAROGONAS, 2015) proposed a static event-triggered mechanism (ETM), while (ZHANG *et al.*, 2021) employed an adaptive ETM; however, both were developed in disturbance-free scenarios. In (DOLK *et al.*, 2017), a minimum waiting time was enforced to ensure Zeno-free behavior. Additionally, dynamic ETMs were developed to further reduce the number of triggering events. However, the event-triggered control (ETC) is designed based on a two-step approach (emulation), which can lead to more conservative design conditions. The work in (DOLK *et al.*, 2017) only accounted for network delays without considering uncertainties. Based on the discretization of the platooning system, another discrete-time ETC scheme was proposed in (LI *et al.*, 2019), which takes into account unreliable communication links. Due to the discretization and sampling nature of this co-design approach, Zeno behavior can be naturally avoided. However, this approach requires that all vehicles sample the information at the same time, which is not realistic, even with the same sampling frequency.

Accounting for external disturbances, effective ETC approaches were proposed for cooperative ACC in (SU *et al.*, 2024; GE *et al.*, 2024), considering periodic event-triggered control. These approaches can avoid Zeno behavior, as the inter-event time is limited by the sampling time. (WU *et al.*, 2021) developed a fully distributed ETM for distributed control of vehicular platoons with nonzero input of the leader vehicle and actuator uncertainties while ensuring Zeno-free behavior. The works in (WU *et al.*, 2021; SU *et al.*, 2024) considered static ETMs, while the ETM in (GE *et al.*, 2024) is adaptive, which can significantly reduce the number of transmitting events. Furthermore, in (SU *et al.*, 2024; WU *et al.*, 2021), multiple communication topologies were considered, while the work (GE *et al.*, 2024) focuses on the predecessor-follower (PF) topology. All the mentioned works evaluated individual and string stability considering the combined dynamics of all vehicles of the platoon, from the leader to the last vehicle, which can result in scalability issues. As shown in (DOLK *et al.*, 2017), the specificity of the PF topology can be exploited to reduce the analysis problem to a subset of vehicles, facilitating the scalability of the platoon.

1.1 Objective and contributions

The main objective of this thesis is to design string-stable controllers for cooperative ACC vehicle platoons subject to uncertainties under event-triggered communication. To address the uncertainty issue in platooning control, we propose a disturbance observer-based compensation technique that combines feedback linearization with disturbance compensation. Mismatches caused by parametric uncertainties and exogenous disturbance effects are modeled as a single virtual disturbance signal, which is estimated and compensated using a disturbance observer (DOB). The DOB-based disturbance estimate is directly integrated into the feedback control law. To address the impact of disturbance estimation error, we propose an extension of the $\mathcal{L}_2$ norm stability conditions to assess string stability. Specifically, classical string stability can be ensured in the presence of significant uncertainties through effective disturbance compensation.

To increase communication efficiency, we propose dynamic event-triggered controllers for CACC platoons that ensures both individual vehicle stability and $\mathcal{L}_2$ string stability of the platoon. We define interconnected subsystems that model the interaction between consecutive vehicles such that by evaluating the $\mathcal{L}_2$ stability of a single subsystem, the individual and $\mathcal{L}_2$ string stability can be ensured for the platoon independently of the number of vehicles, thus facilitating platoon scalability. To avoid Zeno behavior, a minimum waiting time is imposed between consecutive transmissions. Considering the communication time delay and the imposed waiting time, we define a switching ETC and consequently model the system as switching. Based on this switching, along with a proper choice of Lyapunov-Krasovskii functionals (LKF), both the controller and the ETM can be designed within a single optimization problem subject to linear matrix inequality (LMI) constraints. Additionally, we employ suitable relaxation techniques to achieve less conservative conditions. Furthermore, considering the feedback linearization technique employed in the vehicular platoon, we propose co-design conditions for event-triggered control of feedback linearizable systems, assuming that the states necessary for the feedback linearization procedure are updated based on the event-triggering conditions. Specifically, the main contributions of this PhD can be summarized as follows.

- A DOB-based disturbance compensation scheme is proposed for feedback linearization control of nonhomogeneous platoons, along with proper extensions to string stability analysis to account for disturbance estimation error.
- A switched dynamic ETM is proposed to ensure string stability of the platoon subject to network-induced delays, while minimizing the number of transmissions and avoiding Zeno behavior.
- Event-triggered control co-design conditions are proposed for nonlinear systems considering a feedback linearization control law, where the states utilized for feedback

linearization are updated according to an event-triggering condition.

1.2 Organization

This PhD manuscript is organized as follows.

In Chapter 2, we introduce the platooning control problem, discuss results about event-triggered control, and present properties used to prove Zeno-free behavior. Subsequently, a succinct introduction to the sector nonlinearity approach and delay systems is provided, with a brief explanation of the stability analysis utilizing LMI constraints.

In Chapter 3, we address the problem of control design for cooperative adaptive cruise control vehicular platoons, assuming continuous communication. Considering uncertain vehicle model parameters, we propose feedback linearization along with disturbance observer compensation to handle the effects of uncertainties. Various approaches to modeling vehicle interaction are presented and proposed, along with string stability analysis conditions that account for uncertainty compensation. Simulations are provided to validate the DOB compensation, and the platoon performance is evaluated.

In Chapter 4, communication is assumed to be event-based, and event-triggered controllers are designed for efficient communication between vehicles. We propose dynamic event-triggered control with an enforced minimum waiting time and a switching model of the problem to account for this enforced time. Design conditions are proposed for scenarios with and without delays, and numerical examples are provided to validate the proposed approach.

In Chapter 5, event-triggered controllers are proposed for a class of nonlinear feedback linearizable MIMO systems. In this approach, mismatches between nonlinearities arise from the sample-and-hold process intrinsic to the event-triggered controller. With some assumptions, these mismatches are explicitly incorporated into the controller and event-triggering mechanism design conditions. Numerical examples are provided to validate the proposed approach, and the results are compared with others in the literature.

Finally, in Chapter 6, we present the concluding remarks of this PhD work and provide an outlook on future perspectives for this research.

1.2.1 Personal publications related to the PhD project

Chapters 3 and 4 mainly address event-triggered control for nonhomogeneous CACC vehicular platoons using DOB-based uncertainty compensation. The materials in these chapters are presented in the following publication and submission.

- SILVA, R.; NGUYEN, A.; GUERRA, T.-M.; SOUZA, F.; FREZZATTO, L. Switched dynamic event-triggered control for string stability of nonhomogeneous vehicle

platoons with uncertainty compensation. *IEEE Transactions on Intelligent Vehicles*, doi: 10.1109/TIV.2024.3385575, p. 1–15, 2024.

- SILVA, R.; NGUYEN, A.; GUERRA, T.-M.; SOUZA, F.; FREZZATTO, L. Dynamic event-triggered CACC co-design for heterogeneous vehicular platoons under uncertainties and network delays, *IEEE Transactions on Intelligent Transportation Systems* ***(Submitted)***, 2024.

The results of feedback linearization with event-triggered control in Chapter 5 pertain to the following submission.

- SILVA, R. N.; SOUZA, F. O.; NGUYEN, A.; GUERRA, T.; FREZZATTO, L. Event-triggered control co-design for MIMO systems via feedback linearization with tolerated nonlinearity mismatches, *IEEE Transactions on Automatic Control* ***(Third revision)***, 2022.

Apart of the results presented in this work the following result was published and presented in a conference.

- SILVA, R. N.; FREZZATTO, L.; SOUZA, F. O.; CAMPOS, V. C. S. Event-triggered control of TS fuzzy systems with guaranteed membership function mismatch. *IFAC-PapersOnLine*, Elsevier BV, v. 54, n. 4, p. 74–79, out. 2021.

2 Basic aspects about platooning and event-triggering control

2.1 Introduction

As the manuscript is related to Event-Triggered Control (ETC) on one side and platooning on the other, this first chapter will describe some bases and technical aspects useful for both topics. Some mathematical preliminaries and notations used all along the work are summarized in the first section. The second section recalls the main challenges of control for platooning, including individual and string stability. As a part of the communication will be considered as event-triggered, the section three presents the main principles of ETC stability including the input-to-state stability conditions. As usual in this field, the so-called Zeno behavior has to be avoided, the section three also gives the way to determine a positive lower bound of inter event times. The systems used in this thesis are generally nonlinear and, excepted for pure feedback linearization, the way to deal with their stability analysis and/or stabilization will require a polytopic description. A quick recall of such a representation is done in section four. As the communication can also be delayed, section five gives some classical tools for time delay systems stability, especially the use of Lyapunov-Krasovskii functionals. At last, all along the thesis, in order to derive results, we use the framework of Linear Matrix Inequalities (LMI) constraints. Therefore, some definitions and useful technical lemmas conclude the chapter.

Notations:

Sets: $\mathbb{N}$ denotes the set of natural numbers including zero, $\mathbb{R}^n$ denotes the n-dimensional Euclidean space, $\mathbb{R}^{n\times m}$ is the set of $n \times m$ matrices with real entries.

Vectors: For $x \in \mathbb{R}^n$ and $y \in \mathbb{R}^m$, $\|x\|$ stands for the vector Euclidean norm of x, $\mathrm{col}\{x,\ y\}$ stands for $[x^T\ y^T]^T$.

Matrices: For a matrix X, X^T denotes its transpose, X^{-1} its inverse, $\mathrm{Tr}(X)$ its trace, and $\mathrm{He}(X) = X^T + X$. For a symmetric matrix P, $\lambda_{\min}(P)$ and $\lambda_{\max}(P)$ stands for the minimum and maximum eigenvalues of P, respectively. For a symmetric matrix P, $P \succ 0$ (respectively, $P \prec 0$) stands for a positive (respectively negative) definite matrix. The symbol $*$ in a matrix denotes a symmetric component. $[X]_{i,j}$ stands for the element of X in position i, j. For matrices Y_1, Y_2, $\ldots$, Y_p, not necessarily square, $\mathrm{diag}(Y_1,\ Y_2,\ \ldots,\ Y_p)$ stands for a block diagonal matrix with entries Y_i for $i = 1, \ldots, p$. For matrices $\mathbf{e}_i$ and A_i, for $i = 1, \ldots, N$, with appropriate dimensions,

we denote $\text{col}\{\mathbf{e}_1, \ldots, \mathbf{e}_n\} = \text{diag}(A_1, A_2, \ldots, A_n)$, which means that

$$\left[\begin{array}{c} \mathbf{e}_1 \\ \hline \mathbf{e}_2 \\ \hline \vdots \\ \hline \mathbf{e}_n \end{array}\right] = \left[\begin{array}{cccc} A_1 & 0 & \ldots & 0 \\ \hline 0 & A_2 & \ldots & 0 \\ \hline \vdots & \vdots & \ddots & \vdots \\ \hline 0 & 0 & \ldots 0 & A_n \end{array}\right]. \tag{2.1}$$

Functions: For $x \in \mathcal{X}$ and $\mathcal{S} \subseteq \mathbb{R}^{n\times m}$, a function $f : \mathcal{X} \to \mathcal{S}$ is denoted $f(x)$. Functions are denoted as $f(x)$ whether they are scalar ($n = m = 1$), vector-valued ($m = 1$), or matrix functions ($m, n > 1$). For a vector-valued function $f(x)$, $J_f(x)$ stands for the Jacobian of f. To avoid confusion between variables defined as e (error signals for example), exponential functions are denoted as e^x, where e is Euler's constant.

$\mathcal{K}$ and $\mathcal{K}_\infty$ functions: A continuous function $\alpha : [0, a] \to [0, \infty]$ is said to be a $\mathcal{K}$-function (on short $\mathcal{K}$-function), if:

- $\alpha(x)$ is strictly increasing;
- $\alpha(0) = 0$.

Moreover, a continuous function $\alpha : [0, \infty] \to [0, \infty]$ is said to be a $\mathcal{K}_\infty$-function if:

- $\alpha(x)$ is a $\mathcal{K}$-function;
- $\lim_{r\to\infty} \alpha(r) = \infty$.

Lie derivative: For functions, $f(x)$ and $h(x)$, the Lie derivative of $h(x)$ in the direction of $f(x)$ is defined as

$$\mathcal{L}_f h(x) = \frac{\partial h}{\partial x} f(x) \tag{2.2}$$

Moreover, the n-th Lie derivative of $h(x)$ at $f(x)$ direction is given by $\mathcal{L}_f^{(n)} h(x) = \mathcal{L}_f \mathcal{L}_f^{(n-1)} h(x)$.

Simplex: A unit simplex with m vertices is denoted as

$$\Upsilon_m = \left\{ \upsilon \in \mathbb{R}^n : \sum_{i=1}^{m} \upsilon_i = 1, \quad \upsilon_i \geq 0, \quad i = 1, \ldots, n \right\}. \tag{2.3}$$

and, given $\upsilon(x) = \text{col}\{\upsilon_1(x), \ \ldots, \ \upsilon_n(x)\}$ a vector-valued function, $\upsilon(x) \in \Upsilon_n$ for $x \in \mathcal{X}$, means that $\sum_{i=1}^{n} \upsilon_i(x) = 1$, $\upsilon_i(x) \geq 0$, for $i = 1, \ldots, n$ and all $x \in \mathcal{X}$.

The notations being defined the first topic of the thesis is introduced in the next section.

2.2 Introduction to longitudinal platooning

With the increase of vehicle circulation, automatic and intelligent vehicles are still considered a promising approach to reduce traffic, reduce fuel consumption, and improve

safe transportation (LESCH *et al.*, 2022; YU; WANG, 2021; WANG *et al.*, 2018; MAHFOUZ *et al.*, 2023). These aspects motivated the study of vehicles with adaptive cruise control (ACC) and Cooperative ACC (CACC) systems. Both ACC and Cooperative ACC allow vehicles to travel in strings while maintaining a safe and short distance that, in most cases, is difficult to be achieved by the human alone (MAHFOUZ *et al.*, 2023; WANG *et al.*, 2018). This short distancing allows aerodynamic drag reduction, which in turn can reduce fuel consumption (YU; WANG, 2021; MAHFOUZ *et al.*, 2023; LESCH *et al.*, 2022). Furthermore, with an optimized distance spacing, traffic flow improves, avoiding congestion.

The ACC and Cooperative ACC systems needs to ensure a suitable distance between vehicles. In order to achieve this goal, a distance policy is defined which depends of the vehicle velocity. To achieve platooning the measurements required are the inter vehicles distance and the velocity difference. The Cooperative ACC differs from the ACC by introducing a communication system that allows vehicles to share information, Figure 2.1. As shown in some practical applications (DARBHA *et al.*, 2019; MILANES *et al.*, 2014; DEY *et al.*, 2016) sharing information can improve platoon performance and, from a theoretical point of view, allows shorter distance policies (DARBHA *et al.*, 2019) without compromising safety.

In addition to achieve and maintain the desired distance policy the string stability is a desired property, which ensures that small disturbances are not amplified throughout the platoon. While individual stability guarantee platoon formation, string stability ensures that fast disturbances affecting the leader or other vehicles will not cause excessive changes in the formation, for example, avoiding vehicles suddenly braking.

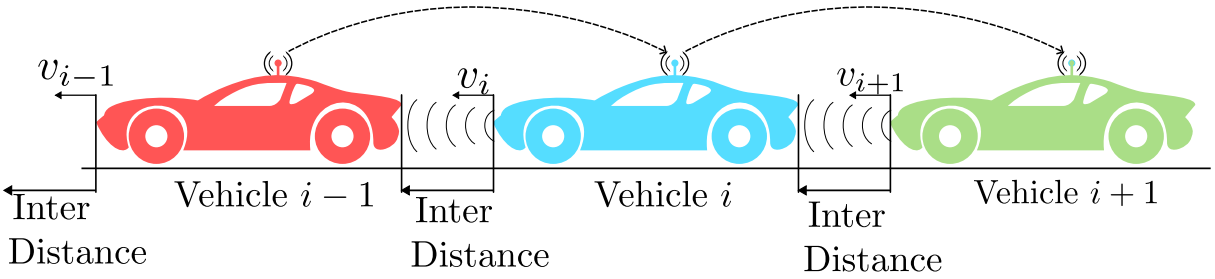

Figure 2.1 – Cooperative ACC vehicle platooning illustration where Vehicle i receives information from Vehicle $i-1$ and transmit to Vehicle $i+1$.

For ACC and Cooperative ACC, ensuring distance policy has been achieved using methods such as Sliding Mode Control (XIAO; GAO, 2011; SAWANT *et al.*, 2021), Model Predictive Control (LIN; NGUYEN, 2020; ASADI; VAHIDI, 2011; MOSER *et al.*, 2018), Fuzzy Control (NARANJO *et al.*, 2003; PANANURAK *et al.*, 2009), Neuro-Fuzzy Control (LIN; NGUYEN, 2020), Model free approach (POLACK *et al.*, 2017; MENHOUR *et al.*, 2018) or Feedback Linearization (DOLK *et al.*, 2017; PLOEG *et al.*, 2014; ZHENG *et al.*, 2016; WANG *et al.*, 2022b; SU *et al.*, 2024; ZHU *et al.*, 2020). Among all the re-

ferenced approaches, feedback linearization is commonly used, often in combination with other methods such as Sliding Mode Control and Model Predictive Control. Linearization is primarily utilized to reduce the problem of designing controllers for longitudinal platoons to a linear control problem where all vehicle dynamics are homogeneous. However, parametric uncertainties and unmeasured external variables can interfere with the feedback linearization, causing mismatches and resulting in non-homogeneous platooning systems (GUO *et al.*, 2016; GAO *et al.*, 2016; HUANG; KARIMI, 2021; JU *et al.*, 2022b).

Works such as (WANG *et al.*, 2022a; LUO *et al.*, 2021) introduce disturbance compensation to handle uncertainties, but without addressing the issue of string stability. Alternative approaches handle the uncertainties via filtering (GAO *et al.*, 2016) or by proposing Lyapunov-like string stability conditions with disturbances. These works evaluate string stability based on the overall platoon dynamics, describing the relationship between the input of the leader and the output of the last vehicle. Note that the need to consider the overall platoon dynamics can significantly increase the complexity of stability analysis.

String stability is a property constantly referenced in this thesis. As there exist many mathematical definitions in the literature (FENG *et al.*, 2019), we formalize the string stability conditions considered in this thesis. They are based on the $\mathcal{L}_2$ string stability proposed in (PLOEG *et al.*, 2014), and are defined as follows.

Definition 2.1. *Let $\bar{x}_i$ be the states and $\bar{x}(t) = \mathrm{col}(\bar{x}_1, \ldots, \bar{x}_N)$ be the lumped state of all vehicles. Moreover, let u_0 be an exogenous input, and $z_i = h(\bar{x}_i)$ be a performance output for vehicle i. The vehicular platoon is $\mathcal{L}_2$ string stable if there exist a constant γ_0 and a $\mathcal{K}$-function $\rho(\cdot)$ such that for any initial condition $\bar{x}(0)$, we have*

$$\|z_i\|_{\mathcal{L}_2} \leq \gamma_0 \|u_0\|_{\mathcal{L}_2} + \rho(\|\bar{x}(0)\|), \quad i = 1, \ldots, N. \tag{2.4}$$

In Definition 2.1, the exogenous input u_0 refers to the leader input, while z_i is a performance output for each vehicle which can vary according to the model used for vehicle interaction. The different models used for the vehicles, the vehicles interactions, the measurements required, the considered uncertainties, individual and string stability will be detailed in Chapter 3.

In this thesis, we will explore the case where the communication between vehicles is event-triggered, next section presents the main principles of ETC

2.3 Introduction to event-triggered control

Event triggered control (ETC) stands for a control approach where the signals utilized for computing the control law are updated, according to a event triggering mechanism. The signals utilized by the control law are samples of the measured signals which are

held constant between updates and are only updated whenever a triggering conditions is achieved. This event conditions are functions based on the error between the signals current value and its last sample. The paper of (TABUADA, 2007) presents a methodology to design event-triggered controllers and conditions for nonlinear systems based on an input-to-state stability (ISS) criterion (PENG; LI, 2018; HEEMELS *et al.*, 2012). Those results were fundamental for other event-triggering conditions proposed in literature such as (GIRARD, 2015; MOREIRA *et al.*, 2016) applied for perturbed systems models. Different approaches can be considered with different modelings, like hybrid systems (ABDELRAHIM *et al.*, 2017), piecewise models (HEEMELS *et al.*, 2012), and time delay systems with Lyapunov-Krasoviskii functionals (YAN *et al.*, 2019).

2.3.1 Input-to-state stability conditions

For this thesis the event-triggered controller is designed similar to (TABUADA, 2007), based on ISS conditions. For a better comprehension we revisit the results and proofs in (TABUADA, 2007). To this end, consider the following nonlinear system

$$\dot{x} = f(x, u) \tag{2.5}$$

with $x \in \mathbb{R}^{n_x}$ the system states and $u \in \mathbb{R}^{n_u}$ the control input given by

$$u = \kappa(x + e) \tag{2.6}$$

where $e \in \mathbb{R}^{n_x}$ can stand for an error in the measurement of x. Substituting (2.6) in (2.5), yields

$$\dot{x} = f(x, k(x + e)), \tag{2.7}$$

therefore, the control law is designed to render an ISS closed-loop system with respect to e. The definition of input-to-state stability is given as follows.

Definition 2.2 ((SONTAG; WANG, 1996))**.** *A smooth positive definite function $V(x)$ is said to be an ISS Lyapunov function for the closed-loop system* (2.7) *if there exist $\mathcal{K}_\infty$ functions $\alpha_1(\cdot)$, $\alpha_2(\cdot)$, $\alpha_3(\cdot)$ and $\gamma(\cdot)$ satisfying*

$$\alpha_1(\|x\|) \leq V(x) \leq \alpha_2(\|x\|) \tag{2.8}$$

$$\frac{\partial V}{\partial x} f(x, \kappa(x + e)) \leq -\alpha_3(\|x\|) + \gamma(\|e\|) \tag{2.9}$$

Consider the control loop shown in Figure 2.2. The event triggering mechanism measure all the states and, according to the difference between the measured states $x(t)$ and the lest transmitted (sampled) state $x(t_k)$, determine when to update the signal transmitted to the controller $x(t_k)$. The measurement error is caused by the difference between the transmitted (sampled) state $x(t_k)$, used to compute the control law, and the continuous state $x(t)$. Therefore the control input (2.6) can be written as $u(t_k) = \kappa(x(t_k))$ and

$e(t) = x(t_k) - x(t)$ where $t_k \in \{t_0, t_1, t_2, \dots\}$ is the time sequence of increasing sample instants. When the sampling is periodic, the difference $t_{k+1} - t_k = T$, $T > 0$, is the sampling period. For the context of event-triggered control, the sampling time is neither periodic nor specified in advance. The sampling instants are achieved by an event-triggering condition based on the states of the system and the measurement error.

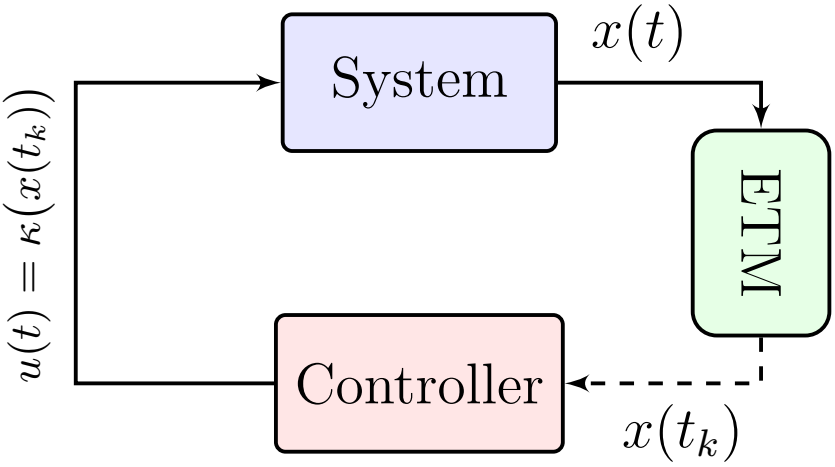

Figure 2.2 – Event triggering control loop

Assuming that the closed-loop system is ISS, the event conditions can be defined based on inequality (2.9). For this end, as in (TABUADA, 2007), let us rewrite (2.9) as

$$\frac{\partial V}{\partial x} f(x, \kappa(x+e)) \leq -(1-\sigma)\alpha_3(\|x\|) + (\gamma(\|e\|) - \sigma\alpha_3(\|x\|)) \,. \tag{2.10}$$

Notice that making

$$\gamma(\|e\|) - \sigma\alpha_3(\|x\|) \leq 0 \tag{2.11}$$

in (2.10) we have

$$\frac{\partial V}{\partial x} f(x, \kappa(x+e)) \leq -(1-\sigma)\alpha_3(\|x\|). \tag{2.12}$$

For $\sigma \in (0, 1)$, the condition (2.12) implies that $\dot{V} < 0$ for $x \neq 0$, *i.e.*, the system is asymptotically stable. To ensure that (2.11) holds an event condition can be defined

$$\begin{aligned} t_0 &= 0 \\ t_{k+1} &= \inf\{t > t_k \ : \ \gamma(\| \underbrace{x(t_k) - x(t)}_{e(t)} \|) - \sigma\alpha_3(\|x(t)\|) > 0\} \end{aligned} \tag{2.13}$$

The methodology consists in a two step approach: first it designs a control law (2.6) such that the closed-loop system (2.7) is ISS and in the second step defines an event-triggering condition. Alternatively both controller and ETM can be designed in a single step. We differentiate those two cases as follows:

- **Emulation**: Is a two step procedure where the controller is designed in the first step to ensure Input-to-State stability and in the second step the ETM is designed based on the controller.
- **Co-design**: Fixing the ETM structure, both controller and ETM parameters are designed within a single optimization problem

As an example of co-design consider $f(x,u) = Ax + Bu$ in (2.5) and a control input $u = \kappa(x+e) = Kx + Ke$ in (2.6) where K is a matrix to be designed, it follows from (2.7) that

$$\dot{x} = (Ax + BK)x + BKe. \tag{2.14}$$

Let Q_e, Q_x be positive definite matrices to be designed. Defining an event triggering condition

$$\begin{aligned} t_0 &= 0 \\ t_{k+1} &= \inf\{t > t_k \ : \ e(t)^T Q_e e(t) - x(t)^T Q_x x(t) > 0\} \end{aligned} \tag{2.15}$$

ensures that another sample is not taken from the system while $e(t)^T Q_e e(t) - x(t)^T Q_x x(t) \leq 0$. Choosing a Lyapunov function $V(x) = x^T P x$, with P a positive definite matrix, it suffices that

$$\dot{V} \leq e^T Q_e e - x^T Q_x x \tag{2.16}$$

to ensure asymptotic stability for the closed-loop system under ETM (2.15). In this approach Q_e, Q_x, P and K are design parameters that can be determined simultaneously via semi-definite programming.

2.3.2 Positive lower bound of inter event times

Throughout this thesis an important property to be ensured is Zeno-free behavior, this can be achieved ensuring the existence of a positive lower bound between events i.e., for $t_k \in t_0, t_1, \ldots$ a sequence generated by the event triggering mechanism, it exists a positive lower bound $\varepsilon > 0$ such that $t_{k+1} - t_k > \varepsilon$ for all $k \geq 0$. Ensuring the existence of a lower bound requires some assumptions regarding the system nonlinearities, the Lipschitz continuity being the main one. This assumption is commonly used in this thesis and its definition and properties are recalled thereafter (WEAVER, 1999).

Definition 2.3. *A function $f : \mathcal{X} \to \mathcal{Y}$ is Lipschitz continuous at $\mathcal{X}$ if there is a positive constant L such that*

$$\|f(x_1) - f(x_2)\| \leq L\|x_1 - x_2\| \tag{2.17}$$

for every $x_1, x_2 \in \mathcal{X}$.

Remark 2.1. Definition 2.3 is made considering a particular 2-norm, but a general definition for Lipschitz continuity considers a metric space, with its respective metrics.

Lemma 2.1. *Let $a(x)$, $b(x)$, $f(x)$ and $g(y)$ be Lipschitz continuous functions in compact sets $\mathcal{X}$ and $\mathcal{Y}$ Then, the following properties hold*

- *Multiplication: The function $a(x)b(x)$ is Lipschitz on $\mathcal{X}$;*
- *Division: If $a(x)^{-1}$ is bounded, then $b(x)/a(x)$ is Lipschitz on $\mathcal{X}$;*
- *Composition: If $f : \mathcal{X} \to \mathcal{Y}$ and $g : \mathcal{Y} \to \mathcal{X}$, then the composition $(g \circ f)(x)$ is Lipschitz continuous.*

Moreover to prove the existence of a lower bound of IET we consider a generalization of a well known result in literature named Grönwall-Bellman lemma (BELLMAN, 1943) or just Grönwall's lemma:

Lemma 2.2. *(PACHPATTE, 1997) Let $v : [t_0, T] \to \mathbb{R}$ be a bounded nonnegative piecewise continuous function, $\alpha : [t_0, T] \to \mathbb{R}$ a nonnegative integrable function and $\beta : [t_0, T] \to \mathbb{R}$ a continuous positive nondecreasing function. If*

$$v(t) \leq \beta(t) + \int_{t_0}^{t} \alpha(\tau)v(\tau)d\tau \tag{2.18}$$

for all $t \in [t_0, T]$. Then

$$v(t) \leq \beta(t)e^{\int_{t_0}^{t} \alpha(\tau)d\tau} \tag{2.19}$$

Another important inequality refers to the exponential function e^x.

Lemma 2.3. *Let $x \in \mathbb{R}$, such that $x < 1$, then*

$$\mathrm{e}^x < \frac{1}{1-x} \tag{2.20}$$

Proof. For the proof we distinguish the following two cases.

Case 1) $0 \leq x < 1$. For this case from power series expansion, we have

$$\mathrm{e}^x = \sum_{n=0}^{\infty} \frac{x^n}{n!}. \tag{2.21}$$

Since $0 \leq x < 1$, the series converges, and since $x^n/n! \leq x^n$, from (2.21) it follows that

$$\mathrm{e}^x = \sum_{n=0}^{\infty} \frac{x^n}{n!} \leq \sum_{n=0}^{\infty} x^n = \frac{1}{1-x} \tag{2.22}$$

Case 2) $x < 0$. Take $y > 0$, then we have that $\mathrm{e}^y > 1 + y$ and, consequently, $\mathrm{e}^{-y} < (1+y)^{-1}$. Making $x = -y < 0$ yields

$$e^x < \frac{1}{1-x} \tag{2.23}$$

Combining Cases 1 and 2 it follows that (2.20) holds for $x < 1$, finishing the proof.

□

In this work, in many scenarios we are interested not only in the stability of the system, but in the relationship between an certain input and output. This can be evaluated in terms of $\mathcal{L}_2$ stability analysis described in the next section.

2.4 $\mathcal{L}_2$ stability

From the definition presented in (KHALIL, 2002), a nonlinear system

$$\begin{aligned} \dot{x} &= f(x,u) \\ y &= h(x,u) \end{aligned} \tag{2.24}$$

with x being the states, u an input and y the output, is called finite gain $\mathcal{L}_2$ stable ($\mathcal{L}_2$ stable for short) from u to y if there exists a finite positive gain γ and a positive β such that

$$\|y\|_{\mathcal{L}_2} \leq \gamma \|u\|_{\mathcal{L}_2} + \beta \tag{2.25}$$

where $\|y\|_{\mathcal{L}_2} = \sqrt{\int_0^\infty \|y(t)\|^2 dt}$. Similarly to the Input-to-state stability conditions from Definition 2.2, the input-to-output stability can also be evaluated in terms of Lyapunov stability analysis.

Lemma 2.4. *Consider the nonlinear system* (2.24)*. If there exists a positive definite function $V(x)$ and positive constants α_1, α_2, and γ such that*

$$\alpha_1 \|x\|^2 \leq V(x) \leq \alpha_2 \|x\|^2 \tag{2.26}$$

$$\dot{V} = \frac{\partial V}{\partial x} f(x, \kappa(x+e)) \leq \gamma^2 \|u\| - \|y\| \tag{2.27}$$

then the system is finite-gain $\mathcal{L}_\in$ stable, and its $\mathcal{L}_2$ gain is less than or equal to γ.

Proof. First, notice that for $u = 0$ the conditions (2.26) and (2.27) imply asymptotic stability. Now, considering $u \neq 0$, integrating both sides of (2.27) from $t = 0$ to $t = \tau$ yields

$$V(x(t)) - V(x(0)) \leq \gamma^2 \int_0^\tau \|u(t)\|^2 dt - \int_0^\tau \|y(t)\|^2 dt \tag{2.28}$$

$$\int_0^\tau \|y(t)\|^2 dt + V(x(t)) \leq \gamma^2 \int_0^\tau \|u(t)\|^2 dt + V(x(0)). \tag{2.29}$$

Since $V(x(t))$ is positive definite, i.e., $V(x(t)) \geq 0$, we have that (2.29) implies

$$\int_0^\tau \|y(t)\|^2 dt \leq \gamma^2 \int_0^\tau \|u(t)\|^2 dt + V(x(0)) \tag{2.30}$$

Taking the square root of both sides of (2.30), defining $\beta = \sqrt{V(x(0))}$ and making $t \to \infty$, condition (2.30) implies

$$\|y\|_{\mathcal{L}_2} \leq \gamma \|u\|_{\mathcal{L}_2} + \beta \tag{2.31}$$

concluding the proof. □

The conditions of Lemma 2.4 will be referred to as $\mathcal{L}_2$ stability conditions and, as will be further discussed in Section 2.7, in this work these conditions will be evaluated in terms of an optimization subject to LMI constraints. Moreover, the models considered throughout this work are nonlinear. When we do not use feedback linearization, the way to deal with their stability/stabilization is to build exact polytopic representations described in the next section.

2.5 Sector nonlinearity

In this thesis we consider the class of affine in the control systems with a constant input matrix:

$$\dot{x} = F(x)x + Bu \tag{2.32}$$

with $x \in \mathbb{R}^{n_x}$ the system states, $u \in \mathbb{R}^{n_u}$ the input and $F(x) \in \mathbb{R}^{n_x \times n_x}$ a matrix such that $[F(x)]_{i,j} = f_{i,j}(x)$ where $f_{i,j}(x)$, for $i, j = 1, \ldots, n_x$ are nonlinear functions of x. We assume that $F(x)$ can be written as

$$F(x) = \sum_{i=1}^{p} \upsilon_i(x) M_i \tag{2.33}$$

where M_i are called vertices and $\upsilon(x) = \text{col}\{\upsilon_1(x), \ldots, \upsilon_p(x)\}$ is such that $\upsilon(x) \geq 0$ belongs to a unity simplex (i.e., $\upsilon(x) \in \Upsilon_p$). This assumption seems restrictive but writing $F(x)$ as in (2.33) is possible for a large class of systems. To this purpose we consider a sector nonlinearity approach as in (TANAKA; WANG, 2001) to write the nonlinearities as a convex sum of known vertices weighted by nonlinear functions that belong to an unit simplex.

For example, given a nonlinear function $f(x)$ with $x \in \mathbb{R}^{n_x}$, we desire to write it as $f(x) = (a_1\upsilon_1(x) + a_2\upsilon_2(x))$, with $\upsilon(x) \in \Upsilon_p$ where $\upsilon(x) = \text{col}\{\upsilon_1(x), \upsilon_2(x)\}$. The main idea is to find a sector such that $a_1 x \leq f(x)x \leq a_2 x$. As pointed in (TANAKA; WANG, 2001) and (OHTAKE *et al.*, 2003), it may not be possible to achieve a sector globally, but it is possible for some bounded regions $\|x\| \leq \bar{x}$. This assumption is not restrictive for control purposes, since in real systems applications, signals are commonly bounded.

Following the steps of (OHTAKE *et al.*, 2003), assuming that $f(x)$ is bounded such that $f^{\min} \leq f(x) \leq f^{\max}$, which allows to write

$$f(x) = \upsilon_1(x) f^{\min} + \upsilon_2(x) f^{\max}. \tag{2.34}$$

Imposing that $\upsilon_1(x) + \upsilon_2(x) = 1$, we can determine that

$$\upsilon_1(x) = \frac{f^{\max} - f(x)}{f^{\max} - f^{\min}}, \quad \upsilon_2(x) = 1 - \upsilon_1(x) = \frac{f(x) - f^{\min}}{f^{\max} - f^{\min}}. \tag{2.35}$$

where $\upsilon_1(x), \upsilon_2(x) \geq 0$. As an example, consider the nonlinearity $f(x) = \frac{\sin(x)}{x}$. The function $f(x)$ has a maximum $f^{\max} = 1$ and a minimum $f^{\min} \approx -0.2172$. Therefore

$f(x) = \upsilon_1(x)(-0.2172) + \upsilon_2(x)(1)$ with $\upsilon_1(x) = (1 - \sin(x)/x)/1.21723$ and $\upsilon_2(x) = 1 - \upsilon_1(x)$.

For matrix functions, such as $F(x)$, the same methodology can be applied, considering each element of $F(x)$. Consider that

$$F(x) = \begin{bmatrix} f_{1,1}(x) & f_{1,2}(x) & \dots & f_{1,n_x}(x) \\ f_{2,1}(x) & f_{2,2}(x) & \dots & f_{2,n_x}(x) \\ \vdots & \vdots & \ddots & \vdots \\ f_{n_x,1}(x) & f_{n_x,2}(x) & \dots & f_{n_x,n_x}(x) \end{bmatrix} \tag{2.36}$$

and $f_{i,j}(x)$ are bounded such that, $f_{i,j}^{\min} \leq f_{i,j}(x) \leq f_{i,j}^{\max}$, for $i, j = 1, \dots, n_x$. To simplify, let us considered the case where $n_x = 2$ and

$$F(x) = \begin{bmatrix} 1 & f_{1,2}(x) \\ f_{2,1}(x) & 1 \end{bmatrix} \begin{bmatrix} x_1 \\ x_2 \end{bmatrix}. \tag{2.37}$$

From the sector nonlinearity approach we can write $f_{1,2}(x) = \upsilon_1^1(x) f_{1,2}^{\min} + \upsilon_2^1(x) f_{1,2}^{\max}$ and $f_{2,1}(x) = \upsilon_1^2(x) f_{2,1}^{\min} + \upsilon_2^2(x) f_{2,1}^{\max}$. Hence $F(x)$ in (2.37) can be rewritten as

$$F(x) = \begin{bmatrix} 1 & \upsilon_1^1(x) f_{1,2}^{\min} + \upsilon_2^1(x) f_{1,2}^{\max} \\ \upsilon_1^2(x) f_{2,1}^{\min} + \upsilon_2^2(x) f_{2,1}^{\max} & 1 \end{bmatrix} \tag{2.38}$$

with vectors $\upsilon^1(x), \upsilon^2(x) \in \Upsilon_2$. From (2.38) we can rewrite it as

$$\begin{aligned} F(x) = \upsilon_1^1(x) & \begin{bmatrix} 1 & f_{1,2}^{\min} \\ \upsilon_1^2(x) f_{2,1}^{\min} + \upsilon_2^2(x) f_{2,1}^{\max} & 1 \end{bmatrix} \\ + \upsilon_2^1(x) & \begin{bmatrix} 1 & f_{1,2}^{\max} \\ \upsilon_1^2(x) f_{2,1}^{\min} + \upsilon_2^2(x) f_{2,1}^{\max} & 1 \end{bmatrix} \end{aligned} \tag{2.39}$$

Repeating the same process we get

$$F(x) = \hat{\upsilon}_1(x) M_1 + \hat{\upsilon}_2(x) M_2 + \hat{\upsilon}_3(x) M_3 + \hat{\upsilon}_4(x) M_4 \tag{2.40}$$

with

$$\begin{aligned} &\hat{\upsilon}_1(x) = \upsilon_1^1(x)\upsilon_1^2(x), \quad \hat{\upsilon}_2(x) = \upsilon_1^1(x)\upsilon_2^2(x), \\ &\hat{\upsilon}_3(x) = \upsilon_2^1(x)\upsilon_1^2(x), \quad \hat{\upsilon}_4(x) = \upsilon_2^1(x)\upsilon_2^2(x), \\ &M_1 = \begin{bmatrix} 1 & f_{1,2}^{\min} \\ f_{2,1}^{\min} & 1 \end{bmatrix}, \quad M_2 = \begin{bmatrix} 1 & f_{1,2}^{\min} \\ f_{2,1}^{\max} & 1 \end{bmatrix}, \\ &M_3 = \begin{bmatrix} 1 & f_{1,2}^{\max} \\ f_{2,1}^{\min} & 1 \end{bmatrix}, \quad M_4 = \begin{bmatrix} 1 & f_{1,2}^{\max} \\ f_{2,1}^{\max} & 1 \end{bmatrix}. \end{aligned} \tag{2.41}$$

2.6 System with time delays

Throughout this thesis, in addition to event triggered control we consider also phenomenona as transmission delays. To design controller under ETC along with time delays we use a Lyapunov-based approach (FRIDMAN, 2014; LIU *et al.*, 2019; GU; NICULESCU, 2003). The classical way to handle this problem is the Lyapunov–Krasovskii approach, which is used not only for time delay systems but for sampled data systems, networked connected systems and event triggered controller (FRIDMAN, 2014). The main idea is to use so called Lyapunov–Krasovskii functional (LKF) to evaluate stability conditions. In this section we present some classical lemmas related to LKF and also focus on the time derivative of the functionals.

Lemma 2.5 (Jensen's inequality (GU *et al.*, 2003))**.** *For a given matrix $R \succ 0$ of appropriate dimension, and for a continuous function $\phi \in [a,b] \to \mathbb{R}^n$, the following inequality holds:*

$$\int_a^b \dot{\phi}(s)^T R \dot{\phi}(s) ds \geq \frac{1}{b-a} \psi(\phi)^T R \psi(\phi) \tag{2.42}$$

with $\psi(\phi) = \int_a^b \dot{\phi}(s) ds$.

Lemma 2.6 (Delay-dependent reciprocally convex inequality (SEURET; GOUAISBAUT, 2018))**.** *Consider two matrices of appropriate dimensions $R_1 \succ 0$ and $R_2 \succ 0$. If there are symmetric matrices X_1, X_2, and matrices Y_1, Y_2 such that*

$$\begin{bmatrix} R_1 & 0 \\ 0 & R_2 \end{bmatrix} - \alpha \begin{bmatrix} X_1 & Y_1 \\ Y_1^T & 0 \end{bmatrix} - (1-\alpha) \begin{bmatrix} 0 & Y_2 \\ Y_2^T & X_2 \end{bmatrix} \succeq 0 \tag{2.43}$$

holds for $\alpha = 0$ and $\alpha = 1$, then the following inequality holds for all $\alpha \in (0,1)$:

$$\begin{bmatrix} \frac{1}{\alpha} R_1 & 0 \\ 0 & \frac{1}{1-\alpha} R_2 \end{bmatrix} \succeq \begin{bmatrix} R_1 & 0 \\ 0 & R_2 \end{bmatrix} + (1-\alpha) \begin{bmatrix} X_1 & Y_2 \\ Y_2^T & 0 \end{bmatrix} + \alpha \begin{bmatrix} 0 & Y_1 \\ Y_1^T & X_2 \end{bmatrix}. \tag{2.44}$$

Lemma 2.7. *Leibniz Integral Rule (PROTTER; MORREY, 1985)*

$$\frac{d}{dt}\left(\int_{a(t)}^{b(t)} f(t,s) ds \right) = f(t,b(t)) \frac{d}{dt} b(t) - f(t,a(t)) \frac{d}{dt} a(t) + \int_{a(t)}^{b(t)} \frac{\partial}{\partial t} f(t,s) ds \tag{2.45}$$

For Chapter 4 the following functionals are used for the proofs of the main Theorems in Section 4.5.

$$V_S = \int_{t-\tau_1}^{t-\tau_2} \mathrm{e}^{2\alpha(s-t)} x^T(s) S x(s) ds \tag{2.46}$$

$$V_R = (\tau_1 - \tau_2) \int_{-\tau_1}^{-\tau_2} \int_{t+\theta}^{t} \mathrm{e}^{2\alpha(s-t)} \dot{x}^T(s) R \dot{x}(s) ds d\theta \tag{2.47}$$

The time derivative of those functionals are important for the proofs and will be discussed in this Section. For this purpose we introduce the following lemmas.

Lemma 2.8. *Let V_S be defined as in* (2.46)*. Its time derivative is given by*

$$\dot{V}_S = -2\alpha V_s + \mathrm{e}^{-2\alpha\tau_2} x^T(t-\tau_2) S x(t-\tau_2) - \mathrm{e}^{-2\alpha\tau_1} x^T(t-\tau_1) S x(t-\tau_1) \tag{2.48}$$

Proof. To prove, let $a(t) = t - \tau_1$ and $b(t) = t - \tau_2$ and $f(s,t) = e^{2\alpha(s-t)} x^T(s) S x(s) ds$, then

$$\frac{d}{dt} a(t) = \frac{d}{dt} b(t) = 1, \tag{2.49}$$

$$\frac{\partial}{\partial t} f(t,s) = \frac{\partial}{\partial t}(e^{2\alpha(s-t)}) x^T(s) S x(s) = -2\alpha \underbrace{\mathrm{e}^{2\alpha(s-t)} x^T(s) S x(s)}_{f(t,s)}. \tag{2.50}$$

Thus, from Lemma 2.7, we have that

$$\begin{aligned}
\dot{V}_s &= f(t, t-\tau_2) - f(t, t-\tau_1) + \int_{t-\tau_1}^{t-\tau_2} -2\alpha f(t,s) ds \\
&= e^{2\alpha(-\tau_2)} x^T(t-\tau_2) S x(t-\tau_2) - e^{2\alpha(-\tau_1)} x^T(t-\tau_1) S x(t-\tau_1) - 2\alpha \underbrace{\int_{t-\tau_1}^{t-\tau_2} f(t,s) d_s}_{V_s} \\
&= e^{-2\alpha\tau_2} x^T(t-\tau_2) S x(t-\tau_2) - e^{-2\alpha\tau_1} x^T(t-\tau_1) S x(t-\tau_1) - 2\alpha V_s
\end{aligned} \tag{2.51}$$

concluding the proof. □

Lemma 2.9. *Let V_R be defined as in* (2.47) *with $\tau_1 > \tau_2$. The time derivative of V_R is upper bounded such that*

$$\dot{V}_R \leq -2\alpha V_R + (\tau_1 - \tau_2)^2 \dot{x}^T(t) R \dot{x}(t) - (\tau_1 - \tau_2) \inf_{s\in[\tau_2,\tau_1]} \left\{ e^{-2\alpha s} \right\} \int_{t-\tau_1}^{t-\tau_2} \dot{x}^T(s) R \dot{x}(s) ds \tag{2.52}$$

Proof. To prove, let

$$v_R = \int_{t+\theta}^{t} e^{2\alpha(s-t)} \dot{x}^T(s) R \dot{x}(s) ds, \tag{2.53}$$

Invoking Lemma 2.7, the partial derivative of (2.53) with respect to t is

$$\begin{aligned}
\frac{\partial}{\partial t} v_R &= \frac{\partial}{\partial t} \int_{t+\theta}^{t} e^{2\alpha(s-t)} \dot{x}^T(s) R \dot{x}(s) ds \\
&= -2\alpha v_R + \dot{x}^T(t) R \dot{x}(t) - e^{2\alpha\theta} \dot{x}^T(t+\theta) R \dot{x}(t+\theta)
\end{aligned} \tag{2.54}$$

From the definition of (2.53) we can write $V_R = (\tau_1 - \tau_2) \int_{-\tau_1}^{-\tau_2} v_R(t,\theta) d\theta$. Therefore From Lemma 2.7 and (2.54) we have that

$$\begin{aligned}
\frac{\dot{V}_R}{\tau_1 - \tau_2} &= \int_{-\tau_1}^{-\tau_2} \frac{\partial}{\partial t} v_R(t,\theta) d\theta \\
&= -2\alpha \int_{-\tau_1}^{-\tau_2} v_R d\theta + \int_{-\tau_1}^{-\tau_2} \dot{x}^T(t) R \dot{x}(t) d\theta - \int_{-\tau_1}^{-\tau_2} e^{2\alpha\theta} \dot{x}^T(t+\theta) R \dot{x}(t+\theta) d\theta \\
&= -2\alpha \frac{V_R}{\tau_1 - \tau_2} + (\tau_1 - \tau_2) \dot{x}^T(t) R \dot{x}(t) - \int_{-\tau_1}^{-\tau_2} e^{2\alpha\theta} \dot{x}^T(t+\theta) R \dot{x}(t+\theta) d\theta \\
&\leq -2\alpha \frac{V_R}{\tau_1 - \tau_2} + (\tau_1 - \tau_2) \dot{x}^T(t) R \dot{x}(t) - \inf_{s\in[\tau_2,\tau_1]} \left\{ e^{-2\alpha s} \right\} \int_{-\tau_1}^{-\tau_2} \dot{x}^T(t+\theta) R \dot{x}(t+\theta) d\theta
\end{aligned}$$

$$= -2\alpha\frac{V_R}{\tau_1-\tau_2} + (\tau_1-\tau_2)\dot{x}^T(t)R\dot{x}(t) - \inf_{s\in[\tau_2,\tau_1]}\left\{e^{-2\alpha s}\right\}\int_{t-\tau_1}^{t-\tau_2}\dot{x}^T(s)R\dot{x}(s)ds \tag{2.55}$$

where, for the last line, we substitute $t+\theta = s$. Multiplying (2.55) by $\tau_1-\tau_2$ yields (2.52), concluding the proof. □

In this thesis the conditions are mainly written as an optimization subject to linear matrix inequalities constraints. A summary of LMI tools are presented in next section.

2.7 Linear matrix inequality

Linear matrix inequalities (LMI) is an important and powerful tool utilized in control area for stability analysis and control design. A large class of control problems can be written as an optimization problem subject to LMI constraints. To illustrate this tool we will present the design of controllers for a class of nonlinear system described by sector nonlinearity approach discussed in Section 2.5. Consider the affine in the control system

$$\dot{x} = F(x)x + Bu \tag{2.56}$$

let $u = K(x)x$ be its control input. Therefore the closed loop system is

$$\dot{x} = (F(x) + BK(x))x. \tag{2.57}$$

Choosing a quadratic Lyapunov function candidate $V = x^TPx$ with $P \succ 0$, taking its time derivative yields the condition

$$x^T\Big((F(x)+BK(x))^TP + P(F(x)+BK(x))\Big)x \leq 0 \tag{2.58}$$

and a sufficient condition of stability is given by the matrix inequality

$$(F(x)+BK(x))^TP + P(F(x)+BK(x)) \prec 0. \tag{2.59}$$

Notice that condition (2.59) need to be satisfied for all x. To achieve a finite number of conditions the sector nonlinear approach described in Section 2.5 can come at hand. Therefore we rewrite $F(x)$ with functions $\upsilon_i(x)$ belonging to a unity simplex and we define $K(x)$ using the same functions $\upsilon_i(x)$

$$F(x) = \sum_{i=1}^{p}\upsilon_i(x)M_i, \quad K(x) = \sum_{i=1}^{p}\upsilon_i(x)K_i \tag{2.60}$$

where F_i are known matrices and K_i to be designed. Therefore, we can recast (2.59) as

$$\sum_{i=1}^{p}\upsilon_i(x)\left((M_i+BK_i)^TPx + P(M_i+BK_i)\right) \prec 0 \tag{2.61}$$

From the convexity of $\upsilon(x)$ it follows that matrix inequalities defined at each vertex of the polytope

$$(M_i + BK_i)^T P + P(M_i + BK_i) \prec 0, \quad \text{for } i = 1, \ldots, p \tag{2.62}$$

are sufficient to ensure (2.61). If matrices K_i are given a priori (2.62) provides a set of finite LMI conditions to evaluate the stability of (2.57). More commonly, K_i are matrices to be found, and are part of the optimization problem. To render LMIs from (2.62) we multiply on the left and on the right by P^{-1} which results in

$$P^{-1}M_i^T + P^{-1}K_i^T B^T + M_i P^{-1} + BK_i P^{-1} \prec 0 \tag{2.63}$$

since it is assumed that $P \succ 0$ its inverse exist and it does not changes fact that the condition is negative definite. Performing the change of variables $K_i P^{-1} = Y_i$ and $P^{-1} = W$ in (2.63) results in

$$WM_i^T + Y_i^T B^T + M_i W + BY_i \prec 0, \quad \text{for } i = 1, \ldots, p \tag{2.64}$$

which are linear matrix inequalities in W and M_i. Moreover, as long as the solution is feasible, K_i and P can always be recovered.

Linear matrix inequalities can also be helpful for time delay system via the Lyapunov–Krasovskii approach discussed in Section 2.6. To illustrate we are considering the case of stability analysis of a linear time delay system with constant and bounded time delay τ.

$$\dot{x} = A_1 x + A_0 x(t - \tau). \tag{2.65}$$

The quadratic Lyapunov–Krasovskii functional is chosen as:

$$V = x^T P x + \int_{t-\tau}^{t} x^T(s) S x(s) ds \tag{2.66}$$

from Lemma (2.8) its derivative is

$$\dot{V} = 2x^T(t) P \left(A_1 x + A_0 x(t - \tau)\right) + x^T(t) S x(t) - x^T(t - \tau) S x(t - \tau) \tag{2.67}$$

which can be recast as the LMI constraint in P and S

$$\begin{bmatrix} x(t) & x(t-\tau) \end{bmatrix} \begin{bmatrix} A_1^T P + P A_1 + S & P A_0 \\ * & -S \end{bmatrix} \begin{bmatrix} x(t) \\ x(t-\tau) \end{bmatrix} \leq 0 \tag{2.68}$$

Furthermore, as discussed in 2.4, the $\mathcal{L}_2$-stability from conditions from Lemma 2.4 can be written in terms of Linear matrix inequalities which will be frequently used in this work. For a simple illustration, consider a linear system

$$\begin{aligned} \dot{x} &= Ax + Bu + Dw \\ y &= Cx \end{aligned} \tag{2.69}$$

where x are the system states, u is the control input, y is the system output and w is an exogenous input for which we aim to evaluate $\mathcal{L}_2$ stability. Let $u = Kx$ be the control law. Hence, the closed loop system is

$$\begin{aligned} \dot{x} &= (A + BK)x + Dw \\ y &= Cx \end{aligned} \tag{2.70}$$

Choosing a quadratic Lyapunov function $V(x) = x^T P^{-1} x$ with $P^{-1} \succ 0$, from Lemmma 2.4 condition (2.27), we have

$$\dot{V} = \Big((A + BK)x + Dw\Big)^T P^{-1} x + x^T P^{-1} \Big((A + BK)x + Dw\Big) \leq \gamma^2 w^T w - y^T y. \tag{2.71}$$

Substituting $y = Cx$ and rearranging the terms results in

$$\Big((A + BK)x + Dw\Big)^T P^{-1} x + x^T P^{-1} \Big((A + BK)x + Dw\Big) - \gamma^2 w^T w + x^T C C x \leq 0 \tag{2.72}$$

which can be written as

$$\begin{bmatrix} x^T & w^T \end{bmatrix} \begin{bmatrix} (A + BK)^T P^{-1} + P^{-1}(A + BK) + C^T C & P^{-1} D \\ * & -\gamma^2 I \end{bmatrix} \begin{bmatrix} x \\ w \end{bmatrix} \leq 0, \tag{2.73}$$

resulting in the matrix inequality

$$\begin{bmatrix} (A + BK)^T P^{-1} + P^{-1}(A + BK) + C^T C & P^{-1} D \\ * & -\gamma^2 I \end{bmatrix} \prec 0 \tag{2.74}$$

As previously discussed in the example with the sector nonlinear approach, the matrix inequality (2.74) is not a linear matrix inequality. In an attempt to render an LMI we multiply (2.74) on the left and on the right by $\mathrm{diag}(P, I)$, resulting in

$$\begin{bmatrix} P(A + BK)^T + (A + BK)P + PC^T CP & D \\ * & -\gamma^2 I \end{bmatrix} \prec 0. \tag{2.75}$$

Performing a change of variables $KP = Y$ we have

$$\begin{bmatrix} PA^T + Y^T B^T + AP + BY + PC^T CP & D \\ * & -\gamma^2 I \end{bmatrix} \prec 0. \tag{2.76}$$

However, (2.76) is not a LMI due to the term $PC^T CP$. This condition, as many control and observation problems, cannot be directly written as LMI constraints, however some technical lemmas can be used to recast these problems as LMI constraints. The two most useful lemmas are the Schur's complement and the Finsler's Lemma that are recalled thereafter.

Lemma 2.10 (Schur's complement (BOYD *et al.*, 1994))**.** *Let $\mathcal{M}$ be a block matrix such that*

$$\mathcal{M} = \begin{bmatrix} A & B \\ B^T & C \end{bmatrix} \tag{2.77}$$

the following conditions are equivalent

- $\mathcal{M} \succ 0$
- $A \succ 0$ *and* $C - B^T A^{-1} B \succ 0$,
- $C \succ 0$ *and* $A - BC^{-1}B^T \succ 0$.

For example, turning back $\mathcal{L}_2$ stability problem, condition (2.76) can be written as

$$\begin{bmatrix} PA^T + Y^T B^T + AP + BY & D \\ * & -\gamma^2 I \end{bmatrix} - \begin{bmatrix} PC^T \\ 0 \end{bmatrix} \begin{bmatrix} -I \end{bmatrix} \begin{bmatrix} CP & 0 \end{bmatrix} \prec 0. \tag{2.78}$$

Hence, from Schur's complement, it can be recast as the LMI constraint

$$\begin{bmatrix} PA^T + Y^T B^T + AP + BY + PC^T CP & D & PC^T \\ * & -\gamma^2 I & 0 \\ * & * & -I \end{bmatrix} \prec 0. \tag{2.79}$$

.

Lemma 2.11 (Finsler's lemma (OLIVEIRA; SKELTON, 2001))**.** *Let $\phi \in \mathbb{R}^n$, $\mathcal{M} \in \mathbb{R}^{n \times n}$ and $\mathcal{B} \in \mathbb{R}^{m \times n}$, such that $\mathcal{B}\psi = 0$. Then, the following conditions are equivalent:*

- $\psi^T \mathcal{M} \psi < 0$, *for all* $\phi \neq 0$.
- $\exists \mathcal{X} \in \mathbb{R}^{n \times m}$ *such that* $\mathcal{M} + \mathcal{X}\mathcal{B} + \mathcal{B}^T \mathcal{X}^T \prec 0$.

All the optimization problems used in this thesis are solved with Matlab R2023a, with parser YALMIP R20190425 along with the solver Mosek 10.0.20.

2.8 Conclusion

This chapter has given an overview of the main topics addressed in our work. The issues related to platooning considering communication between them, have been described. Especially, it is important, not only to ensure individual vehicle stability but also to ensure the so-called string stability; in order to avoid inappropriate behaviors. When communication occurs, we consider it as event triggered, thus the need for some extra mathematical tools and properties arealso described. Finally more technical aspects were also presented, concerning the polytopic description of nonlinear models, time delay systems stability, especially the Lyapunov-Krasovskii functional, and finally the optimization tools useful to derive stability/stabilization conditions. Next chapter will start with classical ACC without communication and we demonstrate how to derive individual and string stability conditions for a platoon.

3 Cooperative ACC with continuous communication

3.1 Introduction

In this chapter, we address the control problem of longitudinal cooperative Adaptive Cruise Control (ACC) with continuous communication between vehicles. The platoon formation consists of N vehicles and a leader. The objective is for the N vehicles to follow the leader while maintaining a safe distance between them. At the beginning of this chapter, we explain the platoon problem of interest, the respective distance policy that will be used to ensure a safe distance and present the vehicle longitudinal model. As discussed in the previous chapter, Section 2.2, in practice, vehicle parameters are not precisely known, leading to uncertainties in the model. Due to these uncertainties, the classical feedback linearization approach cannot be applied directly. To compensate for these uncertainties, we propose a disturbance observer to estimate the lumped effect caused by the uncertainties and possible exogenous inputs. Then, the feedback linearization approach is combined with disturbance-based compensation to ensure a linear and homogeneous dynamic. After linearization, we study the individual and string stability of the platoon. To this end, a model describing the interaction between two vehicles, vehicle $i-1$ and vehicle i (immediately behind) is presented. From this modeling, the control law and the signal that will be transmitted from one vehicle to another are defined. Considering this model, to evaluate individual and string stability, we propose an extension to the $\mathcal{L}_2$ norm stability conditions, accounting for the effects of the disturbance compensation. By introducing a filter commonly used for cooperative ACC with non-constant distance policies, an alternative model for the interaction between vehicles is derived, and design conditions for this model are presented. Finally, simulations are performed to evaluate the effectiveness of the disturbance compensation and the platoon performance considering each model of vehicle interaction.

3.2 Platooning control framework

In this chapter we consider a platoon with a leader and N follower vehicles where each vehicle is denoted by Σ_i, with $i = 0, \ldots, N$, where index $i = 0$ is reserved for the leader. The objective is to maintain a safe distance, defined by a distance policy, between vehicle Σ_i and Σ_{i-1}. Consider the platoon shown in Fig 3.1, vehicle Σ_i measures $\hat{p}_i = p_{i-1} - p_i$ and $\Delta v_i = v_{i-1} - v_i$, which are the relative distance and relative velocity between Σ_i and Σ_{i-1}. Vehicle Σ_i receives information only from Σ_{i-1} which will be used by Σ_i to calculate

its control law. This information can consist of internal states or even control inputs of Σ_{i-1} according to the modeling of interest and will be specified in subsequent sections. In the adopted predecessor-follower (PF) communication topology, vehicle Σ_i can only receive information from Σ_{i-1}, which implies that only Σ_1 receives information from the leader Σ_0.

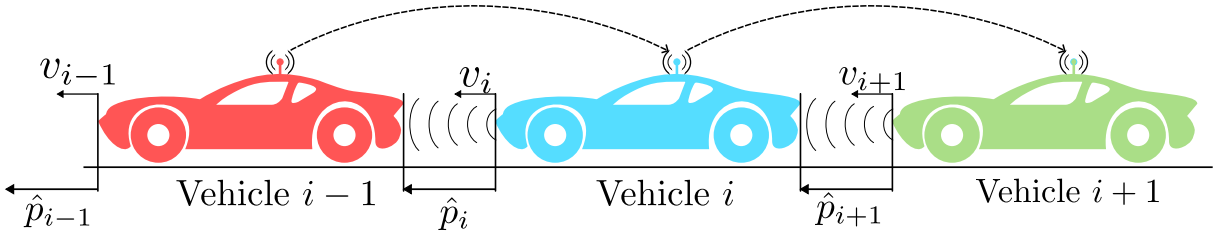

Figure 3.1 – Vehicle platooning PF topology where Σ_i receives information from Σ_{i-1} and transmit to Σ_{i+1}. Vehicle i measures, the relative distance distance $\hat{p}_i = p_{i-1} - p_i - L_{c,i}$ and the velocity difference $\Delta v_i = v_{i-1} - v_i$.

3.2.1 Vehicle Dynamics and Distance Policy

For each vehicle in the platooning system, we consider the following dynamics (TOULOTTE *et al.*, 2008; RAJAMANI, 2012):

$$\dot{p}_i = v_i \tag{3.1a}$$

$$\dot{v}_i = \frac{1}{\boldsymbol{W}_i}\left(\boldsymbol{R}_{h,i}T_i - \boldsymbol{m}_i \mathbf{g} F_{r,i} - \boldsymbol{B}_i v_i - \boldsymbol{C}_i v_i^2\right) \tag{3.1b}$$

$$\dot{T}_i = -\frac{1}{\rho_i}T_i + \frac{1}{\rho_i}u_{e,i} \tag{3.1c}$$

with

$$\boldsymbol{W}_i = \frac{(\boldsymbol{m}_i \boldsymbol{h}_{w,i}^2 + \boldsymbol{J}_{r,i} + \boldsymbol{J}_{f,i})\boldsymbol{R}_{g,i}^2 + \boldsymbol{J}_{e,i}}{\boldsymbol{h}_{w,i}^2 \boldsymbol{R}_{g,i}^2} \tag{3.2}$$

$$\boldsymbol{R}_{h,i} = (\boldsymbol{h}_{w,i}\,\boldsymbol{R}_{g,i})^{-1}. \tag{3.3}$$

where p_i is the vehicle position, v_i is the vehicle velocity, T_i is the engine torque, and $u_{e,i}$ is the input torque (computed torque). $F_{r,i}$ is the rolling resistance coefficient and is dependent on the conditions of the road and the tires, which can vary over time. As $F_{r,i}$ is not known in real time, we consider it as an exogenous input of the system.

The vehicle parameters are explained in Table 3.1, where the subscript i is used to indicate that these values can change among vehicles. We assume that the real values of these parameters are not precisely known. The available values are only approximations, estimated values, or values provided by the manufacturer. In addition, some of those parameter values can change according to the circumstances. For example, the mass ($\boldsymbol{m}_i$)

Table 3.1 – Vehicle model parameters.

Parameters	Description
$\boldsymbol{m}_i$	Mass of the vehicle (kg)
$\boldsymbol{R}_{g,i}$	Gear ratio (–)
$\boldsymbol{h}_{w,i}$	Height of center of wheel (m)
$\boldsymbol{J}_{e,i}$	Engine/transmission inertia (kg·m^2)
$\boldsymbol{J}_{r,i}$	Rear wheel inertia (kg·m^2)
$\mathbf{g}$	Gravitational acceleration (m/s^2)
$\boldsymbol{J}_{f,i}$	Front wheel inertia (kg·m^2)
$\boldsymbol{B}_i$, $\boldsymbol{C}_i$	Resistance force coefficients (kg/s, kg/(m·s))
ρ_i	Time constant of the longitudinal dynamics (s)

can change according to the load transported and the friction changes according to the ground conditions.

Throughout this work, we propose a feedback linearization approach to handle the nonlinearities of the system. To write (3.1) in a feedback linearizable form, let us denote $\dot{v}_i = a_i$, then the acceleration dynamics can be derived from (3.1b) as

$$\dot{a}_i = \frac{1}{\boldsymbol{W}_i}\left(\boldsymbol{R}_{h,i}\dot{T}_i - (\boldsymbol{B}_i + 2\boldsymbol{C}_i v_i)a_i\right) \tag{3.4}$$

From (3.1b), we can write

$$T_i = \frac{1}{\boldsymbol{R}_{h,i}}\left(\boldsymbol{W}_i\dot{v}_i + \boldsymbol{m}_i\mathbf{g}F_{r,i} + \boldsymbol{B}_i v_i + \boldsymbol{C}_i v_i^2\right). \tag{3.5}$$

Substituting (3.5) in (3.1c) and then in (3.4), we obtain

$$\dot{p}_i = v_i \tag{3.6a}$$

$$\dot{v}_i = a_i \tag{3.6b}$$

$$\dot{a}_i = f_i(v_i, a_i) + b_i u_{e,i} - c_i F_{r,i} \tag{3.6c}$$

with

$$\begin{aligned} f_i(v_i, a_i) &= -\left(\frac{1}{\rho_i} + \frac{1}{\boldsymbol{W}_i}\boldsymbol{C}_i v_i\right)a_i - \frac{1}{\boldsymbol{W}_i\rho_i}\left(\boldsymbol{B}_i + \boldsymbol{C}_i v_i\right)(v_i + \rho_i a_i), \\ b_i &= \frac{\boldsymbol{R}_{h,i}}{\boldsymbol{W}_i\rho_i}, \qquad c_i = \frac{\boldsymbol{m}_i g}{\boldsymbol{W}_i\rho_i}, \end{aligned} \tag{3.7}$$

Hence, expression (3.6) is in the feedback linearizing form allowing system nonlinearites to be canceled by an appropriate control law.

The main objective of the platoon is to ensure a safe distance. We define safe distance in terms of the distance policy

$$\Delta p_{d,i} = r_i + h v_i \tag{3.8}$$

where r_i is the standstill distance for each vehicle, and the time gap h is constant and identical for all vehicles of the platoon. This distance policy is referred in the literature

as constant-time headway (CTH), where the safe distance increases proportionally to the vehicle velocity. The case where $h = 0$, is referred to as constant disturbance (CD) and is normally applied to vehicles moving at slow velocities. From the distance policy (3.8), the distance policy error (or tracking error) is defined as

$$\Delta p_i = p_{i-1} - p_i - L_{c,i} - \Delta p_{d,i}. \tag{3.9}$$

where $L_{c,i}$ is the length of the car. The distance error (3.9) is the difference between the vehicles inter distance (accounting for the vehicle length) and the distance policy. Vehicles move in a platoon formation at a safe distance when the distance police is close to zero ($\Delta p_i \approx 0$).

3.3 Control problem formulation

In this section we present the feedback linearizing strategy with a DOB-based uncertainty compensation technique.

3.3.1 DOB-Based Uncertainty Compensation

As discussed in Section 3.1, the vehicle parameters are not precisely known, resulting in an uncertainty associated to the parameters in (3.1). It results that the nonlinearies cannot be perfectly canceled. To account for the uncertainties we group their influence, along with the unmeasured exogenous input, we define nominal values $f_i(v_i, a_i)$ and b_i, and real (possibly time varying) $f_{i,r}(v_i, a_i) = f_i(v_i, a_i) + \Delta f_i$ and $b_{i,r} = b_i + \Delta b_i$. Hence we can write the system (3.6c) as

$$\dot{a}_i = f_i(v_i, a_i) + b_i u_{e,i} - d_i \tag{3.10}$$

where

$$d_i = \Delta f_i + \Delta b_i u_{e,i} + c_i F_{r,i} \tag{3.11}$$

is a *virtual* disturbance, that combines effects caused by parametric uncertainties, given by $\Delta f_i + \Delta b_i u_{e,i}$ and exogenous input $c_i F_{r,i}$.

From expression (3.10), we propose the following disturbance observer;

$$\begin{aligned} \dot{\omega}_i &= \frac{\partial L_i(a_i)}{\partial a_i}(f_i(v_i, a_i) + b_i u_{e,i} - \hat{d}_i) \\ \hat{d}_i &= \omega_i - L_i(a_i) \end{aligned} \tag{3.12}$$

where ω_i is the internal state of the disturbance observer, $L_i(a_i)$ is the observer nonlinear gain, and $\hat{d}_i$ is the estimated disturbance. To assess the convergence of disturbance estimation, let us define $e_{d,i} = \hat{d}_i - d_i$ as the disturbance estimation error, then from (3.10) and (3.12) we can write the estimation error dynamics as

$$\dot{e}_{d,i} = -\frac{\partial L_i(a_i)}{\partial a_i} e_{d,i} - \dot{d}_i. \tag{3.13}$$

The gain $L_i(a_i)$ is designed such that (3.13) is stable. A straightforward choice is to make $L_i(a_i) = L_i a_i$ with $L_i > 0$ a positive constant. In this case we have $\dot{e}_{d,i} = -L_i e_{d,i} - \dot{d}_i$, and, assuming that $\|\dot{d}_i\| \leq \bar{\delta}_i$, its solution satisfies;

$$\|e_{d,i}\| \leq \mathrm{e}^{-L_i t}\|e_{d,i}(0)\| + \frac{1}{L_i}(\mathrm{e}^{-L_i t} - 1)\bar{\delta}_i. \tag{3.14}$$

Hence, the error converges exponentially to a bounded region defined by $\bar{\delta}_i$. Moreover, for slow-varying disturbances (that is, $\bar{\delta}_i \approx 0$), we have $e_{d,i} \to 0$.

Using the estimated disturbance (3.12), we propose the following linearizing control law for system (3.6):

$$u_{e,i} = \underbrace{\frac{1}{b_i}\left(-\frac{1}{\rho_d}a_i - f_i(v_i, a_i) + \frac{1}{\rho_d}u_i\right)}_{\text{linearization}} + \underbrace{\frac{1}{b_i}\hat{d}_i}_{\text{Compensation}} \tag{3.15}$$

where u_i is the control input and ρ_d is a desired platoon time constant, which is specified considering an estimation of the real time constant of the vehicle longitudinal dynamics. In Figure 3.2 we illustrate the feedback linearizing control loop along with the DOB.

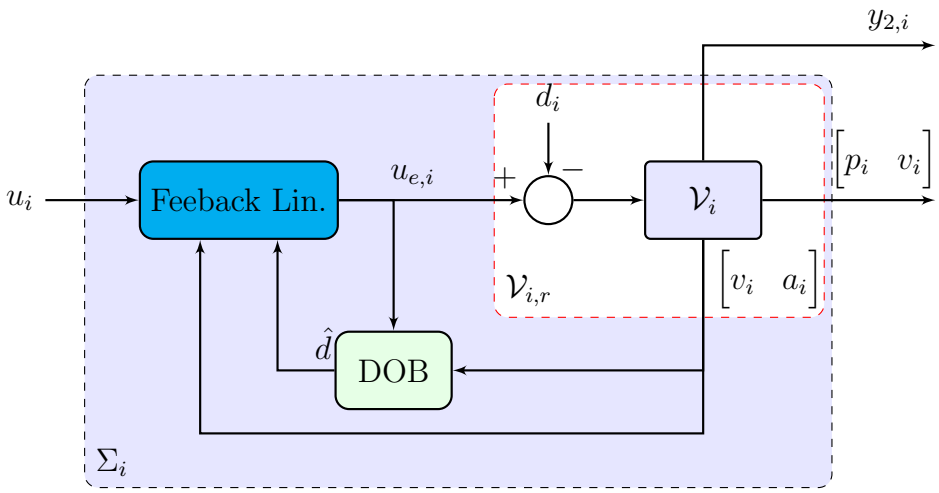

Figure 3.2 – Feeback linearization loop with DOB compensation. $\mathcal{V}_i$ Stand for the nominal dynamical system and d_i is the *virtual* disturbance defined in (3.11).

Applying the control law (3.15) to (3.10) we obtain the linearized dynamics:

$$\begin{cases} \dot{p}_i = v_i \\ \dot{v}_i = a_i \\ \dot{a}_i = -\dfrac{1}{\rho_d}a_i + \dfrac{1}{\rho_d}u_i + e_{d,i} \end{cases} \tag{3.16}$$

Equation (3.16) for $e_{d,i} = 0$ (no disturbance) or with $e_{d,i} = d_i$ (no compensation) represents respectively the common linear dynamics for ACC and CACC.

Generally, the heterogeneity of the platoon is characterized according to ρ_d. There are two cases: ρ_d is constant (homogeneous), ρ_d varies according to the vehicles (heterogeneous, $\rho_{d,i}$). In the second case, if $\rho_{d,i}$ variation is small we can define $\rho_{d,i} = \rho_d + \delta_i^\rho$ and include δ_i^ρ into the disturbances. We bring to attention that this approach is only valid when δ_i^ρ is small enough.

From (3.16), considering the distance policy error (3.9) and defining the velocity error as $\Delta v_i = v_{i-1} - v_i$ we obtain the following dynamics:

$$\Sigma_i : \begin{cases} \Delta\dot{p}_i = \Delta v_i - h a_i \\ \Delta\dot{v}_i = a_{i-1} - a_i \\ \dot{a}_i = -\dfrac{1}{\rho_d} a_i + \dfrac{1}{\rho_d} u_i + e_{d,i} \end{cases} \tag{3.17}$$

for $i = 1, \ldots, N$ and for the leader vehicle, since the leader does not have a reference vehicle to follow, we have

$$\Sigma_0 : \begin{cases} \dot{v}_0 = a_0 \\ \dot{a}_0 = -\dfrac{1}{\rho_d} a_0 + \dfrac{1}{\rho_d} u_0 + e_{d,0} \end{cases} \tag{3.18}$$

Although the leader dynamics is known, its input behavior is considered unknown.

In CACC systems, the control input u_i of system (3.17) is composed of a feedback component $u_{\text{fb},i}(t)$ and a feedforward component $u_{\text{ff},i}(t)$, defined as:

$$u_i(t) = u_{\text{fb},i}(t) + u_{\text{ff},i}(t) \tag{3.19}$$

The feedback component is computed using the signal measured by vehicle Σ_i, while the feedforward component uses information received from Σ_{i-1} as shown in Figure 3.3. We further denote each component as

$$u_{\text{fb},i}(t) = K_1 y_{1,i} \quad u_{\text{ff},i}(t) = K_2 y_{2,i-1} \tag{3.20}$$

where $y_{1,i}$ and $y_{2,i-1}$ are, respectively, the measured signals and information received by Σ_i. To deal with event triggered control, goal of the next chapter, we consider two approaches to model the interaction between vehicles. One called Interconnected and the other one called Overlapping. Their interest is related to the LMI constraints writing in Chapter 4.

3.3.2 Interconnected system

As illustrated in Figure 3.3 the information transmitted only goes from Σ_{i-1} to Σ_i, we define an interconnected system denoted $\Sigma_{i,i-1}$ that represents vehicle Σ_i accounting from the information coming from Σ_{i-1}. Notice that from, system (3.17), we can write for Σ_{i-1}

$$\dot{a}_{i-1} = -\frac{1}{\rho_d} a_{i-1} + \frac{1}{\rho_d} u_{i-1} + e_{d,i-1}. \tag{3.21}$$

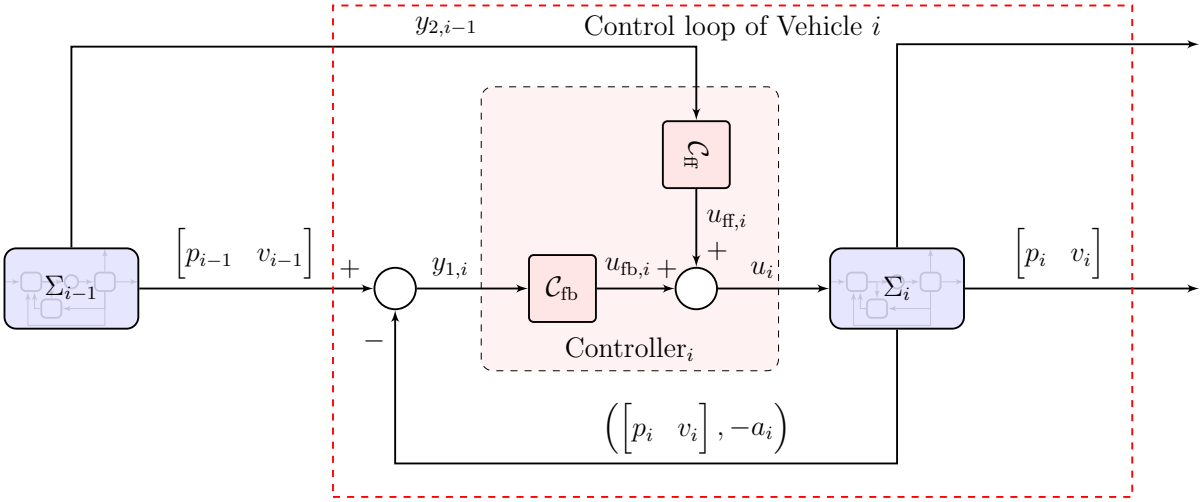

Figure 3.3 – Vehicle communication and control loop. $\mathcal{C}_{\text{fb}}$ and $\mathcal{C}_{\text{ff}}$ stand, respectively, for the feedback and feedforward control law components.

Due to a_{i-1} affecting Σ_i we combine (3.17) with (3.21) to write

$$\Sigma_{i,i-1}: \begin{cases} \dot{x}_i = Ax_i + Bu_i + Du_{i-1} + Ew_{d,i} \\ y_{1,i} = C_1 x_i \\ y_{2,i-1} = C_2 x_i \end{cases} \tag{3.22}$$

with $x_i = \text{col}\{\Delta p_i,\ \Delta v_i,\ a_i,\ a_{i-1}\}$, $w_i = \text{col}\{e_{d,i}, e_{d,i-1}\}$ and matrices

$$A = \begin{bmatrix} 0 & 1 & 0 & 0 \\ 0 & 0 & -1 & 0 \\ 0 & 0 & -\frac{1}{\rho_d} & 0 \\ 0 & 0 & 0 & -\frac{1}{\rho_d} \end{bmatrix} \quad B = \begin{bmatrix} 0 \\ 0 \\ \frac{1}{\rho_d} \\ 0 \end{bmatrix} \quad D = \begin{bmatrix} 0 \\ 0 \\ 0 \\ \frac{1}{\rho_d} \end{bmatrix} \quad E = \begin{bmatrix} 0 & 0 \\ 0 & 0 \\ 1 & 0 \\ 0 & 1 \end{bmatrix} \quad C_1 = \begin{bmatrix} 1 & 0 & 0 & 0 \\ 0 & 1 & 0 & 0 \\ 0 & 0 & 1 & 0 \end{bmatrix}$$
$$C_2 = \begin{bmatrix} 0 & 0 & 0 & 1 \end{bmatrix} \tag{3.23}$$

The output $y_{1,i}$ corresponds to the states measured by Σ_i, while $y_{2,i-1}$ is received from Σ_{i-1} via communication. Model (3.22) comprises the connection between vehicles Σ_i and Σ_{i-1}. It remains to properly define the performance inputs and outputs to evaluate the string stability of the system. First we set the performance output as the control input of Σ_i

$$z_i = u_i \tag{3.24}$$

Hence, for string stability analysis we are going to evaluate the input-output stability between the input u_{i-1} and the output $z_i = u_i$.

Assuming that the communication is sufficiently fast, such that we can approximate the transmission as continuous, $y_{2,i-1}$ is available in real time allowing us to define the control law of system (3.22) as

$$u_i = Kx_i = \underbrace{K_1 y_{1,i}}_{u_{\text{fb},i}} + \underbrace{K_2 y_{2,i-1}}_{u_{\text{ff},i}} \tag{3.25}$$

where $u_{\text{fb},i}$ and $u_{\text{ff},i}$ are, respectively, the feedback and feedforward component of u_i. Notice that we can write $u_i = Kx_i$ since $x_i = \text{col}\{y_{1,i}, y_{2,i-1}\}$. Applying (3.25) to (3.22) and considering the performance output (3.24) we have

$$\Sigma_{i,i-1} : \begin{cases} \dot{x}_i = (A + BK)x_i + Du_{i-1} + Ew_{d,i} \\ z_i = Kx_i \end{cases} \tag{3.26}$$

Thus, for continuous communication, the structure of the system individual vehicle stability can be achieved using any appropriate technique (pole placement, LQR, H_∞ etc.). For $w_{d,i} = 0$ the condition are the same as in (DOLK *et al.*, 2017; PLOEG *et al.*, 2014) and string stability analysis is straightforward. However, the results cannot be extended directly when $w_{d,i} \neq 0$. Based on the $\mathcal{L}_p$ string stability condition

$$\|z_i\|_{\mathcal{L}_2} \leq \gamma_0 \|u_0\|_{\mathcal{L}_2} + \rho(\|\bar{x}(0)\|), \quad i = 1, \ldots, N. \tag{3.27}$$

from Definition 2.1 in Section 2 we propose the following proposition to account for disturbances or estimation error in the platoon string stability analysis

Proposition 3.1. Consider the system $\Sigma_{i,i-1}$ in (3.26). Assume that there exists an upper bound $w_{\max} > 0$ such that $\|w_{d,i}\|_{\mathcal{L}_2} \leq w_{\max}$, for all $i = 0, \ldots, N$. If there exists finite positive scalars $\gamma \leq 1$ and β, such that

$$\|z_i\|_{\mathcal{L}_2} \leq \gamma \|z_{i-1}\|_{\mathcal{L}_2} + \beta \|w_{d,i}\|_{\mathcal{L}_2} \tag{3.28}$$

for all $i = 1, \ldots, N$, with $z_0 = u_0$. Then,

$$\|z_i\|_{\mathcal{L}_2} \leq \|u_0\|_{\mathcal{L}_2} + i\beta w_{\max} \tag{3.29}$$

holds for, all $i = 1, \ldots, N$.

Proof. By recursivity of expression (3.28) starting with $i = 1$, it follows that

$$\|z_i\|_{\mathcal{L}_2} \leq \gamma^i \|z_0\|_{\mathcal{L}_2} + \beta \sum_{j=1}^{i} \gamma^{i-j} \|w_{d,j}\|_{\mathcal{L}_2}. \tag{3.30}$$

Since $\|w_{d,i}\|_{\mathcal{L}_2} \leq w_{\max}$, for $i = 1, \ldots, N$ and $\gamma \leq 1$ it follows that $\gamma^i \leq 1$ and

$$\sum_{j=1}^{i} \gamma^{i-j} \|w_{d,j}\|_{\mathcal{L}_2} \leq \sum_{j=1}^{i} \|w_{d,j}\|_{\mathcal{L}_2} \leq i w_{\max} \tag{3.31}$$

Then, condition (3.30) implies (3.29) for $z_0 = u_0$. This completes the proof. □

Proposition 3.1 can be seen as an extension of the $\mathcal{L}_2$ string stability defined in (PLOEG *et al.*, 2014; FENG *et al.*, 2019) including the effects of disturbances. The condition depends on $w_{d,i} = \text{col}\{e_{d,i}, e_{d,i-1}\}$ and its upper bound. Hence, effective DOB compensation

can reduce the effects of $w_{d,i}$ enabling platoon formations with more vehicles without compromising safety.

Moreover, there is a clear connection between condition (3.28) and the $\mathcal{L}_2$-gain stability conditions (KHALIL, 2002). Hence we can ensure string stability via $\mathcal{L}_2$ stability analysis of system (3.26). The following theorem proposes design conditions to ensure that condition (3.28) in Proposition 3.1 holds for system (3.26)

Theorem 3.1. *Consider the interconnected system $\Sigma_{i,i-1}$ in* (3.26)*. If there exist positive scalars β, $\gamma \leq 1$, a matrix L, and a symmetric matrix $P \succ 0$, of appropriate dimensions, such that the following optimization problem is feasible:*

$$\min \beta \tag{3.32}$$

such that

$$\begin{bmatrix} \mathrm{He}\{AP + BL\} + \alpha P & D & E & L^T \\ * & -\gamma^2 I & 0 & 0 \\ * & * & -\beta^2 I & 0 \\ * & * & * & -I \end{bmatrix} \prec 0 \tag{3.33}$$

Then, the closed-loop system (3.26)*, is $\mathcal{L}_2$ stable and condition* (3.28) *in Proposition 3.1 holds under the control law* (3.25) *with the control gains $K = LP^{-1}$.*

Proof. The proof is straightforward from the proof of $\mathcal{L}_2$ gain condition in Section 2. □

The conditions from Theorem 3.1 provides a controller that satisfies the conditions from Proposition 3.1. However, the optimization will prove one solution from a set of possible ones. Without additional information to limit the set of solution, the controller performance might be inefficient. For this reason we provide some guidelines for the controller design introducing additional information achieved via the error dynamics analysis.

3.3.3 Interconnected model control gain guidelines

Based on Proposition 3.1 we can design the controller gain K in (3.25) such that condition (3.28) holds for the closed loop system (3.26). Although both K_1 and K_2 can be set as unrestricted variables, we can also impose some restrictions on K_2 or even set its value a priori.

Consider the distance policy error Δp_i defined in (3.9). Taking its time derivative twice yields

$$\Delta p_i^{(2)} = a_{i-1} - a_i - \frac{h}{\rho_d}(-a_i + u_i) - h e_{d,i}. \tag{3.34}$$

Substituting the control law u_i (3.25) in (3.34) we have

$$\Delta p_i^{(2)} = \underbrace{-a_i - \frac{h}{\rho_d}(-a_i + K_1 y_{1,i})}_{\text{feedback}} + \underbrace{a_{i-1} - \frac{h}{\rho_d} K_2 y_{2,i-1}}_{\text{feedforward}} - h e_{d,i}. \tag{3.35}$$

Since $y_{2,i-1} = a_{i-1}$ the effects of a_{i-1} in (3.35) can be canceled choosing K_2 such that

$$K_2 \frac{h}{\rho_d} = 1. \tag{3.36}$$

Hence K_2 can be set a priori to minimize the influence of a_{i-1} in the distance policy error dynamics. The main drawback is that the feedback contribution in (3.35) does not directly connect to the distance policy error or its derivative, which will become more evident in the overlapping approach explained in the next section.

Imposing a value to K_2, choosing $P = \text{diag}(P_1,\ P_2)$ and taking advantage that $K_1 C_1 P = K_1 P_1 C_1$. The following Corollary provides design conditions for a predefined K_2.

Corollary 3.1. *Consider the interconnected system $\Sigma_{i,i-1}$ in (3.26). If for a given K_2, there exist positive scalars β, $\gamma \leq 1$, a matrix L_1, symmetric matrix $P = \text{diag}(P_1, P_2) \succ 0$, of appropriate dimensions such that the following optimization problem is feasible:*

$$\min \beta \tag{3.37}$$

such that

$$\begin{bmatrix} \text{He}\left\{(A + BK_2C_2)P + BL_1C_1\right\} + \alpha P & D & E & (K_2C_2P + L_1C_1)^T \\ * & -\gamma^2 I & 0 & 0 \\ * & * & -\beta^2 I & 0 \\ * & * & * & -I \end{bmatrix} \prec 0 \tag{3.38}$$

Then, the closed-loop system (3.26), is $\mathcal{L}_2$ stable and condition (3.28) in Proposition 3.1 holds under the control law (3.25) with the control gain K_2 and $K_1 = L_1 P_1^{-1}$.

Perfect canceling only occurs for continuous communication and in the absence of delays. Therefore, instead of using Corollary 3.1 with K_2 fixed according to equality (3.36), we can use the conditions from Theorem 3.1 including a norm-bounded constraint in the optimization problem such as:

$$\|K_2^* - K_2\| \leq \bar{\kappa} \tag{3.39}$$

where $K_2^* = \frac{\rho_d}{h}$ is the ideal given feedforward control gain from (3.36).

3.3.4 Overlapping model

The error dynamics analysis in the previous section allows to set K_2 a priori but not K_1. In this section we show that, introducing a filter and augmenting the dynamics we can model the vehicles interaction such that both K_2 and K_1 can be designed a priori. To differentiate it from the interconnected model $\Sigma_{i,i-1}$ we denote it as Overlapping model.

Before defining the interaction between vehicles for this approach we introduce the filter

$$h\dot{u}_i + u_i = \xi_i. \tag{3.40}$$

where ξ_i is the new control input to be designed. Filtering is a common approach in CACC systems with a CTH distance policy and is used for pre-compensation of distance policy (DOLK *et al.*, 2017; PLOEG *et al.*, 2011; PLOEG *et al.*, 2014). We will turn back to its interest in Section 3.3.5. Thus, we introduce u_i as a new state variable and from model (3.17) and filter (3.40), we have from Σ_{i-1}

$$\begin{aligned}\dot{a}_{i-1} &= -\frac{1}{\rho_d}a_{i-1} + \frac{1}{\rho_d}u_{i-1} + e_{d,i-1}.\\ \dot{u}_{i-1} &= -\frac{1}{h}u_i + \frac{1}{h}\xi_i\end{aligned} \tag{3.41}$$

Combining (3.17) with (3.41) and (3.40) we write

$$\Xi_{i,i-1}: \begin{cases}\dot{\bar{x}}_i = \bar{A}\bar{x}_i + \bar{B}\xi_i + D\xi_{i-1} + \bar{E}w_{d,i}\\ \bar{y}_{1,i} = \bar{C}_1\bar{x}_i\\ \bar{y}_{2,i-1} = \bar{C}_2\bar{x}_i\end{cases} \tag{3.42}$$

with $\bar{x}_i = \text{col}\{\Delta p_i,\ \Delta v_i,\ a_i,\ u_i,\ a_{i-1},\ u_{i-1}\}$, $w_{d,i} = \text{col}\{e_{d,i}, e_{d,i-1}\}$ and matrices

$$\bar{A} = \begin{bmatrix}0 & 1 & 0 & 0 & 0 & 0\\ 0 & 0 & -1 & 0 & 0 & 0\\ 0 & 0 & -\frac{1}{\rho_d} & \frac{1}{\rho_d} & 0 & 0\\ 0 & 0 & 0 & -\frac{1}{h} & 0 & 0\\ 0 & 0 & 0 & 0 & -\frac{1}{\rho_d} & 0\\ 0 & 0 & 0 & 0 & 0 & -\frac{1}{h}\end{bmatrix}, \bar{B} = \begin{bmatrix}0\\0\\0\\\frac{1}{h}\\0\\0\end{bmatrix}, \bar{D} = \begin{bmatrix}0\\0\\0\\0\\0\\\frac{1}{h}\end{bmatrix}, \bar{E} = \begin{bmatrix}0 & 0\\0 & 0\\1 & 0\\0 & 0\\0 & 1\\0 & 0\end{bmatrix},$$

$$\bar{C}_1 = \begin{bmatrix}1 & 0 & 0 & 0 & 0 & 0\\ 0 & 1 & 0 & 0 & 0 & 0\\ 0 & 0 & 1 & 0 & 0 & 0\\ 0 & 0 & 0 & 1 & 0 & 0\end{bmatrix}, \bar{C}_2 = \begin{bmatrix}0 & 0 & 0 & 0 & 1 & 0\\ 0 & 0 & 0 & 0 & 0 & 1\end{bmatrix} \tag{3.43}$$

The output $\bar{y}_{1,i}$ is the states measured by Σ_i including the filter state u_i. Meanwhile $\bar{y}_{2,i-1} = [a_{i-1},\ u_{i-1}]$ is the information sent to Σ_i by Σ_{i-1} via communication. We now define the performance output as

$$\bar{z}_i = \xi_i \tag{3.44}$$

which allows to assess the interaction between vehicles Σ_i and Σ_{i-1} via the input-output stability ξ_{i-1} to ξ_i. Similarly to the interconnected problem, for a sufficiently fast communication, control law of system (3.42) is decomposed with a feedback part (K_1) and a feedforward part (K_2):

$$\xi_i = \bar{K}\bar{x}_i = \underbrace{\bar{K}_1\bar{y}_{1,i}}_{\xi_{\text{fb},i}} + \underbrace{\bar{K}_2\bar{y}_{2,i-1}}_{\xi_{\text{ff},i}}, \tag{3.45}$$

with

$$\bar{K}_1 = \begin{bmatrix}\bar{K}_{11} & \bar{K}_{12} & \bar{K}_{13} & \bar{K}_{14}\end{bmatrix} \quad \bar{K}_2 = \begin{bmatrix}\bar{K}_{12} & \bar{K}_{22}\end{bmatrix} \tag{3.46}$$

and the closed-loop overlapping system can be written as

$$\Xi_{i,i-1}: \begin{cases} \dot{\bar{x}}_i = (\bar{A} + \bar{B}\bar{K})\bar{x}_i + D\xi_{i-1} + \bar{E}w_{d,i} \\ \bar{z}_i = \bar{K}\bar{x}_i \end{cases} \tag{3.47}$$

For the overlapping model individual and string stability analyses can be evaluated based on Proposition 3.1. However, special attention is necessary regarding the interaction between Σ_1 and Σ_0 (leader). The leader control input u_0 is not a design parameter, hence we cannot introduce the filter in the control law. To handle this we assume that there exists ξ_0, such that $h\dot{u}_0 = u_0 + \xi_0$, which is not a strong assumption since, as long as u_0 is continuously differentiable, ξ_0 can always be found. We can now include the interaction between Σ_1 and Σ_0 in the $\Xi_{i,i-1}$ system and stability can be evaluated based on Proposition 3.1 without further modifications.

The controller gain $\bar{K}$ can be designed based optimization problem similar to the interconnected system that is not described here but is straightforward from Theorem 3.1. Also similar to the interconnected case we provide some guidelines for the controller design introducing additional information achieved via the error dynamics analysis.

3.3.5 Overlapping model control gain guidelines

As in Section 3.3.3 we can also attain some insights on the design of $\bar{K}_1$ and $\bar{K}_2$ studying the system error dynamics. Differentiating (3.34), and organizing the terms we have

$$\begin{aligned} \Delta p_i^{(3)} &= \frac{1}{\rho_d}(-a_{i-1} + u_{i-1}) + he_{d,i-1} - \frac{1}{\rho_d}(-a_i + u_i) + he_{d,i} \\ &\quad - \frac{h}{\rho_d}\left(-\frac{1}{\rho_d}(-a_i + u_i) + he_{d,i} + \dot{u}_i\right) + h\dot{e}_{d,i} \\ &= \underbrace{-\frac{1}{\rho_d}\left(a_{i-1} - a_i - \frac{h}{\rho_d}(-a_i + u_i) - he_{d,i}\right)}_{\Delta p_i^{(2)}} \\ &\quad - \frac{1}{\rho_d}(\underbrace{h\dot{u}_i + u_i}_{\xi_i} - u_{i-1}) + e_{d,i-1} - e_{d,i} - h\dot{e}_{d,i}. \end{aligned} \tag{3.48}$$

Looking at (3.48) it is clear the filter (3.40) and we can write

$$\Delta p_i^{(3)} = -\frac{1}{\rho_d}\Delta p_i^{(2)} - \frac{1}{\rho_d}(\xi_i + u_{i-1}) + e_{d,i-1} - e_{d,i} - h\dot{e}_{d,i}. \tag{3.49}$$

Furthermore, substituting the control law (3.45) in the last line of (3.49) yields

$$\Delta p_i^{(3)} = -\frac{1}{\rho_d}(\Delta p_i^{(2)} - \bar{K}_1\bar{y}_{1,i}) + \frac{1}{\rho_d}(u_{i-1} - \bar{K}_2\bar{y}_{2,i-1}) + e_{d,i-1} - e_{d,i} - h\dot{e}_{d,i}. \tag{3.50}$$

Equivalently to the interconnected case, it is straightforward to cancel the effect of u_{i-1} by choosing $\bar{K}_2 = [0\ 1]$. Nevertheless, the second degree of freedom can be used to

propose other appropriate choices. Notice that from the linearized dynamic (3.16)

$$\dot{a}_{i-1} = -\frac{1}{\rho_d}a_{i-1} + \frac{1}{\rho_d}u_{i-1} + e_{d,i-1}. \tag{3.51}$$

Hence in steady state, $a_{i-1} \to u_{i-1} + \rho_d e_{d,i}$. Therefore, the feedforward component in (3.45) converges to

$$\bar{K}_2\bar{y}_{2,i-1} = (\bar{K}_{21} + \bar{K}_{22})u_{i-1} + \bar{K}_{21}\rho_d e_{d,i-1}. \tag{3.52}$$

Choosing $\bar{K}_{21}$ and $\bar{K}_{22}$ such that $\bar{K}_{21} + \bar{K}_{22} = 1$, and substituting (3.52) in (3.50) gives

$$\Delta p_i^{(3)} = -\frac{1}{\rho_d}(\Delta p_i^{(2)} - \bar{K}_1\bar{y}_{1,i}) + \frac{1}{\rho_d}\cancelto{0}{(u_{i-1} - u_{i-1})} + \left(e_{d,i-1} - \bar{K}_{21}e_{d,i-1}\right) - e_{d,i} - h\dot{e}_{d,i} \tag{3.53}$$

Therefore, it is possible to compensate for the effects of both u_{i-1} and $e_{d,i-1}$ in steady state.

Remark 3.1. Considering the system (3.47) with control law (3.45), the feedforward control gain $\bar{K}_2 = [\bar{K}_{21}\ \bar{K}_{22}]$ can be chosen such that $\bar{K}_{21} + \bar{K}_{22} = 1$, to compensate for u_{i-1} and $e_{d,i-1}$ in the distance policy error dynamics (3.50).

Due to the lower triangular structure of (3.49) the control gain $\bar{K}_1$ can also be easily designed by imposing some structure to $\bar{K}_1$ assuming that $e_{d,i} = 0$. From (PLOEG *et al.*, 2011) we have the following remark:

Remark 3.2. Considering the system (3.47) with control law (3.45), for every $K_p, K_d > 0$ and $K_d > K_p\rho_d$, choosing $\bar{K}_1 = \begin{bmatrix} K_p & K_d & -hK_d & 0 \end{bmatrix}$ ensure individual vehicle stability and, consequently, stability of $\Xi_{i,i-1}$.

To demonstrate we set the structure for $\bar{K}_1$ as $\bar{K}_1 = \begin{bmatrix} K_p & K_d & -hK_d & 0 \end{bmatrix}$ which produces the feedback control component

$$\bar{K}_1\bar{y}_{1,i} = K_p\Delta p_i^{(0)} + K_d\Delta p_i^{(1)} = K_p\Delta p_i + K_d\Delta v_i - K_d h a_i \tag{3.54}$$

For simplicity, consider that the feedforward component u_{i-1} is perfectly canceled, moreover we assume that $e_{d,i} = 0$. From (3.51), filter (3.40) and introducing u_i as a new state we can write the augmented closed loop dynamics as

$$\begin{bmatrix} \Delta p_i^{(1)} \\ \Delta p_i^{(2)} \\ \Delta p_i^{(3)} \\ \dot{u}_i \end{bmatrix} = \left[\begin{array}{ccc|c} 0 & 1 & 0 & 0 \\ 0 & 0 & 1 & 0 \\ -\frac{K_p}{\rho_d} & -\frac{K_d}{\rho_d} & -\frac{1}{\rho_d} & 0 \\ \hline \frac{K_p}{h} & \frac{K_d}{h} & 0 & -\frac{1}{h} \end{array}\right] \begin{bmatrix} \Delta p_i^{(0)} \\ \Delta p_i^{(1)} \\ \Delta p_i^{(2)} \\ u_i \end{bmatrix} + \begin{bmatrix} 0 \\ 0 \\ 0 \\ \frac{1}{h} \end{bmatrix} u_{\text{ff},i} \tag{3.55}$$

In view of the lower triangular structure, applying the Routh-Hurwitz stability criterion, we can conclude that (3.55) can be stabilized for $h > 0$, choosing $K_p, K_d > 0$ and $K_d > K_p\rho_d$. Those conditions ensure individual vehicular stability and the study of string stability in the frequency domain is done in (PLOEG *et al.*, 2011; PLOEG *et al.*, 2014).

Imposing the above structures to $\bar{K}_1$ and $\bar{K}_2$, simplifies the design conditions. However, translating those constraints into an optimization problem with LMI constraints necessitates bounds that may result in conservative conditions. The design proposed is a two-step procedure where $\bar{K}_1$ and $\bar{K}_2$ are designed a priori based on Remarks 3.2 and 3.1, and we evaluate the $\mathcal{L}_2$ string stability conditions to verify whether the conditions hold in the presence of disturbances or for noncontinuous communication with communication delays, as will be discussed in Chapter 4.

In comparison to the interconnected model, the overlapping model introduces a filter to compensate for the effects of the constant time headway distance policy. Moreover, as individual stability can be ensured directly from Remark 3.2 and Remark 3.1, the controller is designed in a two-step approach, where in the first step the, gains are designed according to Remark 3.2 and Remark 3.1, and string stability is evaluated using Theorem 3.1. Unlike the interconnect system, the constraints in the individual stability analysis difficult the designing conditions in an one-step approach.

The two systems, interconnected and overlapping, also differ in terms of convergence rate and maximum distance policy error, as will be shown in the next section.

3.4 Examples

This section presents illustrative results and comparative studies to show the effectiveness of the proposed DOB and controller design conditions. We present how different choices of DOB gains and control gains can influence the distance policy error. Moreover, we also illustrate the effectiveness of the design conditions based on the interconnected system $\Sigma_{i,i-1}$ and the overlapping system $\Xi_{i,i-1}$ and, how different choices of feedforward control can affect the system dynamics.

Remark 3.3. Whenever a $\tilde{a}$ appears in a variable, it represents the values used for the simulation that may differ from the nominal values used to design the control.

3.4.1 Test 1. Performance evaluation of the DOB

In this section we show the interest of adding the DOB compensation, presented in Figure 3.3. We consider two vehicles the leader Σ_0 and one follower Σ_1. Table 3.2 gives the parameters of each vehicle. In rows Σ_0 and Σ_1 are the values used to calculate the feedback linearizing control law. In rows $\tilde{\Sigma}_0$ and $\tilde{\Sigma}_1$ are the values used for the simulation. The rolling resistance coefficient F_r is considered constant for all vehicles, i.e., $F_r = 0.015$ (sec/kg). However, it is assumed to be unknown.

The desired distance policy $\Delta p_{d,1} = r_1 + hv_1$ is set with $r_1 = 2$ (m) and $h = 0.6$ (sec), the platoon time constant is $\rho_d = 0.1$. For the DOB (3.12) we use a linear observer gain

Table 3.2 – Nominal values of the vehicle parameters (Σ_i columns) and respective values used for simulation ($\tilde{\Sigma}_i$).

Vehicle	r	$\boldsymbol{m}$	$\boldsymbol{h}_w$	$\boldsymbol{J}_r$	$\boldsymbol{J}_e$	$\boldsymbol{R}_g$	$\boldsymbol{B}$	$\boldsymbol{C}$	ρ
Σ_0		1724	0.28	0.75	0.14	0.10	7.35	0.05	0.05
$\tilde{\Sigma}_0$		1724	0.25	1.05	0.14	0.13	8.09	0.06	0.08
Σ_1	2.5	2241	0.63	0.97	0.35	0.18	13.96	0.11	0.10
$\tilde{\Sigma}_1$		2017	0.51	0.68	0.46	0.18	11.17	0.16	0.09

$L(a_1) = L_1 a_1$ with $L_1 = 50$. We choose the gains as

$$\bar{K}_1 = \begin{bmatrix} 0.2 & 0.7 & -0.42 & 0 \end{bmatrix} \quad \bar{K}_2 = \begin{bmatrix} 0 & 1 \end{bmatrix} \tag{3.56}$$

according to Remark 3.2 and 3.1. The speed profile is defined for the trials with three parts: Acceleration, constant speed and braking, Figure 3.4 left. In the nominal case, i.e. without uncertainties, the velocity of Σ_0 and Σ_1, the distance policy error Δp, are shown Figure 3.4. As expected the distance policy error is very small, less than 4×10^{-3} (m).

The second trial considers the uncertainties in Table 3.2, i.e. the rows $\tilde{\Sigma}_0$ and $\tilde{\Sigma}_1$. Figure 3.5 (top) gives the results without DOB and presents an error up to 4 (m); Figure 3.5 (middle) the results with DOB and the error up to 0.02 (m) that shows the importance of estimating the *virtual* disturbance. The bottom left part of Figure 3.5 shows the linear control input u_1 (3.45) in both cases (blue without DOB and red with DOB). At last, bottom right shows the estimation of the disturbance $\hat{d}_0$ and $\hat{d}_1$.

The next section presents results in simulation for platooning with disturbances and uncertainties.

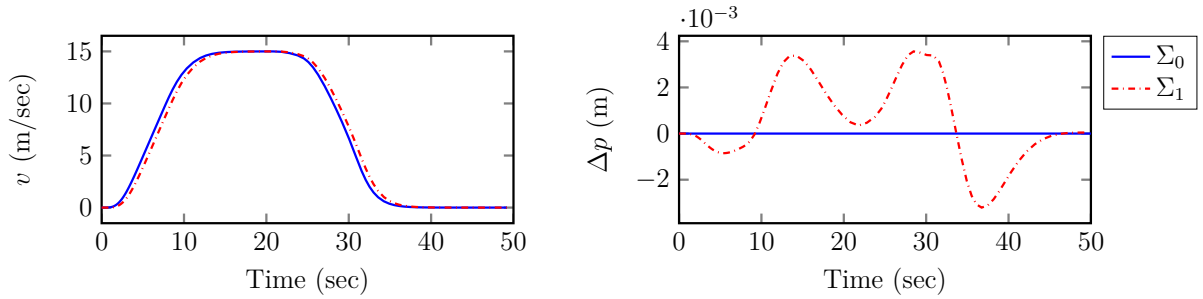

Figure 3.4 – Test 1. Velocity (left) and distance policy error (right), of Σ_0 and Σ_1 for the nominal case.

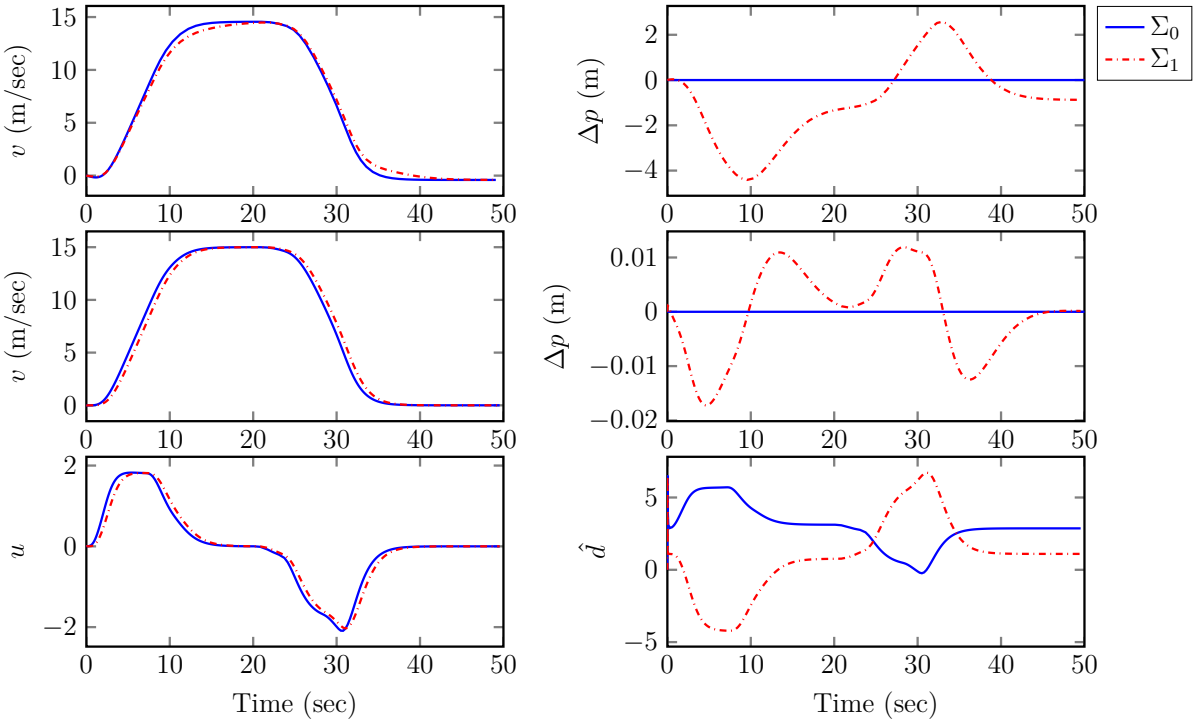

Figure 3.5 – Test 1. Velocity, distance policy error vehicles without DOB compensation (top) , with DOB compensation (middle) and respective control input (bottom left) and disturbance estimation (bottom right) of Σ_0 and Σ_1.

3.4.2 Test 2. Platooning

In these tests, we consider platoon setups with one leader (Σ_0) and four to ten followers (Σ_1 to Σ_{10}). In order to define different platoon formations we define a base of parameters denoted Σ_j^b for $j = 0, \ldots, 5$ whose parameters are described in Table 3.3. The rows Σ_0^b to Σ_4^b are the base values used to calculate the feedback linearizing control law, whereas rows $\tilde{\Sigma}_0^b$ to $\tilde{\Sigma}_4^b$ are the values used for the simulation.

We consider N followers and we define an ordered set of $N+1$ indexes, $\mathbb{J}$, with values belonging to the set $\{0, \ldots, 4\}$. The platoon is defined with vehicles

$$\Sigma_i = \Sigma_{\mathbb{J}(i)}^b. \tag{3.57}$$

For example, with $N = 4$ and $\mathbb{J} = \{0, 3, 4, 1, 0\}$ the platooning is defined with the vehicles having the parameters

$$\left\{\Sigma_0, \quad \Sigma_1, \quad \Sigma_2, \quad \Sigma_3, \quad \Sigma_4\right\} = \left\{\Sigma_0^b, \quad \Sigma_3^b, \quad \Sigma_4^b, \quad \Sigma_1^b, \quad \Sigma_0^b\right\} \tag{3.58}$$

Similar to Test 1 the following parameters are chosen: the rolling resistance coefficient F_r is constant for all vehicles, i.e., $F_r = 0.015$ (sec/kg), $h = 0.6$ (1/sec) and the platoon time constant is $\rho_d = 0.1$. The DOB is designed in the same way as in Test 1 with $L_i = L = 50$ for all Σ_i with $i \in \{0, 1, \ldots, N\}$. The speed profile is the same as for Test 1 with three portions: Acceleration, constant speed and braking.

Table 3.3 – Nominal base values for the vehicle parameters (Σ_i^b columns) and respective values used for simulation ($\tilde{\Sigma}_i^b$).

Vehicle	r	$\boldsymbol{m}$	$\boldsymbol{h}_w$	$\boldsymbol{J}_r$	$\boldsymbol{J}_e$	$\boldsymbol{R}_g$	$\boldsymbol{B}$	$\boldsymbol{C}$	ρ
Σ_0^b		1724	0.28	0.75	0.14	0.10	7.35	0.05	0.05
$\tilde{\Sigma}_0^b$		1724	0.25	1.05	0.14	0.13	8.09	0.06	0.08
Σ_1^b	2.5	2241	0.63	0.97	0.35	0.18	13.96	0.11	0.10
$\tilde{\Sigma}_1^b$		2017	0.51	0.68	0.46	0.18	11.17	0.16	0.09
Σ_2^b	2.5	2930	0.41	1.57	0.27	0.20	11.02	0.08	0.08
$\tilde{\Sigma}_2^b$		2637	0.33	1.26	0.40	0.30	8.82	0.05	0.06
Σ_3^b	2.5	3620	0.63	0.82	0.27	0.11	13.96	0.11	0.12
$\tilde{\Sigma}_3^b$		3258	0.89	1.15	0.40	0.08	15.36	0.16	0.12
Σ_4^b	2.5	3965	0.52	1.72	0.24	0.11	8.09	0.06	0.08
$\tilde{\Sigma}_4^b$		5947	0.63	2.41	0.29	0.14	11.32	0.08	0.11

We will investigate the two approaches to model the interaction between vehicles. We recall that their interest will be explicit in Chapter 4.

3.4.2.1 Test 2.1 - Interconnected system

Consider a platoon with one leader and $N = 6$ followers we define the platoon as $\Sigma_i = \Sigma^b_{\mathbb{J}(i)}$ with set $\mathbb{J} = \{0, 4, 1, 3, 2, 4, 1\}$. This platoon is voluntarily set with Σ_0 the lighter vehicle followed by the heaviest one Σ_4, with Σ_4 repeated at the penultimate position. The controller is designed according to Corollary 3.1 with $K_2 = \frac{\tau_d}{h} = 0.1667$. Solving the optimization problem (3.37) with $\alpha = 0.001$ we obtain

$$P = \begin{bmatrix} 1.5797 & -0.3920 & -0.0398 & 0 \\ -0.3920 & 2.0983 & -0.1904 & 0 \\ -0.0398 & -0.1904 & 0.0211 & 0 \\ 0 & 0 & 0 & 0.1001 \end{bmatrix}, \quad \begin{array}{l} \beta = 10.0108, \\ K_1 = \begin{bmatrix} 0.4620 & 1.5488 & -0.1760 \end{bmatrix} \end{array} \tag{3.59}$$

Figure 3.6 gives the velocity (top left) and distance policy error (top right) for each vehicle and shows that the vehicles are able to follow the velocity profile with a distance policy error up to 0.2 (m). The bottom part of Figure 3.6 shows the control input (bottom left) and estimated disturbance $\hat{d}$ (bottom right) of each vehicle. The values of $\hat{d}(t)$ are larger for vehicles Σ_1 and Σ_5 since their base values are both Σ^b_4, which presents larger mass and uncertainty m.

Comparing the maximum values of distance policy error in Test 1 (up to 0.02) and Test 2.1 (up to 0.2) there is difference in the controller designed considering the Interconnected and the Overlapping model. Further comparison will be provided in Test 2.3.

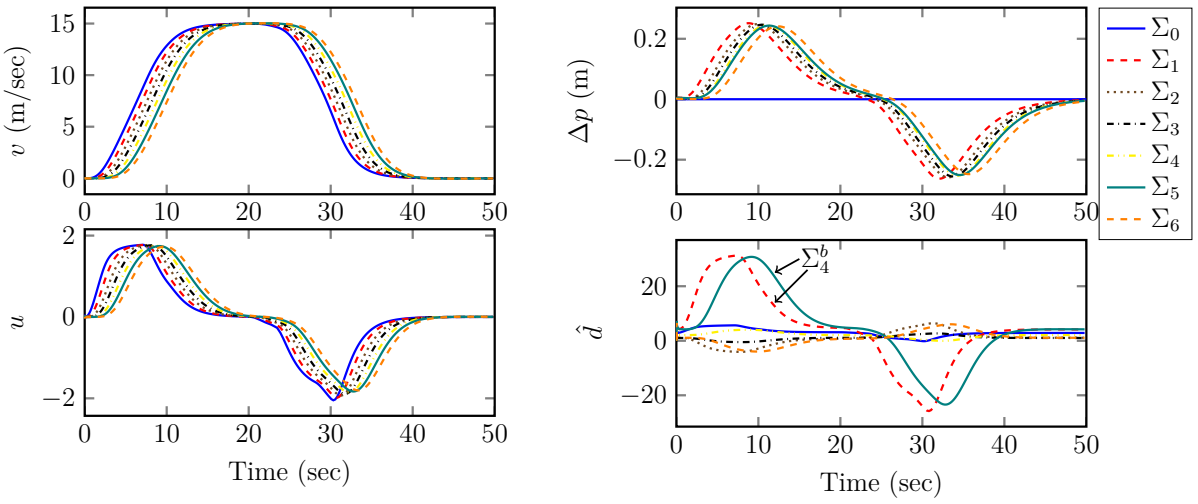

Figure 3.6 – Test 2.1: Platoon $\mathbb{J} = \{0, 4, 1, 3, 2, 4, 1\}$. Velocity (top left), distance policy error (top right), control input (bottom left) and disturbance estimation (bottom right) of each vehicle with a controller designed according to Corollary 3.1.

3.4.2.2 Test 2.2 - Overlapping system

Consider for this test a platoon with $N = 4$ followers and platoon $\Sigma_i = \Sigma^b_{\mathbb{J}(i)}$ with $\mathbb{J} = \{0, 4, 1, 3, 2\}$ again the platoon is voluntarily set with Σ_0 the lighter vehicle followed by the heaviest one Σ_4. The controller is chosen as in Test 1 with

$$\bar{K}_1 = \begin{bmatrix} 0.2 & 0.7 & -0.42 & 0 \end{bmatrix} \quad \bar{K}_2 = \begin{bmatrix} 0 & 1 \end{bmatrix} \tag{3.60}$$

Figure 3.7 (top left) gives the velocity, (top right) the distance policy error, (bottom right) the control input and (bottom left) the disturbance estimation $\hat{d}$. Similar to Test 2.1 the platoon is able to follow the speed profile, however, with smaller values of distance policy error, (up to 0.05 (m) in comparison to 0.2 (m) in Test 2.1 with the interconnected system). As in Test 2.1 the value of $\hat{d}(t)$ is larger for vehicle Σ_1 because of the larger uncertainty.

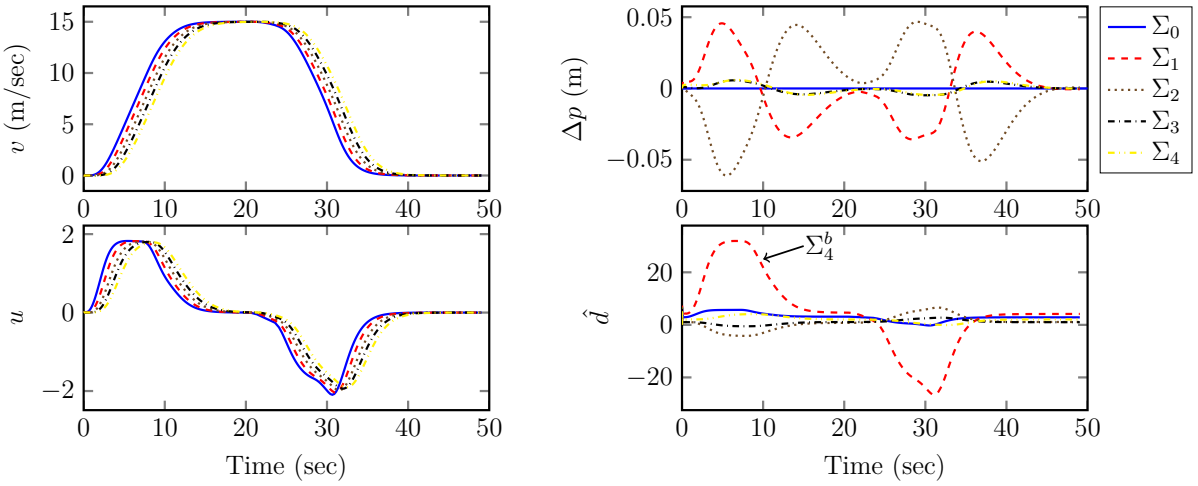

Figure 3.7 – Test 2.2: Platoon $\mathbb{J} = \{0, 4, 1, 3, 2\}$. Velocity (top left), distance policy error (top right), control input (bottom left) and disturbance estimation (bottom right) of each vehicle with $\bar{K}_1 = \begin{bmatrix} 0.2 & 0.7 & -0.42 & 0 \end{bmatrix}$ and $\bar{K}_2 = \begin{bmatrix} 0 & 1 \end{bmatrix}$.

3.4.2.3 Test 2.3 - Comparison: Interconnected and Overlapping

In order to show a larger platoon, we use with $N = 10$ followers and $\Sigma_i = \Sigma^b_{\mathbb{J}(i)}$ with set $\mathbb{J} = \{0, 4, 2, 1, 3, 3, 2, 4, 0, 3, 1\}$. The controller for the interconnected system and overlapping system chosen, respectively, as in Tests 2.1 and 2.2. We select three vehicles for comparison: Σ_2, Σ_7 and Σ_{10}. Vehicle Σ_2 is chosen since it provides the largest Δp in both modelings, Σ_7 is chosen because its base value presents the largest uncertainty and Σ_{10} is chosen to evaluated the effects for the last vehicle.

Left side of Figure 3.8 shows the velocity and the right side the distance policy error Δp of the 4 selected vehicles. Comparing the results from the Interconnected system (top) with the overlapping (bottom), it is noticeable the difference in Δp, with the maximum value of

0.05 (m) for the Overlapping system, compared with a maximum value of 0.2 (m) for the Interconnected system. The behavior of Δp does not change significantly between vehicles for the interconnected system, while there are significant variations for the Overlapping ones.

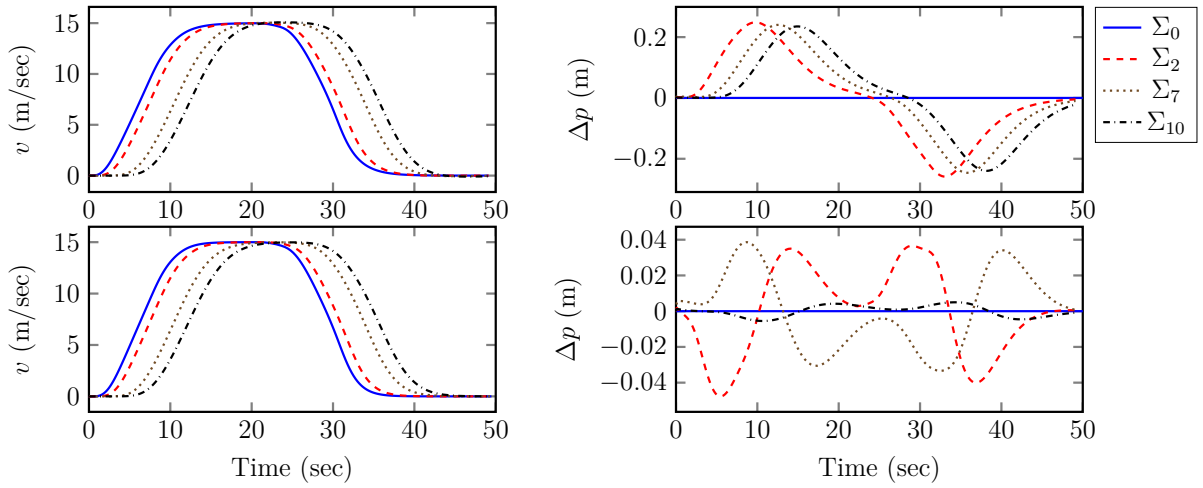

Figure 3.8 – Test 2.3: Velocity (left), and distance policy error (right), of vehicles Σ_2, Σ_7 and Σ_{10} designed considering the Interconnected (top) and Overlapping (bottom) systems.

3.4.2.4 Test 2.4 - Comparison: Non zero initial conditions

The simulations until now were all performed with $\left[\Delta p(0), \Delta v(0), a(0)\right] = 0$, i.e., the platoon is already in the desired formation. In order to show the performance with non-zero initial conditions, we consider a platoon with the same setup as in Test 2.3 ($\mathbb{J} = 0, 4, 2, 1, 3, 3, 2, 4, 0, 3, 1$) and the same controllers. In this test, the focus is on the transient behavior until the vehicles achieve formation. For this reason, all vehicles were selected, and we focus on the initial instants of the velocity profile.

The left side of Figure 3.9 shows the velocity, and the right side shows the distance policy error Δp of all vehicles. Looking at the velocity of each vehicle, we notice that, unlike in the other tests where the initial error is zero, the vehicles exhibit a transient behavior to adjust their positions and reduce the distance policy error. Comparing the results from the interconnected system (top) with the overlapping system (bottom), both approaches successfully drive the vehicles to formation. However, the overlapping approach provides faster convergence, with vehicles reaching formation within 10 seconds, while the interconnected approach required more time and, as in Test 2.3, presented high values of Δp.

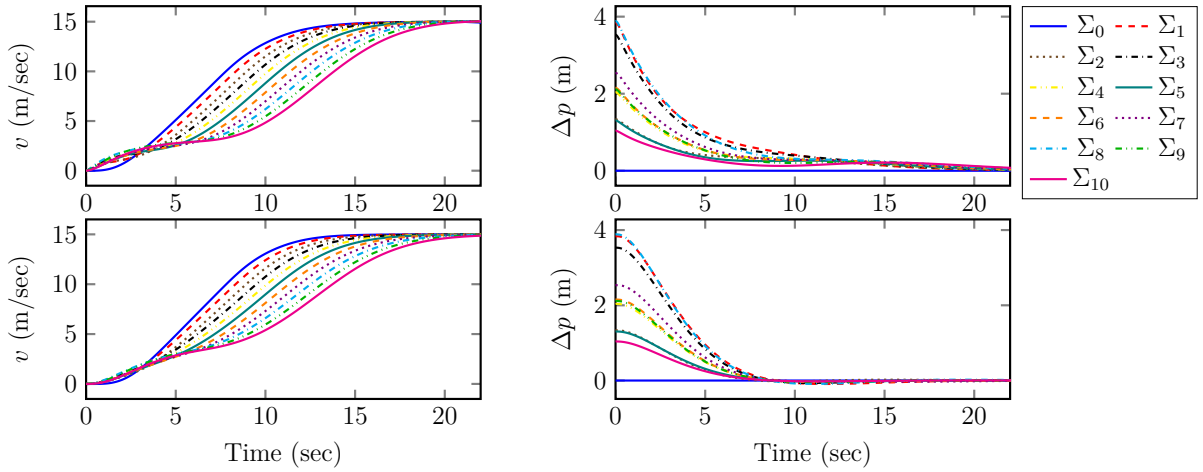

Figure 3.9 – Test 2.4: Velocity (left), and distance policy error (right), of vehicles Σ_1, to Σ_10 the Interconnected (top) and Overlapping (bottom) systems, stating with non zero initial conditions.

3.5 Conclusion

Considering the control communication between vehicles in the predecessor-follower flow topology, extended $\mathcal{L}_2$ string stability condition have been proposed for platoons subject to uncertainties. To effectively compensate for the uncertainties of the platooning system, treated as a virtual disturbance, a DOB-based uncertainty estimation is included in the feedback linearization control law. As a result, string stability and the stability of individual vehicles can be evaluated in a manner similar to the classical CACC design conditions. Moreover sufficient LMI conditions are presented to ensure $\mathcal{L}_2$ stability between the vehicle systems Σ_i and Σ_{i-1} considering different models of vehicle interaction. Through simulations and comparisons, we illustrate that the proposed DOB-based compensation can effectively handle the system uncertainties, how each model can lead to different performances in the platoon system.

4 CACC platoon with event-triggering communication

4.1 Introduction

Cooperative adaptive cruise control differs from adaptive cruise control by introducing a communication system that allows vehicles to share information. Sharing information can improve platoon performance and allow shorter distance policies without compromising safety. Introducing communication requires accounting for possible delays and efficient use of the network. In this chapter, the main subject is the communication mechanism between vehicles in cooperative ACC. To improve communication efficiency, an event-triggered communication mechanism is considered. Since the system models are assumed to be affected by uncertainties, to avoid Zeno behavior, a minimum waiting time is enforced in the event-triggering mechanism. Because of time delays, information transmitted is only received after a time interval. Accounting for enforced time and delays, the time intervals of transmission and reception are divided into subintervals, and the vehicle linearized dynamics is modeled as a switching system that switches according to each time interval. The event-triggering control is designed considering this switching system model, and a dynamic event mechanism is proposed to reduce the number of events. To ensure individual and string stability, as proposed in the previous chapter Section 3.3.2, design conditions are derived for the cases with and without delay. Both conditions are formulated as an optimization problem subject to LMI constraints. Finally, simulations are performed to evaluate the efficiency of the designed controller and event mechanism.

4.2 Platoon modeling with event triggered control

As it was presented in Chapter 3, communication plays an important role in the CACC system. So far the communication was assumed to be continuous (fast enough), where information shared by vehicles is available in real time. However, even under periodic communication, transmitting data continuously can overload the communication network. Instead of continuous communication, we consider that states are transmitted according to an event triggering mechanism which evaluates under what conditions new information is transmitted. Moreover we account for possible communication delays induced by the network.

Consider a platoon with a leader and N follower vehicles denoted by Σ_i, with $i = 0, \ldots, N$ shown in Figure 4.1, as in Chapter 3. Vehicle Σ_i receives information from Σ_{i-1} and transmits to Σ_{i+1}, where the transmission is subject to network induced delays.

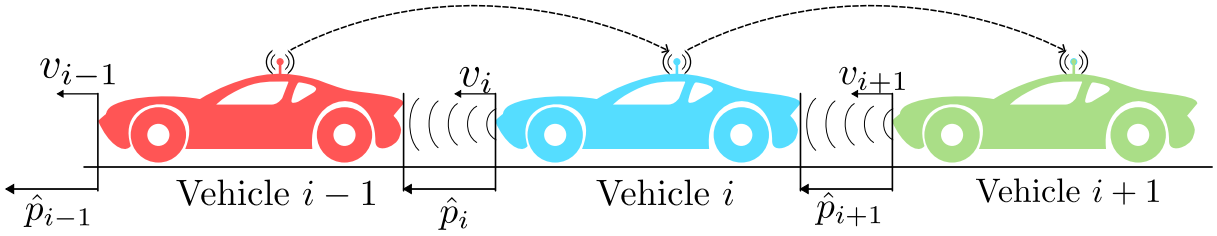

Figure 4.1 – Vehicle platooning PF topology where Σ_i receives information from Σ_{i-1} subjected to a time delay $\tau^*(t)$ and transmits to Σ_i at time $t_{k,i}$ generated according to an event triggering mechanism.

The control law of Σ_i is computed based on two signals. The signal $y_{1,i}$ measured by Σ_i and $y_{2,i-1}$ which is received from Σ_{i-1} by Σ_i. In addition, due to network-induced delays, the transmitted state $y_{2,i-1}$ arrives at Σ_i after a time delay $\tau^*_{i-1}(t)$, Figure 4.2. Here we assume that $\tau^*_i(t) \in (0, \tau_m]$ for all i, where the scalar $\tau_m > 0$ is the maximum allowable delay.

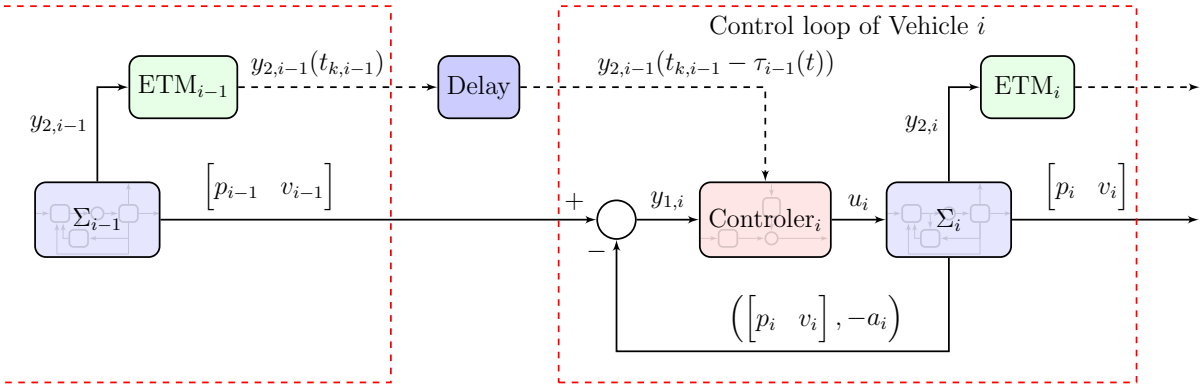

Figure 4.2 – Communication loop of the proposed event-triggered CACC setup.

We assume that all the states required for feedback linearization are not related to the communication, therefore available for computing the feedback linearizing control law. Therefore, both linearization and DOB compensation as defined in the previous chapter, can be applied rendering the linear systems Σ_i

$$\Sigma_i : \begin{cases} \Delta\dot{p}_i = \Delta v_i - h a_i \\ \Delta\dot{v}_i = a_{i-1} - a_i \\ \dot{a}_i = -\dfrac{1}{\rho_d} a_i + \dfrac{1}{\rho_d} u_i + e_{d,i} \end{cases} \tag{4.1}$$

for $i = 1, \ldots, N$ and

$$\Sigma_0 : \begin{cases} \dot{v}_0 = a_0 \\ \dot{a}_0 = -\dfrac{1}{\rho_d} a_0 + \dfrac{1}{\rho_d} u_0 + e_{d,0} \end{cases} \tag{4.2}$$

for the leader Σ_0, which are repeated therein for clarity. However, since the information required for computing the feedforward component of the control law is not continuously

available, the control law is recast as

$$u_i(t) = \underbrace{K_1 y_{1,i}}_{u_{\text{fb},i}} + \underbrace{K_2 y_{2,i-1}(t_{k,i-1})}_{u_{\text{ff},i}} \tag{4.3}$$

where $t_{k,i-1}$ is the time instant such that Σ_{i-1} transmits $y_{2,i-1}$ to Σ_i, which is not the same time that the information is received due to network induced delay $\tau^*_{i-1}(t)$. Based on those conditions we propose an event triggered control law with an appropriate event triggering mechanism with Zeno-free behavior. The conditions are derived based on the Interconnected ($\Sigma_{i,i-1}$) and Overlapping ($\Xi_{i,i-1}$) models. Due to the similarity in structures we restrict the discussion in this Chapter concerning the $\Sigma_{i,i-1}$ model.

Along with the ETC we also propose appropriate design conditions to ensure string stability of the platoon under the event-triggered communication. Two cases are considered based on the delay assumptions. In a delay free scenario we consider an emulation approach. In this case, a two-step procedure takes place: the controller is designed first to ensure string stability under continuous communication; second the ETC is designed with conditions to re-evaluate string stability under event triggering communication. In the presence of delays both control law and ETM are co-designed and the maximum admissible delay τ_m is searched as the maximum value such that the design conditions are feasible.

Both emulation and co-design conditions can be applied to interconnected $\Sigma_{i,i-1}$ and overlapping $\Xi_{i,i-1}$ models. Nonetheless, as discussed in Section 3.4, designing the controller for $\Xi_{i,i-1}$ is simpler and does not require further analysis, making it more appropriated for the emulation case. The model $\Sigma_{i,i-1}$ will be used for co-design with additional constraints to account for norm bound condition (3.39).

4.3 Event-triggered communication under time-delay effects

In this section we first characterize the receiving and transmitting time intervals and the respective subdivision that will be used. According to those intervals we propose an ETM with an enforced minimum time between transmissions which ensures a Zeno-free behavior.

To characterize both the ETM communication and the transmission delay, let $\{t_{k,i}\}$ for $k \in \mathbb{N}^+$ be a strictly increasing sequence of sampling instants, i.e., $t_{k+1,i} > t_{k,i}$, produced by the ETM of vehicle i. Moreover, let $\tau^*_{k,i} \in (0, \tau_m]$ be a network-induced delay with τ_m the maximum value. The signal $y_{2,i+1}$ is transmitted by Σ_i at time $t_{k,i}$ and, due to the network delay, it is received by Σ_{i+1} at time $t_{k,i} + \tau^*_{k,i}$. We then, respectively, define the following transmission $\mathcal{T}$ and receiving $\mathcal{R}$ time intervals:

$$\mathcal{T}_{k,i} = [t_{k,i}, t_{k+1,i}], \quad \mathcal{R}_{k,i} = [t_{k,i} + \tau^*_{k,i}, t_{k+1,i} + \tau^*_{k+1,i}]. \tag{4.4}$$

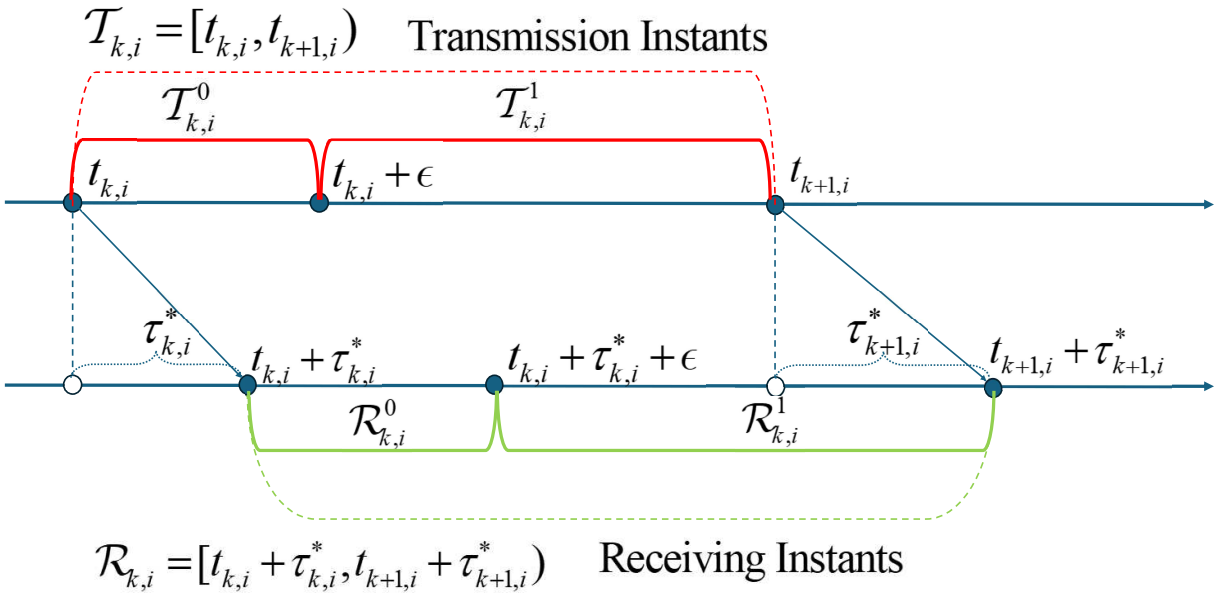

Figure 4.3 – Illustration of the transmission from vehicle Σ_i and the receiving time intervals for Σ_{i+1} with respective interval subdivisions.

Furthermore, considering a fixed time duration $\varepsilon > 0$ such that $\Delta t_{k,i} = t_{k+1,i} - t_{k,i} \geq \varepsilon$, we can further divide the time intervals $\mathcal{R}_{k,i}$ and $\mathcal{T}_{k,i}$ as

$$\begin{aligned} \mathcal{T}^0_{k,i} &= [t_{k,i}, t_{k,i} + \varepsilon], & \mathcal{T}^1_{k,i} &= [t_{k,i} + \varepsilon, t_{k+1,i}], \\ \mathcal{R}^0_{k,i} &= [t_{k,i} + \tau^*_{k,i}, t_{k,i} + \tau^*_{k,i} + \varepsilon], & \mathcal{R}^1_{k,i} &= [t_{k,i} + \tau^*_{k,i} + \varepsilon, t_{k+1,i} + \tau^*_{k+1,i}] \end{aligned} \tag{4.5}$$

where the waiting time $\varepsilon > 0$ represents a minimum inter-event time (IET). In Figure 4.3, we illustrate the transmission and receiving time intervals. In the transmission time axis, information is transmitted by vehicle Σ_i at instant $t_{k,i}$ defined by an event triggering mechanism and is received by vehicle Σ_{i+1} at instant $t_{k,i} + \tau^*_{k,i}$. No information is transmitted for a time interval given by ϵ, and at $t_{k+1,i} \geq t_{k,i} + \epsilon$ a new transmission occurs from Σ_i.

To ensure that $\Delta t_{k,i} = t_{k+1,i} - t_{k,i} \geq \varepsilon$, the sequence $\{t_{k,i}\}$ is generated according to the following proposed event triggering mechanism (ETM):

$$\begin{aligned} t_{0,i} &= 0 \\ t_{k+1,i} &= \inf\{t > t_{k,i} + \varepsilon : \ \theta \Lambda_i\Big(y_{2,i}(t), y_{2,i}(t_{k,i})\Big) - \zeta_i > 0\} \end{aligned} \tag{4.6}$$

where $\varepsilon > 0$ and $\theta > 0$ are design parameters, and

$$\Lambda_i\Big(y_{2,i}(t), y_{2,i}(t_{k,i})\Big) = \Big(y_{2,i}(t) - y_{2,i}(t_{k,i})\Big)^T Q_e \Big(y_{2,i}(t) - y_{2,i}(t_{k,i})\Big) - y^T_{2,i}(t) Q_x y_{2,i}(t) \tag{4.7}$$

for $t \in \mathcal{T}_{k,i}$ with Q_e and Q_x symmetric positive definite matrices to be designed. The dynamic variable $\zeta_i(t)$ has the following switching dynamics:

$$\dot{\zeta}_i = \begin{cases} -\lambda \zeta_i & \text{for } t \in \mathcal{T}^0_{k,i} \\ -\lambda \zeta_i + \Lambda_i\Big(y_{2,i}(t), y_{2,i}(t_{k,i})\Big) & \text{for } t \in \mathcal{T}^1_{k,i} \end{cases} \tag{4.8}$$

where $\zeta_i(0) = 0$, and λ is a positive scalar to be designed. Note that the positive constant ε enforces a minimum waiting time between consecutive events, i.e., $t_{k+1,i} - t_{k,i} \geq \varepsilon$, to ensure Zeno-free behavior.

The following lemma states that $\zeta_i(t)$, as defined in (4.8), remains non-negative for all $t \geq 0$ and will be important for the proofs in Section 4.5.

Lemma 4.1. *Consider the variable $\zeta_i(t)$, defined in* (4.8)*, with $\zeta_i(0) \geq 0$. Then, we have $\zeta_i(t) \geq 0$, for all $t \geq 0$.*

Proof. We distinguish the following two cases.
• For $t \in \mathcal{T}^0_{k,i}$, it follows from (4.8) that $\dot{\zeta}_i = -\lambda\zeta_i$. Then, it is clear that, for $\zeta_i(t_{k,i}) \geq 0$, we have $\zeta_i(t) \geq 0$, for $\forall t \in \mathcal{T}^0_{k,i}$.
• For $t \in \mathcal{T}^1_{k,i}$, the ETM (4.6) imposes that

$$\Lambda_i < \zeta_i/\theta, \tag{4.9}$$

which, combining with the dynamic equation from (4.8), leads to

$$\dot{\zeta}_i \geq -\lambda\zeta_i - \frac{1}{\theta}\zeta_i \tag{4.10}$$

Then, by the comparison lemma (KHALIL, 2002), it follows that for $\zeta_i(t_{k,i} + \varepsilon) \geq 0$, we have $\zeta_i(t) \geq 0$, for $\forall t \in \mathcal{T}^1_{k,i}$.

Combining the above cases, and from the continuity of $\zeta_i(t)$, it follows that, for $t_0 = 0$ and $\zeta_i(0) \geq 0$, then we have $\zeta_i(t) \geq 0$, for $\forall t \geq 0$. □

Accounting for the sub-division in the time intervals given in (4.5), we define two cases with their respective artificial delays.
• For $t \in \mathcal{R}^0_{k,i}$ we define a virtual delay $\tau_i(t) = t - t_{k,i}$ and write

$$y_{2,i}(t_{k,i}) = y_{2,i}(t - \tau_i(t)) \tag{4.11}$$

with $\tau_i(t) \leq \tau_m + \varepsilon = \tau_M$.
• For $t \in \mathcal{R}^1_{k,i}$ we define the error between the continuous state and the last transmitted state as

$$e_i(t) = y_{2,i}(t - \eta_i(t)) - y_{2,i}(t_{k,i}) \tag{4.12}$$

where $\eta_i(t)$ is an artificial delay, with $t - \eta_i(t) \in \mathcal{T}^1_{k,i}$. Consequently, we have $\eta_i(t) \in (0, \tau_m]$.

According to the ETC and the time interval divisions next section proposes a switching model that will be used for designing the ETM and the control law.

4.4 Switching Model

Based on (4.11) and (4.12), and inspired by (SELIVANOV; FRIDMAN, 2016), we can rewrite the control input (4.3) as

$$u_i(t) = K_1 y_{1,i} + \Big(1 - \chi(t)\Big) K_2 y_{2,i-1}\Big(t - \tau_{i-1}(t)\Big)$$

$$+ \chi(t)K_2\Big(y_{2,i-1}(t-\eta_{i-1}(t)) - e_{i-1}(t)\Big) \tag{4.13}$$

where the switching variable $\chi(t)$ is such that

$$\chi(t) = \begin{cases} 0 & \text{for } t \in \mathcal{R}^0_{k,i} \\ 1 & \text{for } t \in \mathcal{R}^1_{k,i} \end{cases} \tag{4.14}$$

The control law is defined as a switching control law, based on the partition of the receiving time interval.Then, applying the control law (4.13) to system $\Sigma_{i,i-1}$ defined in (3.26), we can rewrite the closed-loop system as

$$\Sigma^{\chi}_{i,i-1} : \begin{cases} \dot{x}_i = (A + BK_1C_1)x_i + Du_{i-1} + Ew_{d,i} \\ \qquad + (1-\chi(t))BK_2C_2x_i(t-\tau_{i-1}(t)) \\ \qquad\quad + \chi(t)BK_2(C_2x_i(t-\eta_{i-1}(t)) - e_{i-1}) \\ z_i = K_1C_1x_i + (1-\chi(t))K_2C_2x_i(t-\tau_{i-1}(t)) \\ \qquad + \chi(t)BK_2(C_2x_i(t-\eta_{i-1}(t)) - e_{i-1}) \end{cases} \tag{4.15}$$

for $t \in \mathcal{R}_{k,i}$. Hence, for $t \in \mathcal{R}^0_{k,i}$, we have $\Sigma^0_{i,i-1}$, while we have $\Sigma^1_{i,i-1}$, for $t \in \mathcal{R}^1_{k,i}$. System (4.15) is a switching model of the Interconnected system (3.26) presented in Chapter 3 based on the partition of the time intervals and delay. Using the same switching modeling concept, and the error definition in (4.12), we can also rewrite the dynamics of ζ_i as

$$\dot{\zeta}_i = -\lambda\zeta_i + \chi(t)\left(e_i^TQ_ee_i - x_i^T(t-\eta_i)C_2^TQ_xC_2x_i(t-\eta_i)\right) \tag{4.16}$$

for $t \in \mathcal{R}_{k,i}$.

Our aim is to design the ETM (4.6) to ensure the individual stability of each vehicle and the string stability of the platoon.

4.5 Individual and string stability with ETC

4.5.1 Problem Formulation

The platooning control problem with cooperative adaptive cruiser control (CACC) is to design K_1 and K_2 of the control law (4.3) and the event-triggering mechanism (4.6) such the distance policy error $\Delta p_i \to 0$. Moreover, the conditions are derived by assessing the $\mathcal{L}_2$ stability of $\Sigma_{i,i-1}$, and must verify the following requirements

- Ensure individual stability and string stability of the platoon.
- Minimize the influence of the disturbance estimation error via $\mathcal{L}_2$ norm.
- Reduce the number of transmissions for the ETM and avoid Zeno behavior.

This section presents our main results of switched dynamic $\mathcal{L}_2$ event-triggered control for vehicle platoons. The switched dynamic ETC design is recast as an optimization problem under LMI constraints. We consider two different cases, the emulation approach in a free delay scenario, and the co-design approach accounting for network-induced delays.

4.5.2 Delay free ETC emulation design conditions

In the delay free case $\tau^*(t) = 0$ for all t, therefore, from the time partition proposed in Section 4.4, $\mathcal{T}_{k,i} = \mathcal{R}_{k,i} = [t_{k,i}, t_{k+1,i}]$. The switching model (4.15) corresponds to $\eta(t) = 0$ for all t and $\tau_m = 0$.

Under those conditions, considering the gain K_1 and K_2 designed a priori according to Remark 3.2 and Remark 3.1 respectfully, the following theorem provides conditions to ensure the $\mathcal{L}_2$ stability defined in Proposition 3.1 of the switched system (4.15) under event triggering condition (4.6).

Theorem 4.1. *Consider the interconnected switching $\Sigma^{\chi}_{i,i-1}$ in (4.15) and the event-triggering condition (4.6) with $\zeta_i(0) = 0$. For given positive scalars δ, α, ε and control gains K_1 and K_2, if there exist positive scalars β, $\gamma \leq 1$, matrices P_1, P_2, X, X_1, Y_1, Y_2, Y_3 and symmetric matrices $P \succ 0$, $U \succ 0$, $Q_e \succ 0$ and $Q_x \succ 0$ of appropriate dimensions such that the following optimization problem is feasible:*

$$\min \operatorname{Tr}(Q_e) + \beta^2 \tag{4.17}$$

$$\Theta \succ 0, \quad \Psi \prec 0, \quad \Phi \prec 0, \quad \Omega \prec 0 \tag{4.18}$$

$$Q_x - \delta I \succ 0 \tag{4.19}$$

where

$$\Theta = \begin{bmatrix} P + \varepsilon\Theta_{11} & \varepsilon\Theta_{12} \\ * & \varepsilon\Theta_{22} \end{bmatrix} \tag{4.20}$$

$$\Phi = \begin{bmatrix} \Phi_{11} & \Phi_{12} & \Phi_{13} & P_1D & P_1E & C_1^TK_1^T \\ * & -P_2 - P_2^T + U & P_2BK_2C_2 + Y_2 + \varepsilon\Theta_{12} & P_2D & P_2E & 0 \\ * & * & Y_3 + Y_3^T + \Theta_{22} + 2\alpha\varepsilon\Theta_{22} & 0 & 0 & C_2^TK_2^T \\ * & * & * & -\gamma^2 I & 0 & 0 \\ * & * & * & * & -\beta^2 I & 0 \\ * & * & * & * & * & -I \end{bmatrix} \tag{4.21}$$

$$\Psi = \begin{bmatrix} \Psi_{11} & \Psi_{12} & \Psi_{13} & C_1^TK_1^T & P_1D & P_1E & \varepsilon Y_1^T \\ * & -P_2 - P_2^T & P_2BK_2C_2 + Y_2 & 0 & P_2D & P_2E & \varepsilon Y_2^T \\ * & * & Y_3 + Y_3^T + \Theta_{22} & C_2^TK_2^T & 0 & 0 & \varepsilon Y_3^T \\ * & * & * & -I & 0 & 0 & 0 \\ * & * & * & * & -\gamma^2 I & 0 & 0 \\ * & * & * & * & * & -\beta^2 I & 0 \\ * & * & * & * & * & * & -T\mathrm{e}^{-2\alpha}U \end{bmatrix} \tag{4.22}$$

$$\Omega = \begin{bmatrix} \Omega_{11} & (A+BK_1C_1)^TP_2^T - P_1 & P_1BK_2 & P_1D & P_1E & K^T \\ * & -P_2 - P_2^T & P_2BK_2 & P_2D & P_2E & 0 \\ * & * & -Q_e & 0 & 0 & -K_2^T \\ * & * & * & -\gamma^2 I & 0 & 0 \\ * & * & * & * & -\beta^2 I & 0 \\ * & * & * & * & * & -I \end{bmatrix} \tag{4.23}$$

with

$$\begin{aligned} &\Theta_{11} = \tfrac{X+X^T}{2}, \quad \Theta_{12} = X_1 - X, \quad \Theta_{22} = -X_1 - X_2^T + \Theta_{11} \\ &\Psi_{11} = \mathrm{He}\{(A+BK_1C_1)^TP_1^T\} + 2\alpha P - Y_1 - Y_1 - \Theta_{11} \\ &\Psi_{12} = (A+BK_1C_1)^TP_2^T - P_1 + P - Y_2^T \\ &\Psi_{13} = P_1BK_2C_2 + Y_1 - Y_3^T + \Theta_{12}, \\ &\Phi_{11} = \Psi_{11} + 2\alpha\varepsilon\Theta_{11}, \\ &\Phi_{12} = \Psi_{12} + \varepsilon\Theta_{11}, \\ &\Phi_{13} = \Psi_{13} + 2\alpha\varepsilon\Theta_{12} \\ &\Omega_{11} = \mathrm{He}\{(A+BKC)^TP_1^T\} + 2\alpha P + C_2^TQ_xC_2 \end{aligned}$$

Then, the interconnected switching system $\Sigma_{i,i-1}^{\chi}$ *in* (4.15) *is stable under the event-triggering condition* (4.6)*. Moreover, the dynamics of* ζ_i *is stable and condition* $\|z_i\| \leq \gamma\|z_{i-1}\| + \beta\|\omega_{\max}\|$ (3.28) *in Proposition 3.1 holds for system* (4.15) *with an* $\mathcal{L}_2$ *gain less than or equal to* β*.*

Proof. When there is no possible confusion, we omit the subscript i in x_i, z_i, e_{i-1}, u_{i-1}, $t_{k,i}$ and $w_{d,i}$. For the stability analysis of system (4.15), we consider the Lyapunov-Krasovskii functional candidate

$$V^{\chi}(t,x,\zeta) = x^TPx + \zeta + (1-\chi)(V_1+V_2) \tag{4.24}$$

with

$$V_1 = (\varepsilon - \tau(t)) \begin{bmatrix} x \\ x(t_k) \end{bmatrix}^T \begin{bmatrix} \Theta_{11} & \Theta_{12} \\ * & \Theta_{22} \end{bmatrix} \begin{bmatrix} x \\ x(t_k) \end{bmatrix} \tag{4.25}$$

$$V_2 = (\varepsilon - \tau(t)) \int_{t-\tau(t)}^{t} \mathrm{e}^{2\alpha(s-t)}\dot{x}^T(s)U\dot{x}(s)ds. \tag{4.26}$$

Notice that at switching instants t_k and $t_k + \varepsilon$, i.e., $\tau(t) = 0$ and $\tau(t) = \varepsilon$ respectively,

$$V^0(t_k,x,\zeta) = x^TPx + \zeta + \cancelto{0}{V_1+V_2} = x^TPx + \zeta = V^1(t_k,x,\eta) \tag{4.27}$$

$$V^0(t_k+\varepsilon,x,\zeta) = x^TPx + \zeta + \cancelto{0}{V_1+V_2} = x^TPx + \zeta = V^1(t_k+\varepsilon,x,\eta) \tag{4.28}$$

therefore, during switching instants, $V^0(t,x,\zeta) = V^1(t,x,\zeta)$. Along with the fact that $V^0(t,x,\zeta)$ and $V^1(t,x,\zeta)$ are continuous, this implies that the functional $V^\chi(t,x,\zeta)$ is continuous for all $t \geq 0$. Moreover $V^\chi(t,x,\zeta)$ in (4.24) is a proper LKF for $\Theta \succ 0$ and $P \succ 0$. This can be verified noticing that $V_2 \geq 0$ by construction in (4.26) and from Lemma 4.1, $\zeta \geq 0$ for $\forall t \geq 0$. It remains to prove that $x^T P x + V_1 \geq 0$. Considering the definition of Θ in (4.20), then $\Theta \succ 0$ and $P \succ 0$ is sufficient to ensure that

$$\frac{\varepsilon - \tau(t)}{\varepsilon}\Theta + \frac{\tau(t)}{\varepsilon}\begin{bmatrix} P & 0 \\ 0 & 0 \end{bmatrix} \succeq 0 \tag{4.29}$$

which on its turn, implies $x^T P x + V_1 \geq 0$. Therefore $V^\chi(t,x,\zeta)$ is positive definite.

Due to the switching nature of the problem, we split the analysis based on the time intervals of interest.

Case 1) System $\Sigma^0_{i,i-1}$ and $t \in \mathcal{T}_{k,i} = [t_{k,i}, t_{k,i} + \varepsilon]$

For this time interval, one has $V^0(t,x,\zeta) = x^T P x + \zeta + V_1 + V_2$. We compute

$$\frac{d}{dt}(x^T P x + \zeta) = \dot{x}^T P x + x^T P \dot{x} - \lambda\zeta \tag{4.30}$$

$$\dot{V}_1 = -\begin{bmatrix} x \\ x(t_k) \end{bmatrix}^T \begin{bmatrix} \Theta_{11} & \Theta_{12} \\ * & \Theta_{22} \end{bmatrix} \begin{bmatrix} x \\ x(t_k) \end{bmatrix} + (\varepsilon - \tau(t))\dot{x}^T[2\Theta_{11}x + 2\Theta_{12}x(t_k)] \tag{4.31}$$

$$\dot{V}_2 \leq -2\alpha V_2 - \mathrm{e}^{2\alpha\varepsilon}\int_{t-\tau(t)}^{t} \dot{x}(s)^T U \dot{x}(s) ds + (\varepsilon - \tau(t))\dot{x}^T U \dot{x}. \tag{4.32}$$

Let us define

$$\kappa(t) = \frac{1}{\tau(t)}\int_{t-\tau(t)}^{t} \dot{x}(s) ds \tag{4.33}$$

Then, invoking Jensen's inequality (Lemma 2.5), it follows that

$$-\mathrm{e}^{2\alpha\varepsilon}\int_{t-\tau(t)}^{t} \dot{x}(s)^T U \dot{x}(s) ds \leq -\tau(t)\mathrm{e}^{2\alpha\varepsilon}\kappa(t)^T U \kappa(t) \tag{4.34}$$

Moreover, from the definition of $\kappa(t)$ in (4.33) we have $x(t) = x(t_k) + \tau(t)\kappa(t)$. Then, for any matrices Y_1, Y_2 and Y_3 of suitable dimensions, it follows that

$$0 = \mathrm{He}\{(x^T Y_1 + \dot{x}^T Y_2 + x^T(t_k) Y_3)[x(t_k) - x + \tau\kappa(t)]\} \tag{4.35}$$

Similarly, from the expressions of $\dot{x}$ and z in (4.15) substituting $x(t - \tau_i) = x(t_k)$ we can directly obtain the following null terms:

$$0 = \mathrm{He}\{(x^T P_1 + \dot{x}^T P_2)[(A + BK_1C_1)x + BK_2C_2x(t_k) + Du + Ew_d - \dot{x}]\} \tag{4.36}$$

$$0 = \mathrm{He}\{z^T[K_1C_1x + K_2C_2x(t_k) - z]\}. \tag{4.37}$$

Combining (4.30), (4.31), (4.32), the inequality (4.34), the performance output z in (4.15), and adding the null terms (4.35), (4.36) and (4.37), we can derive the following inequality:

$$\dot{V}^0 + 2\alpha V^0(t,x,0) + \lambda\zeta + z^T z - \gamma^2 u^T u - \beta^2 w_d^T w_d \leq \mu_0^T \mathcal{L}(\tau(t))\mu_0 \tag{4.38}$$

where $\mu_0 = \text{col}\{x, \dot{x}, x(t_k), u, w_d, z, \kappa\}$. The matrix $\mathcal{L}(\tau(t))$ is affine on $\tau(t)$, and can be expressed as

$$\mathcal{L}(\tau(t)) = \frac{\tau(t)}{\varepsilon}\Psi + \frac{\varepsilon - \tau(t)}{\varepsilon}\begin{bmatrix}\Phi & 0\\ * & 0\end{bmatrix} \tag{4.39}$$

where Φ and Ψ are defined in (4.21) and (4.22), respectively. Note from (4.39) that the conditions $\Phi \prec 0$ and $\Psi \prec 0$ from (4.18) ensure that $\mathcal{L}(\tau(t)) \preceq 0$, for all $\tau(t) \in (0, \varepsilon]$.

Case 2) System $\Sigma^1_{i,i-1}$ and $t \in \mathcal{T}^1_{k,i}$

For this time interval, we have $V^\chi(t, x, \zeta) = x^T P x + \zeta$. Taking its time derivative yields

$$\dot{V}^1 = \dot{x}^T P x + x^T P \dot{x} + x^T C_2^T R C_2 x - e_{i-1}^T Q e_{i-1} - \lambda\zeta. \tag{4.40}$$

As in the previous case, we can derive the following null terms from (4.15) for $t \in \mathcal{T}^1_{k,i}$:

$$0 = \text{He}\{(x^T P_1 + \dot{x}^T P_2)[(A + BKC)x + BK_2 e_{i-1} + Du + Ew_d - \dot{x}]\} \tag{4.41}$$

$$0 = \text{He}\{z^T[KCx + K_2 e_{i-1} - z]\}. \tag{4.42}$$

Adding the null terms (4.41) and (4.42) to (4.40), we can derive

$$\dot{V}^1 + 2\alpha V^1(t, x, 0) + \lambda_2\zeta + z^T z - \gamma^2 u^T u - \beta^2 w_d^T w_d \leq \mu_1^T \Omega \mu_1 \tag{4.43}$$

where $\mu_1 = \text{col}\{x, \dot{x}, e_{i-1}, u, w_d, z\}$, and Ω is defined in (4.23). Hence, the condition $\Omega \prec 0$ in (4.18) ensures that $\mu_1^T \Omega \mu_1 \leq 0$.

Then, combining Case 1 and Case 2, from the continuity of the LKF (4.24), if the conditions (4.38) and (4.43) are satisfied, it follows that

$$\dot{V}^\chi + \bar{\alpha} V^\chi(t, x, \zeta) + z^T z - \gamma^2 u^T u - \beta^2 w_d^T w_d \leq 0 \tag{4.44}$$

for $t \geq 0$, with $\bar{\alpha} = \min\{\lambda, 2\alpha\}$. Hence, integrating both sides from 0 to ∞ if follows that

$$\|z\|_{\mathcal{L}_2} \leq \gamma \|u\|_{\mathcal{L}_2} + \beta \|w\|_{\mathcal{L}_2} \tag{4.45}$$

for null initial conditions. Since $\gamma \leq 1$ we recover the condition (3.28) in Proposition 3.1.

Moreover, the LMI constraint (4.19) and the minimization of $\text{Tr}(Q_e)$ in (4.17) are used to maximize the inter-event time of the switched dynamic ETC scheme. This completes the proof. □

4.5.3 Delay free periodic ETC emulation design conditions

To show the generic feature of the proposed ETC method and for comparison purposes, we provide an adaptation of Theorem 4.1 to the case of static periodic ETC design. To this end, we consider the following event-triggering mechanism:

$$\begin{aligned} s_{0,i} &= 0 \\ t_{k+1,i} &= \inf\{t > t_{k,i} + j\varepsilon : \ j \in \mathbb{N} \ \Lambda_i(y_{2,i}(t_{k,i} + j\varepsilon), y_{2,i}(t_{k,i})) > 0\} \end{aligned} \tag{4.46}$$

where

$$\Lambda_i\Big(y_{2,i}(t), y_{2,i}(t_{k,i})\Big) = \Big(y_{2,i}(t) - y_{2,i}(t_{k,i})\Big)^T Q_e\Big(y_{2,i}(t) - y_{2,i}(t_{k,i})\Big) - y_{2,i}^T(t) Q_x y_{2,i}(t) \quad (4.47)$$

is defined in (4.7). In this case we substitute the continuous measured signal $y_{2,i}(t)$ by its sampled variant $y_{2,i}(t_{k,i} + j\varepsilon)$. Let us then redefine $\tau(t) = t - t_{k,i} - j\varepsilon$, then the switching system (4.15) can be recast as

$$\Sigma_{i,i-1} : \begin{cases} \dot{x} = (A + BK_1C_1)x + BK_2C_2x(t - \tau(t)) - BK_2e_{i-1} + Du_{i-1} + Ew_d \\ z = K_1C_1x + K_2C_2x(t - \tau(t)) - K_2e_{i-1}. \end{cases} \quad (4.48)$$

Based on system (4.48) and the event-triggering condition (4.46), we provide the following theorem for static periodic ETC design.

Theorem 4.2. *For given positive scalars δ, α, ε and control gains K_1 and K_2, if there exist positive scalars β, $\gamma \leq 1$, matrices P_1, P_2, X, X_1, Y_1, Y_2, Y_3, and symmetric matrices $P \succ 0$, $U \succ 0$, $Q_e \succ 0$ and $Q_x \succ 0$ of appropriate dimensions such that the following optimization problem is feasible:*

$$\min \mathrm{Tr}(Q_e) + \beta \quad (4.49)$$

$$H_0 \succ 0, \quad Q_x - \delta I \succ 0 \quad (4.50)$$

$$\tilde{\Phi} = \begin{bmatrix} \bar{\Phi} & \Upsilon_1 \\ * & -Q_e \end{bmatrix} \prec 0, \quad \tilde{\Psi} = \begin{bmatrix} \bar{\Psi} & \Upsilon_2 \\ * & -Q_e \end{bmatrix} \prec 0 \quad (4.51)$$

with

$$\bar{\Phi}_{22} = \Phi_{22} + C^T Q_x C, \qquad \bar{\Psi}_{22} = \Psi_{22} + C^T Q_x C$$
$$\bar{\Phi}_{ij} = \Phi_{ij}, \qquad \bar{\Psi}_{ij} = \Psi_{ij}$$
$$\Upsilon_1 = \begin{bmatrix} K_2^T B^T P_1 & K_2^T B^T P_2 & 0 & 0 & 0 & -K_2^T \end{bmatrix}^T.$$
$$\Upsilon_2 = \begin{bmatrix} K_2^T B^T P_1 & K_2^T B^T P_2 & 0 & 0 & 0 & 0 & -K_2^T \end{bmatrix}^T.$$

where matrices Φ_{ij} and Ψ_{ij} are defines in (4.21) *and* (4.22) *in Theorem 4.1. Then, the closed-loop system* (4.48) *is stable under the periodic ETM* (4.46)*. Moreover, condition* (3.28) *in Proposition 3.1 holds for system* (4.48)*.*

Proof. We provide a sketch of this proof in the following, since it follows similar steps to that of Theorem 4.1. Choosing a Lyapunov function candidate $V = x^T Px + V_1 + V_2$, and considering the same time derivatives as in (4.31) and (4.32), and the following null terms:

$$0 = \mathrm{He}\{(x^T P_1 + \dot{x}^T P_2)[(A + BK_1C_1)x + BK_2C_2x(t - \tau) - BK_2e_{i-1} + Du + Ew_d - \dot{x}]\}$$
$$0 = \mathrm{He}\{z^T[K_1C_1x + K_2C_2x(t - \tau) - K_2e_{i-1} - z]\}$$

along with (4.35), as in the proof of Theorem 4.1, we can derive

$$\dot{V} + 2\alpha V + x^T C_2^T R C_2 x - e_{i-1}^T Q e_{i-1} + z^T z - \gamma^2 u^T u - \beta^2 w_d^T w_d \leq \tilde{\mu}^T \mathcal{H}(\tau(t))\tilde{\mu} \quad (4.52)$$

with $\tilde{\mu} = \text{col}(x, \dot{x}, x(t_k), \kappa, u, w_d, z, e_{i-1})$, and

$$\mathcal{H}(\tau(t)) = \frac{\tau(t)}{\varepsilon}\tilde{\Psi} + \frac{\varepsilon - \tau(t)}{\varepsilon}\begin{bmatrix}\tilde{\Phi} & 0\\ 0 & 0\end{bmatrix} \quad (4.53)$$

for $\tau(t) \in (0, \varepsilon]$, where the matrices $\tilde{\Psi}$ and $\tilde{\Phi}$ are defined in (4.51). Notice that the matrix $\mathcal{H}(\tau(t))$ is affine in $\tau(t)$, and condition (4.51) ensures that

$$\tilde{\mu}^T \mathcal{H}(\tau(t))\tilde{\mu} \leq 0. \quad (4.54)$$

From (4.46) we have

$$x(t-\tau)^T C_2^T R C_2 x(t-\tau) - e_{i-1}^T Q e_{i-1} < 0. \quad (4.55)$$

then, it follows from (4.52), (4.54) and (4.55) that

$$\dot{V} + 2\alpha V + z^T z - \gamma^2 u^T u - \beta^2 w_d^T w_d \leq 0. \quad (4.56)$$

Integrating (4.56) from 0 to ∞, we obtain (3.28). This completes the proof. □

Remark 4.1. The designed conditions for the Overlapping system is similar to the interconnected system that is not described here but is straightforward from Theorem 4.1

4.5.4 ETC Co-design conditions

The previous section presented results for switched dynamic $\mathcal{L}_2$ event-triggered control in the delay-free case, next section introduces a communication delay and the way to handle it.

Considering that the communication is affected by network induced delays the following theorem provides conditions to ensure the $\mathcal{L}_2$ stability of the switched system (4.15), as stated in Proposition 3.1 for a given maximum network delay τ_m.

Theorem 4.3. *Consider the interconnected switching system* $\Sigma_{i,i-1}^{\chi}$ *in* (4.15) *and the event-triggering condition* (4.6). *Given a maximum delay* τ_m, *and positive scalars* δ, α, ε, *if there exist positive scalars* β, $\gamma \leq 1$, *matrices* $X = \text{diag}(X_1, X_2)$, L_1, L_2 $\bar{Y}_1$, $\bar{Y}_2$, $\bar{W}_1$, $\bar{W}_2$ *and symmetric matrices* $\bar{P} \succ 0$, $\bar{S}_0 \succ 0$, $\bar{S}_1 \succ 0$, $\bar{R}_0 \succ 0$, $\bar{R}_1 \succ 0$, $\bar{Q}_e \succ 0$ *and* $\bar{Q}_x \succ 0$ *of appropriate dimensions such that the following optimization problem is feasible:*

$$\min \text{Tr}(\bar{Q}_e) + \delta \text{Tr}(\bar{Q}_x) + \beta^2 \quad (4.57)$$

such that

$$\begin{bmatrix} \bar{\Phi}_0 + \bar{\Pi}_0(\tau_m) & \bar{\mathcal{Z}}_0^T & {\mathcal{F}_0}^T \begin{bmatrix} \bar{Y}_1 \\ 0 \end{bmatrix} \\ * & -I & 0 \\ * & * & -\mathrm{e}^{2\alpha\tau_M}\bar{R}_1 \end{bmatrix} \prec 0 \tag{4.58}$$

$$\begin{bmatrix} \bar{\Phi}_0 + \bar{\Pi}_0(\tau_M) & \bar{\mathcal{Z}}_0^T & {\mathcal{F}_0}^T \begin{bmatrix} 0 \\ \bar{Y}_2^T \end{bmatrix} \\ * & -I & 0 \\ * & * & -\mathrm{e}^{2\alpha\tau_M}\bar{R}_1 \end{bmatrix} \prec 0 \tag{4.59}$$

$$\begin{bmatrix} \bar{\Phi}_1 + \bar{\Pi}_1(0) & \bar{\mathcal{Z}}_1^T & \mathbf{v}_5^T X_2^T C_2^T & {\mathcal{F}_1}^T \begin{bmatrix} \bar{W}_1 \\ 0 \end{bmatrix} \\ * & -I & 0 & 0 \\ * & * & -\bar{Q}_x & 0 \\ * & * & * & -\mathrm{e}^{2\alpha\tau_m}\bar{R}_0 \end{bmatrix} \prec 0 \tag{4.60}$$

$$\begin{bmatrix} \bar{\Phi}_1 + \bar{\Pi}_1(\tau_m) & \bar{\mathcal{Z}}_1^T & \mathbf{v}_5^T X_2^T C_2^T & {\mathcal{F}_1}^T \begin{bmatrix} 0 \\ \bar{W}_2^T \end{bmatrix} \\ * & -I & 0 & 0 \\ * & * & -\bar{Q}_x & 0 \\ * & * & * & -\mathrm{e}^{2\alpha\tau_m}\bar{R}_0 \end{bmatrix} \prec 0 \tag{4.61}$$

with

$$\bar{\Phi}_0 = \mathbf{e}_2^T\bar{P}\mathbf{e}_1 + \mathbf{e}_1^T\bar{P}\mathbf{e}_2 - \varphi_m{\mathcal{G}_0}^T\bar{R}_0\mathcal{G}_0 + \bar{\Omega}_0 + \mathrm{He}\left\{\bar{\mathcal{A}}_0\right\},$$
$$\Phi_1 = \mathbf{v}_2^T\bar{P}\mathbf{v}_1 + \mathbf{v}_1^T\bar{P}\mathbf{v}_2 - \varphi_M{\mathcal{G}_1}^T\bar{R}_1\mathcal{G}_1 + \bar{\Omega}_1 + \mathrm{He}\left\{\bar{\mathcal{A}}_1\right\},$$
$$\Pi_0(\tau) = -\varphi_M{\mathcal{F}_0}^T\bar{\mathcal{R}}_0(\tau)\mathcal{F}_0, \quad \mathcal{Z}_0 = L_1C_1\mathbf{e}_2 + L_2C_2\mathbf{e}_5,$$
$$\Pi_1(\tau) = -\varphi_m{\mathcal{F}_1}^T\bar{\mathcal{R}}_1(\tau)\mathcal{F}_1, \quad \mathcal{Z}_1 = L_2C_1\mathbf{v}_2 + L_2C_2\mathbf{v}_5 + L_2\mathbf{v}_8,$$
$$\begin{matrix}\mathcal{G}_0 = \mathbf{e}_2 - \mathbf{e}_1, \\ \mathcal{G}_1 = \mathbf{v}_2 - \mathbf{v}_1,\end{matrix} \quad \mathcal{F}_0 = \begin{bmatrix}\mathbf{e}_3 - \mathbf{e}_5 \\ \mathbf{e}_5 - \mathbf{e}_4\end{bmatrix}, \quad \mathcal{F}_1 = \begin{bmatrix}\mathbf{v}_3 - \mathbf{v}_5 \\ \mathbf{v}_5 - \mathbf{v}_4\end{bmatrix},$$
$$\bar{\Omega}_0 = \mathrm{diag}(\bar{\mathcal{H}}, 2\alpha\bar{P} - \bar{S}_0, \bar{\mathcal{S}}, -\varphi_M\bar{S}_1, 0, -\gamma^2, -\beta^2),$$
$$\bar{\Omega}_1 = \mathrm{diag}(\bar{\mathcal{H}}, 2\alpha\bar{P} - \bar{S}_0, \bar{\mathcal{S}}, -\varphi_M\bar{S}_1, 0, -\gamma^2, -\beta^2, -\bar{Q}_e),$$
$$\bar{\mathcal{H}} = \tau_m^2\bar{R}_0 + \tau_M^2\bar{R}_1, \quad \bar{\mathcal{S}} = \varphi_m(\bar{S}_1 - \bar{S}_0),$$
$$\bar{\mathcal{R}}_0(\tau) = \begin{bmatrix}\bar{R}_1 & 0 \\ 0 & \bar{R}_1\end{bmatrix} + \frac{\tau_M - \tau(t)}{\varepsilon}\begin{bmatrix}\bar{R}_1 & \bar{Y}_2 \\ \bar{Y}_2^T & 0\end{bmatrix} + \frac{\tau(t) - \tau_m}{\varepsilon}\begin{bmatrix}0 & \bar{Y}_1 \\ \bar{Y}_1^T & \bar{R}_1\end{bmatrix},$$
$$\bar{\mathcal{R}}_1(\tau) = \begin{bmatrix}\bar{R}_0 & 0 \\ 0 & \bar{R}_0\end{bmatrix} + \frac{\tau_m - \tau(t)}{\tau_m}\begin{bmatrix}\bar{R}_0 & \bar{W}_2 \\ \bar{W}_2^T & 0\end{bmatrix} + \frac{\tau(t)}{\tau_m}\begin{bmatrix}0 & \bar{W}_1 \\ \bar{W}_1^T & \bar{R}_0\end{bmatrix},$$
$$\bar{\mathcal{A}}_0 = \mathcal{Y}_0(-X\mathbf{e}_1 + (AX + BL_1C_1)\mathbf{e}_2 + BL_2C_2\mathbf{e}_5 + D\mathbf{e}_6 + E\mathbf{e}_7),$$
$$\bar{\mathcal{A}}_1 = \mathcal{Y}_1(-X\mathbf{v}_1 + (AX + BL_1C_1)\mathbf{v}_2 + BL_2C_2\mathbf{v}_5 + D\mathbf{v}_6 + E\mathbf{v}_7 - BL_2\mathbf{v}_8),$$
$$\mathcal{Y}_0 = (\mathbf{e}_1^T\beta_1 + \mathbf{e}_2^T + \mathbf{e}_5^T\beta_2),$$

$$\mathcal{Y}_1 = (\mathbf{v}_1^T\beta_1 + \mathbf{v}_2^T + \mathbf{v}_5^T\beta_2),$$
$$\varphi_m = \mathrm{e}^{-2\alpha\tau_m}, \quad \varphi_M = \mathrm{e}^{-2\alpha\tau_M},$$

where

$$\mathrm{col}\{\mathbf{e}_1, \ldots, \mathbf{e}_7\} = \mathrm{diag}(I_3, I_3, I_3, I_3, I_3, I_1, I_1), \tag{4.62}$$
$$\mathrm{col}\{\mathbf{v}_1, \ldots, \mathbf{v}_8\} = \mathrm{diag}(I_3, I_3, I_3, I_3, I_3, I_1, I_1, I_1). \tag{4.63}$$

Then, the closed-loop interconnected switching system (4.15)*, is* $\mathcal{L}_2$ *stable under the event-triggering condition* (4.6)*. Moreover, the condition* (3.28) *in Proposition 3.1 holds for system* (4.15) *with the control gains* $K_1 = L_1X_1^{-1}$*,* $K_2 = L_2X_2^{-1}$*, and the ETM* (4.6) *with matrices* $Q_e = X_2^{-T}\bar{Q}_eX_2^{-1}$ *and* $Q_x = \bar{Q}_x^{-1}$*.*

Proof. For brevity, we omit the subscript in x_i, z_i, e_{i-1}, u_{i-1}, ζ_{i-1}, $w_{d,i}$. Moreover we denote $\tau_{i-1}(t)$ and $\eta_{i-1}(t)$ as τ, η and $\varphi_m = \mathrm{e}^{-2\alpha\tau_m}$, $\varphi_M = \mathrm{e}^{-2\alpha\tau_M}$.

For the stability analysis of system (4.15), we consider the Lyapunov-Krasovskii functional candidate

$$V(t, x_i, \zeta) = V_P + V_{S_0} + V_{S_1} + V_{R_0} + V_{R_1} + \zeta \tag{4.64}$$

with $V_P = x^TPx$, and

$$V_{S_0} = \int_{t-\tau_m}^{t} \mathrm{e}^{2\alpha(s-t)}x^T(s)S_0x(s)ds \tag{4.65}$$
$$V_{R_0} = \tau_m\int_{-\tau_m}^{0}\int_{t+\theta}^{t} \mathrm{e}^{2\alpha(s-t)}\dot{x}^T(s)R_0\dot{x}(s)dsd\theta \tag{4.66}$$
$$V_{S_1} = \int_{t-\tau_M}^{t-\tau_m} \mathrm{e}^{2\alpha(s-t)}x^T(s)S_1x(s)ds \tag{4.67}$$
$$V_{R_1} = \varepsilon\int_{-\tau_M}^{-\tau_m}\int_{t+\theta}^{t} \mathrm{e}^{2\alpha(s-t)}\dot{x}^T(s)R_1\dot{x}(s)dsd\theta \tag{4.68}$$

We compute the time-derivative of V, defined in (4.64), as

$$\dot{V} = \dot{x}^TVx + x^TV\dot{x} + \dot{V}_{S_0} + \dot{V}_{S_1} + \dot{V}_{R_0} + \dot{V}_{R_1} + \dot{\zeta} \tag{4.69}$$

with

$$\dot{V}_{S_0} = -2\alpha V_{S_0} + x^T(t)S_0x(t) - \varphi_m x^T(t-\tau_m)S_0^m x(t-\tau_m) \tag{4.70}$$
$$\dot{V}_{S_1} = -2\alpha V_{S_1} + \varphi_m x^T(t-\tau_m)S_1x(t-\tau_m) - \varphi_M x^T(t-\tau_M)S_1x(t-\tau_M) \tag{4.71}$$
$$\dot{V}_{R_0} \leq -2\alpha V_{R_0} + \tau_m^2\dot{x}^T(t)R_0\dot{x}(t) - \tau_m\varphi_m\int_{t-\tau_m}^{t}\dot{x}^T(s)R_0\dot{x}(s)ds \tag{4.72}$$
$$\dot{V}_{R_1} \leq -2\alpha V_{R_1} + \tau_M^2\dot{x}^T(t)R_1\dot{x}(t) - \varepsilon\varphi_M\int_{t-\tau_M}^{t-\tau_m}\dot{x}^T(s)R_1\dot{x}(s)ds. \tag{4.73}$$

Consider

$$\mathcal{D}_V = \dot{V} + 2\alpha V(t, x, 0) + \lambda\zeta + z^Tz - \gamma^2u^Tu - \beta^2w^Tw. \tag{4.74}$$

We desire to prove that $\mathcal{D}_V \leq 0$, for $t > 0$. Due to the switching nature of the problem, we split analysis based on the time intervals of interest.

Case 1) $\chi(t) = 0$ and $\tau(t) \in (\tau_m, \tau_M]$

For this interval we define $\mu_0(t) = \text{col}\{\dot{x}, x, x(t-\tau_m), x(t-\tau_M), x(t-\tau), u, w\}$ and $\mathbf{e}_i$ as in (4.62). First, we split the integral term in (4.73) as

$$\int_{t-\tau_M}^{t-\tau_m} \dot{x}^T(s) R_1 \dot{x}(s) ds = \int_{t-\tau}^{t-\tau_m} \dot{x}^T(s) R_1 \dot{x}(s) ds + \int_{t-\tau_M}^{t-\tau} \dot{x}^T(s) R_1 \dot{x}(s) ds. \tag{4.75}$$

Then, applying Jensen's inequality (Lemma 2.5) to (4.72) and (4.75), we have

$$-\tau_m \int_{t-\tau_m}^{t} \dot{x}^T(s) R_0 \dot{x}(s) ds \leq -\mu_0^T \mathcal{G}_0{}^T R_0 \mathcal{G}_0 \mu_0 \tag{4.76}$$

$$-\varepsilon \int_{t-\tau_M}^{t-\tau_m} \dot{x}^T(s) R_1 \dot{x}(s) ds \leq -\mu_0^T \mathcal{F}_0^T \Gamma_0(\tau) \mathcal{F}_0 \mu_0 \tag{4.77}$$

with $\mathcal{G}_0 = \mathbf{e}_2 - \mathbf{e}_3$ and

$$\mathcal{F}_0 = \begin{bmatrix} \mathbf{e}_3 - \mathbf{e}_5 \\ \mathbf{e}_5 - \mathbf{e}_4 \end{bmatrix}, \; \Gamma_0(\tau) = \begin{bmatrix} \frac{\varepsilon}{\tau(t)-\tau_m} R_1 & 0 \\ 0 & \frac{\varepsilon}{\tau_M - \tau(t)} R_1 \end{bmatrix}.$$

Moreover, applying Lemma 2.6, with $X_1 = R_1 - Y_1 R_1^{-1} Y_1^T$ and $X_2 = R_1 - Y_2^T R_1^{-1} Y_2$, it follows from (4.77) that

$$-\varepsilon \int_{t-\tau_M}^{t-\tau_m} \dot{x}^T(s) R_1 \dot{x}(s) ds \leq -\mu_0^T \mathcal{F}_0{}^T \Gamma_0(\tau) \mathcal{F}_0 \mu_0 \tag{4.78}$$

with $\Gamma_0(\tau) = \mathcal{R}_0(\tau) - \mathcal{N}_0(\tau)$,

$$\mathcal{N}_0(\tau) = \begin{bmatrix} \frac{\tau_M - \tau(t)}{\varepsilon} Y_1 R_1^{-1} Y_1^T & 0 \\ 0 & \frac{\tau(t)-\tau_m}{\varepsilon} Y_2^T R_1^{-1} Y_2 \end{bmatrix},$$

$$\mathcal{R}_0(\tau) = \begin{bmatrix} R_1 & 0 \\ 0 & R_1 \end{bmatrix} + \frac{\tau_M - \tau(t)}{\varepsilon} \begin{bmatrix} R_1 & Y_2 \\ Y_2^T & 0 \end{bmatrix} + \frac{\tau(t) - \tau_m}{\varepsilon} \begin{bmatrix} 0 & Y_1 \\ Y_1^T & R_1 \end{bmatrix}.$$

Defining $\mathcal{Z}_0 = \begin{bmatrix} 0 & K_1 C_1 & 0 & 0 & K_2 C_2 & 0 & 0 \end{bmatrix}$ from the performance output ($z_i = u_i$) in (4.15) we can write

$$z = \mathcal{Z}_0 \mu_0. \tag{4.79}$$

Combining into (4.74) relations equations (4.70) to (4.72) and (4.77) to (4.79) and the dynamic of ζ_i in (4.8) yields

$$\mathcal{D}_V \leq \mu_0^T \Big(\mathbf{e}_2^T P \mathbf{e}_1 + \mathbf{e}_1^T P \mathbf{e}_2 + \Omega_0 - \varphi_m \mathcal{G}_0{}^T R_0 \mathcal{G}_0 + \Pi_0(\tau) + \varphi_M \mathcal{F}_0^T \mathcal{N}_0(\tau) \mathcal{F}_0 + \mathcal{Z}_0^T \mathcal{Z}_0 \Big) \mu_0 \tag{4.80}$$

with

$$\Pi_0(\tau) = -\varphi_M \mathcal{F}_0{}^T \mathcal{R}_0(\tau) \mathcal{F}_0, \; \Omega_0 = \text{diag}(\mathcal{H}, 2\alpha P - S_0, \mathcal{S}, -\varphi_M S_1, 0, -\gamma^2, -\beta^2)$$

Furthermore, defining $\mathcal{A}_0 = \begin{bmatrix} -I & A+BK_1C_1 & 0 & 0 & BK_2C_2 & D & E \end{bmatrix}$, it is straightforward from system (4.15) that $\mathcal{A}_0\mu_0 = 0$. Then, for a matrix $X = \text{diag}(X_1, X_2)$ of appropriate dimension, it follows from Lemma 2.11 that

$$\Phi_0 + \Pi_0(\tau) + \varphi_M \mathcal{F}_0^T \mathcal{N}_0(\tau)\mathcal{F}_0 + \mathcal{Z}_0^T\mathcal{Z}_0 \prec 0 \tag{4.81}$$

where

$$\Phi_0 = \mathbf{e}_2^T P\mathbf{e}_1 + \mathbf{e}_1^T P\mathbf{e}_2 + \Omega_0 - \varphi_m {\mathcal{G}_0}^T R_0 \mathcal{G}_0 + \text{He}\left\{\mathcal{X}_0^T\mathcal{A}_0\right\},\ \mathcal{X}_0 = \beta_1 X\mathbf{e}_1 + X\mathbf{e}_2 + \beta_2 X\mathbf{e}_5$$

ensures that $\mathcal{D}_V \leq 0$. By Schur complement lemma (BOYD *et al.*, 1994), we can show that condition (4.81) is equivalent to

$$\begin{bmatrix} \Phi_0 + \Pi_0(\tau) & \mathcal{Z}_0^T & \mathcal{F}_0^T \begin{bmatrix} Y_1 & 0 \\ 0 & Y_2^T \end{bmatrix} \\ * & -I & 0 \\ * & * & -\text{e}^{2\alpha\tau_M} \begin{bmatrix} \frac{\tau_M - \tau(t)}{\varepsilon} R_1 & 0 \\ 0 & \frac{\tau(t)-\tau_m}{\varepsilon} R_1 \end{bmatrix} \end{bmatrix} \prec 0 \tag{4.82}$$

From the convexity of (4.82), the conditions

$$\begin{bmatrix} \Phi_0 + \Pi_0(\tau_m) & \mathcal{Z}_0^T & {\mathcal{F}_0}^T \begin{bmatrix} Y_1 \\ 0 \end{bmatrix} \\ * & -I & 0 \\ * & * & -\text{e}^{2\alpha\tau_M} R_1 \end{bmatrix}, \prec 0 \tag{4.83}$$

$$\begin{bmatrix} \Phi_0 + \Pi_0(\tau_M) & \mathcal{Z}_0^T & {\mathcal{F}_0}^T \begin{bmatrix} 0 \\ Y_2^T \end{bmatrix} \\ * & -I & 0 \\ * & * & -\text{e}^{2\alpha\tau_M} R_1 \end{bmatrix} \prec 0 \tag{4.84}$$

are sufficient to ensure (4.81). Multiplying (4.83) and (4.84) on the right by

$$\text{diag}(X, X, X, X, X, I, I, I, X),$$

and on the left by its transpose, making $\bar{R}_i = X^T R_i X$, $\bar{S}_i = X^T S_i X$, $\bar{Y}_i = X^T Y_i X$, $L_i C_i = K_i X_i C_i = K_i C_i X$, for $i = 1, 2$, and $\bar{P} = X^T P X$, results in conditions (4.58) and (4.59).

Case 2) $\chi(t) = 1$ and $\eta(t) \in (0, \tau_m]$

For this interval, the proof is similar to Case 1, thus some steps are omitted. Let $\mu_1(t) = \text{col}\{\dot{x}, x, x(t-\tau_m), x(t-\tau_M), x(t-\eta), u, w, e\}$ and $\mathbf{v}_i$ as in (4.63). By splitting the integral term in (4.72) as

$$\int_{t-\tau_m}^{t} \dot{x}^T(s) R_0 \dot{x}(s) ds = \int_{t-\eta}^{t} \dot{x}^T(s) R_0 \dot{x}(s) ds + \int_{t-\tau_m}^{t-\eta} \dot{x}^T(s) R_0 \dot{x}(s) ds. \tag{4.85}$$

Invoking Jensen's inequality in Lemma 2.5 and the delay-dependent reciprocally convex inequality in Lemma 2.6, we can bound the integral terms (4.72) and (4.73) as

$$-\tau_m \int_{t-\tau_m}^{t} \dot{x}^T(s) R_0 \dot{x}(s) ds \leq -\mu_1^T \mathcal{F}_1{}^T \Gamma_1(\tau) \mathcal{F}_1 \mu_1 \tag{4.86}$$

$$-\tau_m \int_{t-\tau_M}^{t-\tau_m} \dot{x}^T(s) R_1 \dot{x}(s) ds \leq -\mu_1^T \mathcal{G}_1{}^T R_1 \mathcal{G}_1 \mu_1 \tag{4.87}$$

with

$$\mathcal{G}_1 = \mathbf{v}_2 - \mathbf{v}_3, \quad \Gamma_1(\tau) = \mathcal{R}_1(\tau) - \mathcal{N}_1(\tau), \quad \mathcal{F}_1 = \begin{bmatrix} \mathbf{v}_3 - \mathbf{v}_5 \\ \mathbf{v}_5 - \mathbf{v}_4 \end{bmatrix}$$

$$\mathcal{N}_1(\tau) = \begin{bmatrix} \frac{\tau_m - \tau(t)}{\tau_m} W_1 R_0^{-1} W_1^T & 0 \\ 0 & \frac{\tau(t)}{\tau_m} W_2^T R_0^{-1} W_2 \end{bmatrix}$$

$$\mathcal{R}_1(\tau) = \begin{bmatrix} R_0 & 0 \\ 0 & R_0 \end{bmatrix} + \frac{\tau_m - \tau(t)}{\tau_m} \begin{bmatrix} R_0 & W_2 \\ W_2^T & 0 \end{bmatrix} + \frac{\tau(t)}{\tau_m} \begin{bmatrix} 0 & W_1 \\ W_1^T & R_0 \end{bmatrix}.$$

By defining $\mathcal{A}_1 = \begin{bmatrix} \mathcal{A}_0 & -BK_2 \end{bmatrix}$, $\mathcal{Z}_1 = \begin{bmatrix} \mathcal{Z}_0 & -K_2 \end{bmatrix}$, combining with the dynamics of ζ in (4.8) and from Finsler Lemma 2.11, it follows that

$$\Phi_1 + \Pi_1(\tau) + \varphi_m \mathcal{F}_1^T \mathcal{N}_1(\tau) \mathcal{F}_1 + \mathcal{Z}_1^T \mathcal{Z}_1 + \mathbf{v}_5^T C_2^T Q_x C_2 \mathbf{v}_5 \prec 0 \tag{4.88}$$

with

$$\Phi_1 = \mathbf{v}_2^T P \mathbf{v}_1 + \mathbf{v}_1^T P \mathbf{v}_2 - \varphi_m \mathcal{G}_1{}^T R_1 \mathcal{G}_1 + \Omega_1 + \mathrm{He}\left\{\mathcal{X}_1^T \mathcal{A}_1\right\}, \Pi_1(\tau) = -\varphi_M \mathcal{F}_1{}^T \mathcal{R}_1(\tau) \mathcal{F}_1$$

$$\Omega_1 = \mathrm{diag}(\Omega_0, -Q_x), \mathcal{X}_1 = \beta_1 X \mathbf{v}_1 + X \mathbf{v}_2 + \beta_2 X \mathbf{v}_5$$

which ensures $\mathcal{D}_V \leq 0$. Using again the convexity of the condition (4.88) and Schur complement lemma (BOYD *et al.*, 1994), we have that

$$\begin{bmatrix} \Phi_1 + \Pi_1(0) & \mathcal{Z}_1^T & \mathbf{v}_5^T C_2^T & \mathcal{F}_1{}^T \begin{bmatrix} W_1 \\ 0 \end{bmatrix} \\ * & -I & 0 & 0 \\ * & * & -Q_x^{-1} & 0 \\ * & * & * & -\mathrm{e}^{2\alpha\tau_m} R_0 \end{bmatrix} \prec 0 \tag{4.89}$$

$$\begin{bmatrix} \Phi_1 + \Pi_1(\tau_m) & \mathcal{Z}_1^T & \mathbf{v}_5^T C_2^T & \mathcal{F}_1{}^T \begin{bmatrix} 0 \\ W_2^T \end{bmatrix} \\ * & -I & 0 & 0 \\ * & * & -Q_x^{-1} & 0 \\ * & * & * & -\mathrm{e}^{2\alpha\tau_m} R_0 \end{bmatrix} \prec 0 \tag{4.90}$$

are sufficient to ensure (4.88). Multiplying (4.89) and (4.90) on the right by

$$\mathrm{diag}(X, X, X, X, X, I, I, I, X_2, X) \tag{4.91}$$

and on the left by its transpose, making $\bar{R}_i = X^T R_i X$, $\bar{S}_i = X^T S_i X$, $\bar{W}_i = X^T W_i X$, $L_i C_i = K_i X_i C_i = K_i C_i X$ for $i = 1, 2$, $L_2 = K_2 X_2$ and $\bar{P} = X^T P X$, result in conditions (4.60) and (4.61).

Then, combining Case 1 and Case 2, from the continuity of the LKF (4.64), if the conditions (4.81) and (4.88) are satisfied it follows that

$$\dot{V} + \bar{\alpha} V(t, x, \zeta) + z^T z - \gamma^2 u^T u - \beta^2 w^T w \leq 0 \tag{4.92}$$

with $\bar{\alpha} = \min\{\lambda, 2\alpha\}$, for $t \geq 0$. Hence, integrating both sides from 0 to ∞ we have

$$\|z\|_{\mathcal{L}_2} \leq \gamma \|u\|_{\mathcal{L}_2} + \beta \|w\|_{\mathcal{L}_2} \tag{4.93}$$

for null initial conditions. Since $\gamma \leq 1$ we recover the condition (3.28) in Proposition 3.1. Moreover, $\mathrm{Tr}(\bar{Q}_e) + \delta \mathrm{Tr}(\bar{Q}_x)$ in (4.57) is used to maximize the inter-event time of the switched dynamic ETC scheme. This completes the proof. □

As discussed in Section 3.3.3, we can set the feedforward gain as $K_2 = K_2^* = \frac{\rho_d}{h}$ as in (3.36) to compensate for the effect of a_{i-1} on error dynamics (3.35). However, since perfect compensation can only be possible in the absence of network-induced delays, instead of fixing $K_2 = K_2^*$, we consider a norm-bounded constraint as

$$\|K_2^* - K_2\|^2 < \kappa^2 \tag{4.94}$$

for a sufficient small $\kappa > 0$. Compared to the strict equality $K_2 = K_2^*$, constraint (4.94) provides more flexibility in searching for values of K_2 close to K_2^*. Note that by Schur complement lemma (BOYD *et al.*, 1994), we can show that inequality (4.94) is equivalent to

$$\begin{bmatrix} \kappa^2 & K_2^* - K_2 \\ * & I \end{bmatrix} \succ 0. \tag{4.95}$$

Using the change of variable $K_2 = L_2 X_2^{-1}$ as in Theorem 4.3 and multiplying (4.95) on the left by $\mathrm{diag}(I, X_2^T)$ and on the right by its transpose, it follows that

$$\begin{bmatrix} \kappa^2 & K_2^* X_2 - L_2 \\ * & X_2^T X_2 \end{bmatrix} \succ 0. \tag{4.96}$$

It is clear that the following constraint directly implies (4.96):

$$\begin{bmatrix} \kappa^2 & K_2^* X_2 - L_2 \\ * & X_2 + X_2^T - I \end{bmatrix} \succ 0. \tag{4.97}$$

As a result, when solving the optimization problem in Theorem 4.3, the LMI (4.97) can be directly included to ensure the constraint (4.94) of the feedforward gain K_2.

Remark 4.2. The design conditions for the Overlapping system is similar to the interconnected system that is not described here but is straightforward from Theorem 4.3

4.6 Static ETC conditions

In both emulation and co-design synthesis conditions, retrieving the static ETM conditions is straightforward and it is comprised in the following Corollary.

Corollary 4.1. *Imposing $\theta \to \infty$, the following static ETM can be directly retrieved from* (4.6)*:*

$$\begin{aligned} s_{0,i} &= 0 \\ t_{k+1,i} &= \inf\{t > t_{k,i} + \varepsilon : \ \Lambda_i(y_{2,i}(t), y_{2,i}(t_{k,i})) > 0\} \end{aligned} \tag{4.98}$$

where $\Lambda_i(y_{2,i}(t), y_{2,i}(t_{k,i}))$ is defined in (4.7)*, and matrices Q_x and Q_e are obtained applying Theorem 4.1 or Theorem 4.3.*

For the choice of the control design parameters in Theorem 4.1, Theorem 4.2 and Theorem 4.3, parameters ε (waiting time) and δ are related to the maximum inter event times, while α is related to the convergence. Considering a grid on those values, the conditions are evaluated, and the parameters are chosen considering the trade-off between convergence and the number of events. Moreover, for Theorem 4.3, the conditions are evaluated varying the value of τ_m (maximum delay), to achieve the maximum values such that the conditions are still feasible.

4.7 Examples

In this section we present illustrative results and comparative studies to show the effectiveness of the proposed dynamic ETC platooning control method. We compare the achieved results utilizing the emulation and co-design conditions. We consider a platoon setup with one leader (Σ_0) and four different followers (Σ_1 to Σ_4). Table 4.1 presents the parameters of the vehicles. In columns Σ_i are the values used to calculate the feedback linearizing control law. In columns $\tilde{\Sigma}_i$ are the values used for the simulation. The rolling resistance coefficient F_r is considered constant for all vehicles, i.e., $F_r = 0.015$ (sec/kg). However, it is assumed to be unknown and is not used to compute the feedback linearizing control law (3.15). Moreover, the length of the vehicles, $L_c = 2.5$ (m), is also known for all vehicles.

For disturbance compensation, we utilized the DOB proposed in Chapter 3 equation (3.12) with $L_i = 50$ for all vehicles and simulations. The distance policy parameters from (3.8) are set as $r_i = 2.5$ (m) for $i = 1, 2, 3, 4$, $h = 0.6$ (sec) and the desired time constant is $\rho_d = 0.1$.

We divided the examples in two study cases based on the two approaches discussed in Section 4.5.

- Case 1 – Emulation) We study the case of communication without delay and ETC designed based on Remark 4.1 presented in Section 4.5.2. In the examples we consi-

Table 4.1 – Nominal values of the vehicle parameters and respective true values.

Vehicle	r	$\boldsymbol{m}$	$\boldsymbol{h}_w$	$\boldsymbol{J}_r$	$\boldsymbol{J}_e$	$\boldsymbol{R}_g$	$\boldsymbol{B}$	$\boldsymbol{C}$	ρ
Σ_0		1724	0.28	0.75	0.14	0.10	7.35	0.05	0.05
$\tilde{\Sigma}_0$		1724	0.25	1.05	0.14	0.13	8.09	0.06	0.08
Σ_1	2.5	2241	0.63	0.97	0.35	0.18	13.96	0.11	0.10
$\tilde{\Sigma}_1$		2017	0.51	0.68	0.46	0.18	11.17	0.16	0.09
Σ_2	2.5	2930	0.41	1.57	0.27	0.20	11.02	0.08	0.08
$\tilde{\Sigma}_2$		2637	0.33	1.26	0.40	0.30	8.82	0.05	0.06
Σ_3	2.5	3620	0.63	0.82	0.27	0.11	13.96	0.11	0.12
$\tilde{\Sigma}_3$		3258	0.89	1.15	0.40	0.08	15.36	0.16	0.12
Σ_4	2.5	3965	0.52	1.72	0.24	0.11	8.09	0.06	0.08
$\tilde{\Sigma}_4$		5947	0.63	2.41	0.29	0.14	11.32	0.08	0.11

der the overlapping model $\Xi_{i,i-1}$ (3.42) and the controller defined a priori according to Remark 3.2 and Remark 3.1.

- Case 2 – Co-design) we consider the communication delay and the ETC is designed based on Theorem 4.3 presented in Section 4.5.4 considering the Interconnected model $\Sigma_{i,i-1}$ (3.22).

4.7.1 Case 1 – Emulation

For the emulation approach as discussed in Section 4.5.2 we consider the overlapping system $\Xi_{i,i-1}$ defined in Section 3.3.4, equation (3.50). The controller gains $\bar{K}_1$ and $\bar{K}_2$ are chosen as

$$K_1 = \begin{bmatrix} 0.2 & 0.7 & -0.42 & 0 \end{bmatrix}, \quad K_2 = \begin{bmatrix} -0.2 & 1.2 \end{bmatrix}.$$

the event-triggering condition (4.6) is designed using Theorem 4.1. The optimization problem (4.17) results in $\beta = 2.5$, and

$$Q_e = \begin{bmatrix} 2.77 & -16.61 \\ * & 99.65 \end{bmatrix}, \quad Q_x = \begin{bmatrix} 0.0145 & -0.0132 \\ * & 0.0143 \end{bmatrix}. \tag{4.99}$$

Table 4.2 – ETC and Theorem 4.1 design parameters.

Parameter	ε	δ	α	θ	λ
Value	0.1	0.005	0.01	5	0.01

Figure 4.4 shows the velocity v, the acceleration a, and the distance policy error Δp for each vehicle in the considered platoon. Note that the vehicles in the platoon are able

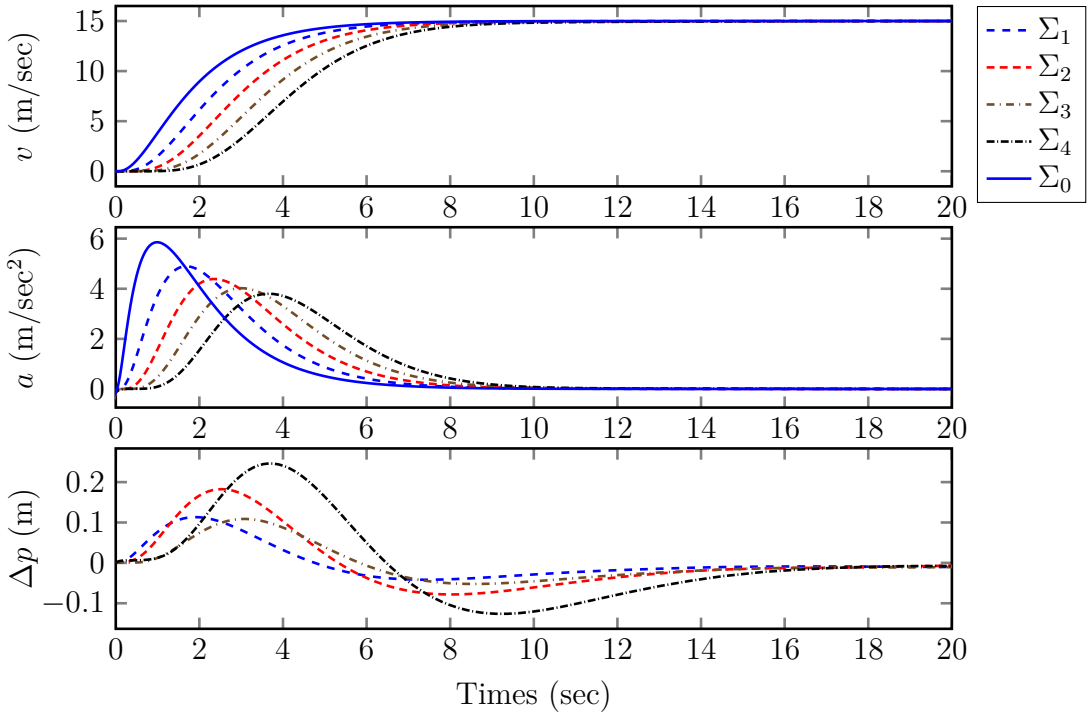

Figure 4.4 – Emulation – Test 1. Velocity v, acceleration a and distance policy error Δp of the platooning vehicles obtained with the switched dynamic ETM (4.6), designed based on Theorem 4.1.

to follow the leader velocity and the distance policy converges to zero without significant oscillations.

Now considering a time-varying velocity reference for a longer simulation time interval of $t_{\text{sim}} = 320$ (sec), as illustrated in Figure 4.5, we observe that the follower vehicles can still correctly follow the leader and maintain the specified distance policy. Figure 4.5 also displays the inter-event time for transmissions to vehicles Σ_1 to Σ_4. Notice that every time the leader changes its velocity, the inter-event time is reduced. However, as the vehicles reach a steady state, the number of transmissions considerably decreases, as evident in the last steady state after 220 seconds.

To further evaluate the platooning control performance, we compare the four following ETMs under the same test conditions as in Figure 4.4:

- Proposed dynamic ETM, designed with Theorem 4.1.
- Dynamic ETM, proposed in (DOLK *et al.*, 2017). Following the same search procedure as in (DOLK *et al.*, 2017), the parameters of the ETM can be determined, as depicted in Table 4.3.
- Static ETM, discussed in Corollary 4.1.
- Periodic ETM, designed with Theorem 4.2.

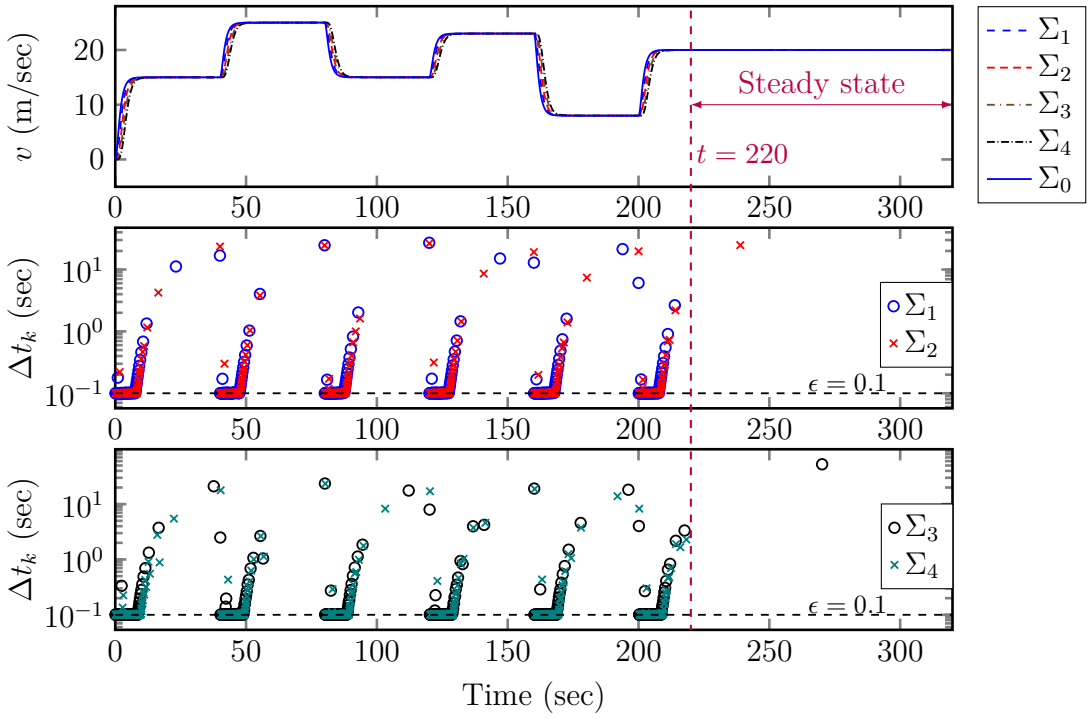

Figure 4.5 – Emulation – Test 1. Platooning with a time-varying velocity reference, and inter-event time for each vehicle obtained with the switched dynamic ETC design from Theorem 4.1.

Table 4.3 – ETM parameters for the ETM in (DOLK *et al.*, 2017).

Parameter	γ	$\tau_{\text{miet}}(\varepsilon)$	$\phi_1(0)$	ϵ	λ	ρ	$\tau_{\text{mad}}(\tau_m)$
Value	8.442	0.072	8.557	0.5	0.305	0.04	0.026

In Figure 4.6, we observe that the distance policy errors do not show significant differences among the considered event-triggering mechanisms. However, in terms of communication, there is a significant difference, as shown in Table 4.4, which summarizes the average time between events during the transient phase T_{avg}, and the number of events N_{event} obtained with the four ETC schemes. In particular, the switched dynamic ETC scheme shows a significant difference compared to the other cases, with almost less than a third of the number of events.

Furthermore, in Table 4.4, we present the ratio of total simulation time to the number of events, denoted as $T_{\text{sim}}/N_{\text{event}}$, with $T_{\text{sim}} = 320$ (sec). When comparing this value with T_{avg}, a significant difference is observed only in the proposed switched dynamic ETC scheme. This is mainly due to the long interval without triggering communication, which is not included in the average. Furthermore, the dynamic ETC method presented in (DOLK *et al.*, 2017) yields a control performance similar to that of the compared static ETC scheme. To better illustrate this difference in triggering communication, Figure 4.7 depicts the inter-event times obtained with different ETMs. Except for the proposed method, the

number of events of the other compared ETMs does not reduce as the platooning system achieves steady state, and the transmission intervals are close to the minimum time.

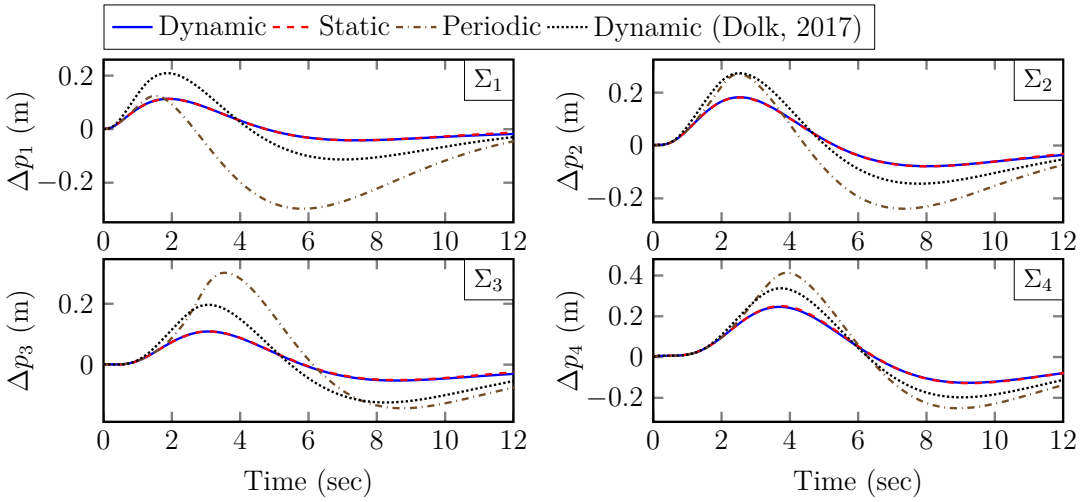

Figure 4.6 – Emulation – Test 2. Distance policy errors Δp_i obtained using the four compared ETMs.

Table 4.4 – Average time between events during the transient phase T_{avg}, number of events N_{event}, and average events during the total simulation time $T_{\text{sim}}/N_{\text{event}}$ obtained with four ETC schemes.

ETC	Indicator	Vehicle			
		1	2	3	4
Dynamic	T_{avg} (sec)	0.40	0.38	0.37	0.35
	N_{event}	534	559	589	617
	$T_{\text{sim}}/N_{\text{event}}$	0.60	0.57	0.54	0.52
Static	T_{avg} (sec)	0.10	0.11	0.11	0.11
	N_{event}	3004	2817	2606	2729
	$T_{\text{sim}}/N_{\text{event}}$	0.11	0.11	0.12	0.12
Periodic	T_{avg} (sec)	0.20	0.22	0.23	0.23
	N_{event}	1953	1701	1385	1439
	$T_{\text{sim}}/N_{\text{event}}$	0.16	0.19	0.23	0.22
Dynamic (DOLK *et al.*, 2017)	T_{avg} (sec)	0.11	0.11	0.11	0.11
	N_{event}	2954	2912	2843	2885
	$T_{\text{sim}}/N_{\text{event}}$	0.11	0.11	0.11	0.11

4.7.2 Case 2 – Co-design

For the co-design approach from Section 4.5.4 the controller gains K_1 and K_2 in (4.13) and the event-triggering condition (4.6) are designed using Theorem 4.3 including the LMI constraint (4.97). Moreover, in all simulations, for each transmission interval, the delay $\tau^*_{k,i}$ is randomly selected between 0 and $\tau_m = 0.006$. Solving the optimization problem

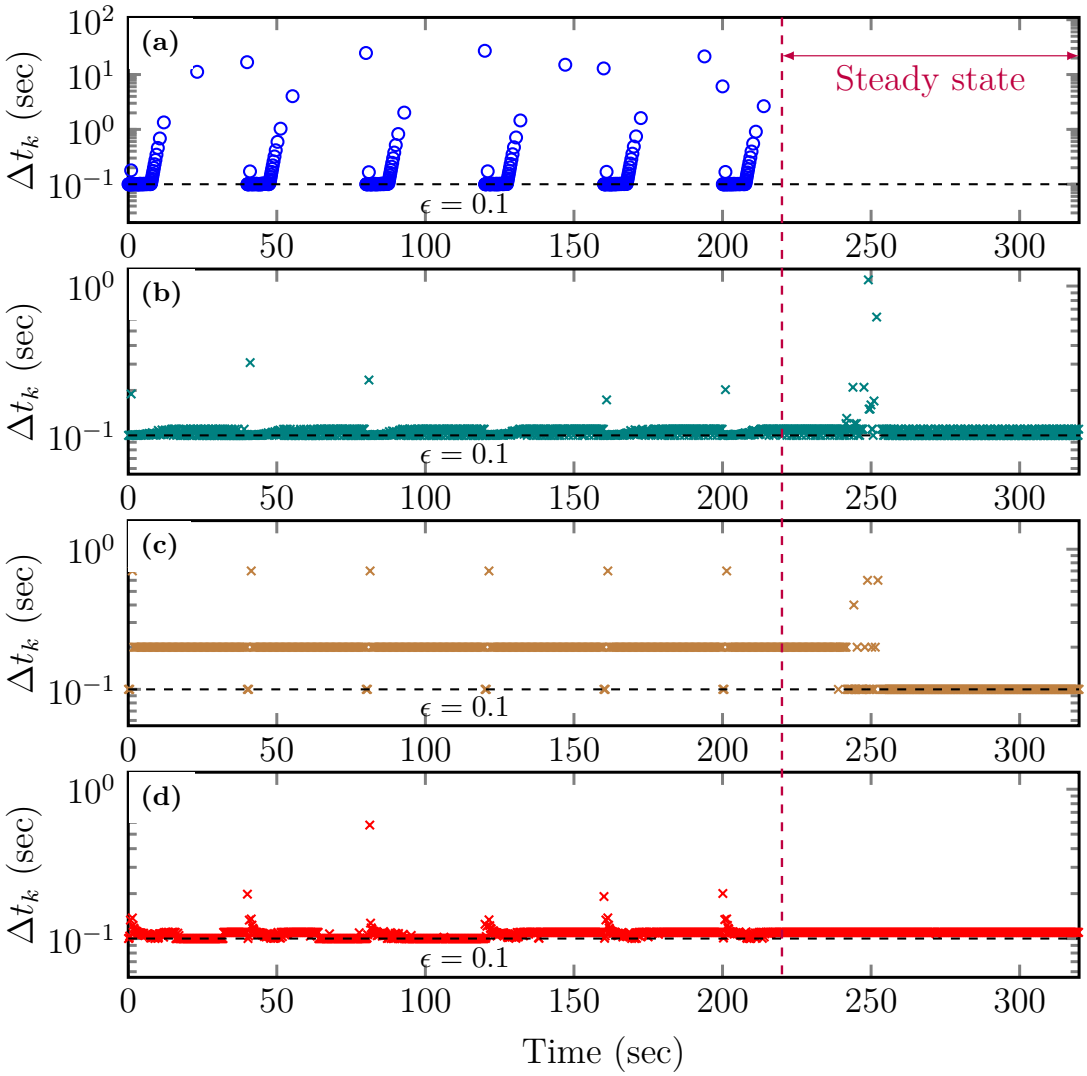

Figure 4.7 – Emulation – Test 2. Inter-event times obtained using the four compared ETMs. (a) Proposed dynamic ETM, (b) Static ETM, (c) Periodic ETM, (d) Dynamic ETM (DOLK *et al.*, 2017).

(4.57) with design parameters provided in Table 4.5, we obtain $\beta = 6.2$, $Q_e = 0.0341$, $Q_x = 1.1 \times 10^{-3}$, and

$$K_1 = \begin{bmatrix} 0.352 & 1.576 & -0.1778 \end{bmatrix}, \quad K_2 = 0.1598. \tag{4.100}$$

Table 4.5 – ETC and Theorem 4.3 design parameters.

Parameter	ε	τ_m	δ	α	θ	λ	β_1	β_2	κ	K_2^*
Value	0.15	0.06	0.1	0.006	1	0.5	0.3	0.2	10^{-4}	0.164

Figure 4.8 shows the velocity v, acceleration a, and the distance policy error Δp for each vehicle in the platoon. Note that the vehicles are able to follow the leader velocity, and the distance policy converges to zero without significant oscillations.

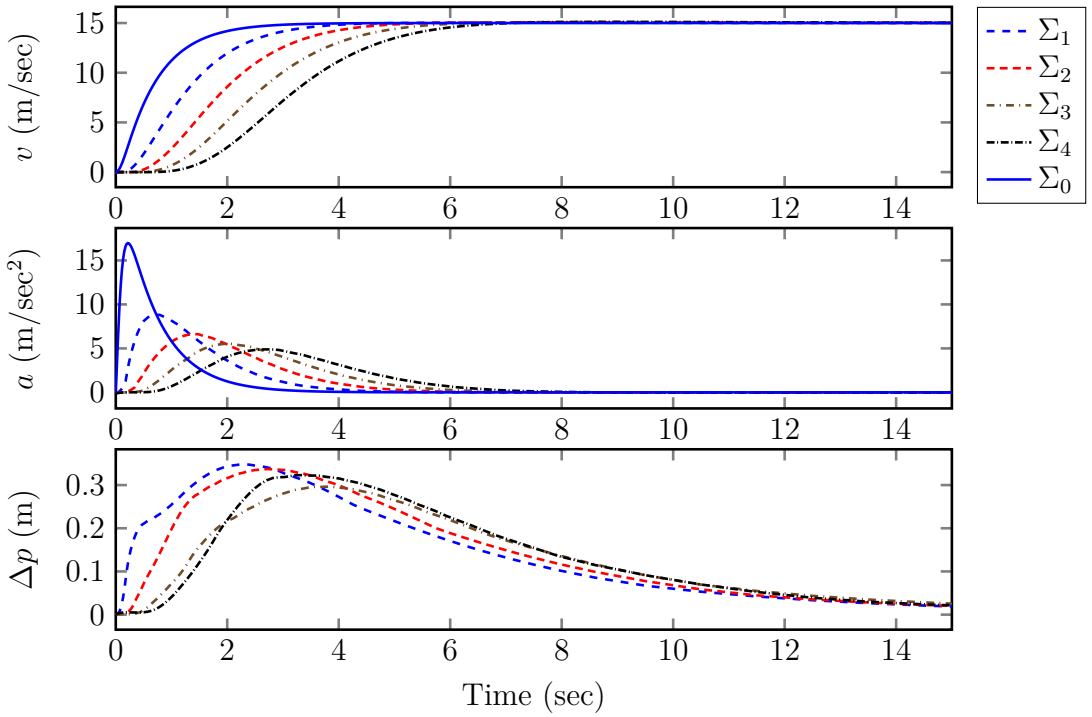

Figure 4.8 – Co-design – Test 2. Velocity v, acceleration a and distance policy error Δp of the platooning vehicles obtained with the switched dynamic ETM (4.6), designed based on Theorem 4.3.

Extending the simulation time to $t_{\text{sim}} = 240$ (sec) and considering a time-varying velocity reference, as depicted in Figure 4.9, we observe that despite constant changes in velocity, the follower vehicles can still accurately follow the leader and maintain the specified distance policy. Figure 4.9 also displays the inter-event time for transmissions to vehicles Σ_1 to Σ_4.

To further evaluate the platooning control performance, we compare the three following ETMs under the same test conditions as in Figure 4.8

- Proposed dynamic ETC, designed with Theorem 4.3.
- Dynamic ETC (controller and ETC), proposed in (DOLK *et al.*, 2017) with the ETC parameters provided in Table 4.6.
- Static ETC, discussed in Corollary 4.1.

Table 4.6 – ETM parameters for the ETM in (DOLK *et al.*, 2017).

Parameter	γ	$\tau_{\text{miet}}(\varepsilon)$	$\phi_1(0)$	ϵ	λ	ρ	$\tau_{\text{mad}}(\tau_m)$
Value	8.442	0.072	8.557	0.5	0.305	0.04	0.026

In Figure 4.10, we observe that the distance policy errors do not show significant differences among the considered event-triggering mechanisms. Examining Table 4.5 and

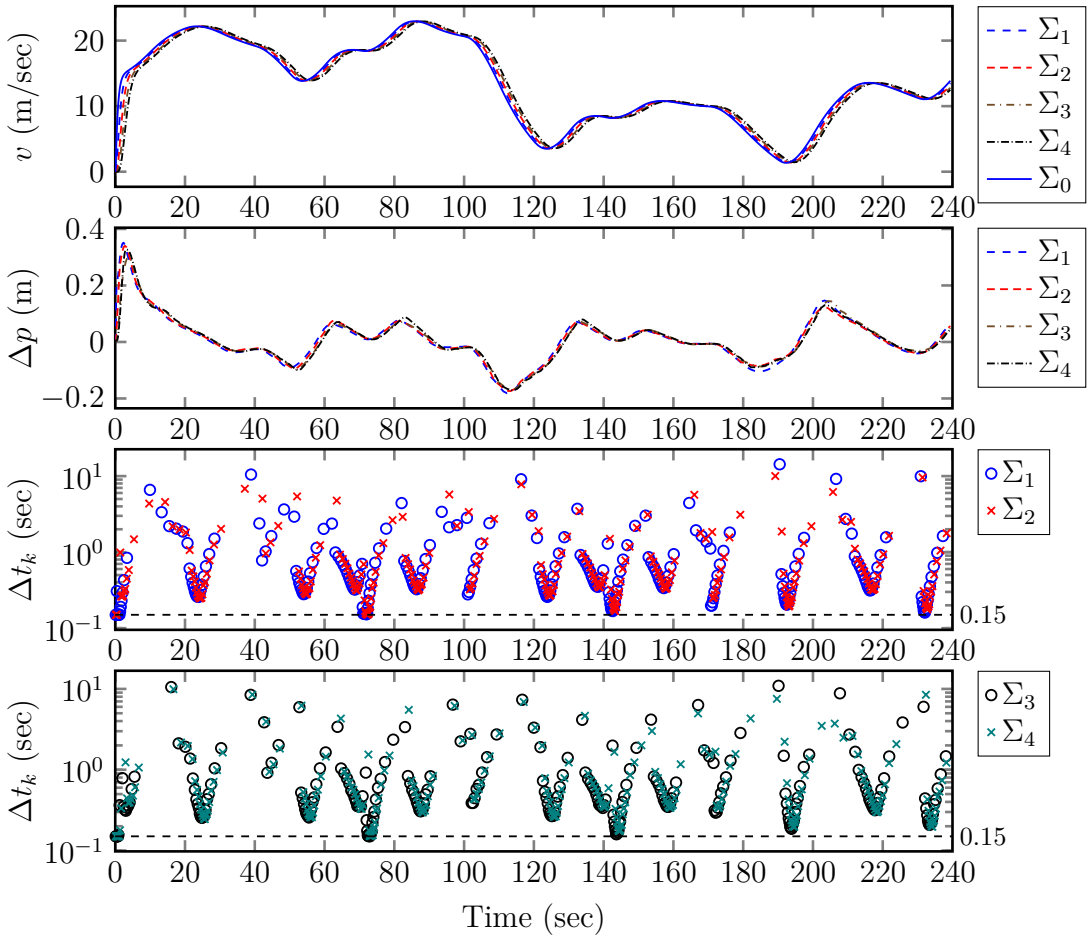

Figure 4.9 – Co-design – Test 2. Platooning with a time-varying velocity reference, and inter-event time for each vehicle obtained with the switched dynamic ETC design from Theorem 4.3.

Table 4.6 and comparing the maximum delay and waiting time (respectively, the τ_{mad} and τ_{meit} for (DOLK *et al.*, 2017)), the proposed approach results in a maximum delay of 0.06 (τ_m) and minimum inter event time of 0.15 (ε), which is more than double of the values achieved by (DOLK *et al.*, 2017).

In terms of communication, there is a significant difference between the approaches. In Figure 4.11 we show the inter-event time for each approach, where it is clear the difference in terms of number of events. For a better comparison, Table 4.7 summarizes the average time between events T_{avg}, and the number of events N_{event} obtained with the three ETC schemes. The switched dynamic ETC scheme, when compared to the static case, renders 2/3 of the events and, consequently, a better average transmission time (T_{avg}). Compared to (DOLK *et al.*, 2017), both dynamic and static ETC present significantly less events, with the dynamic ETM resulting in a tenth of the number of events than the ETM of (DOLK *et al.*, 2017).

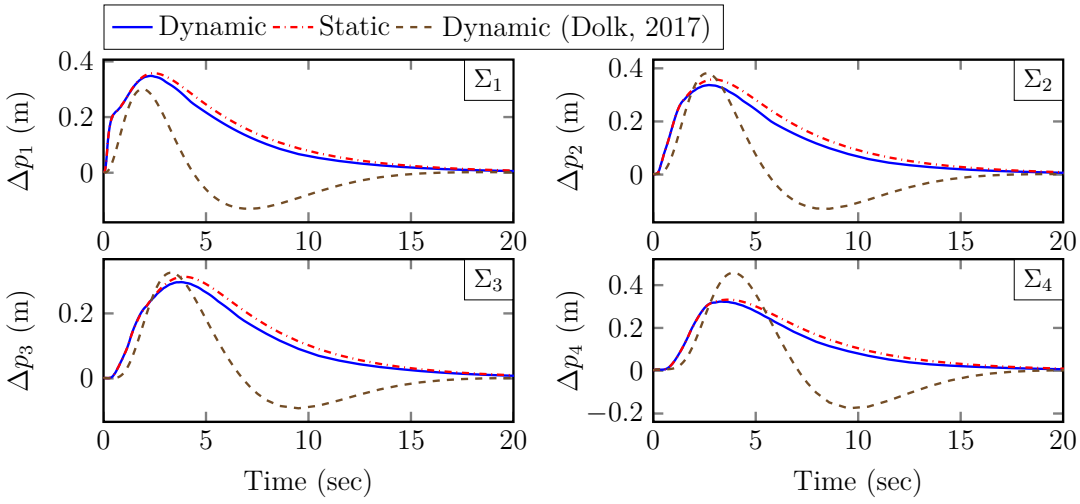

Figure 4.10 – Co-design – Test 2. Distance policy errors Δp_i obtained using the three different ETCs.

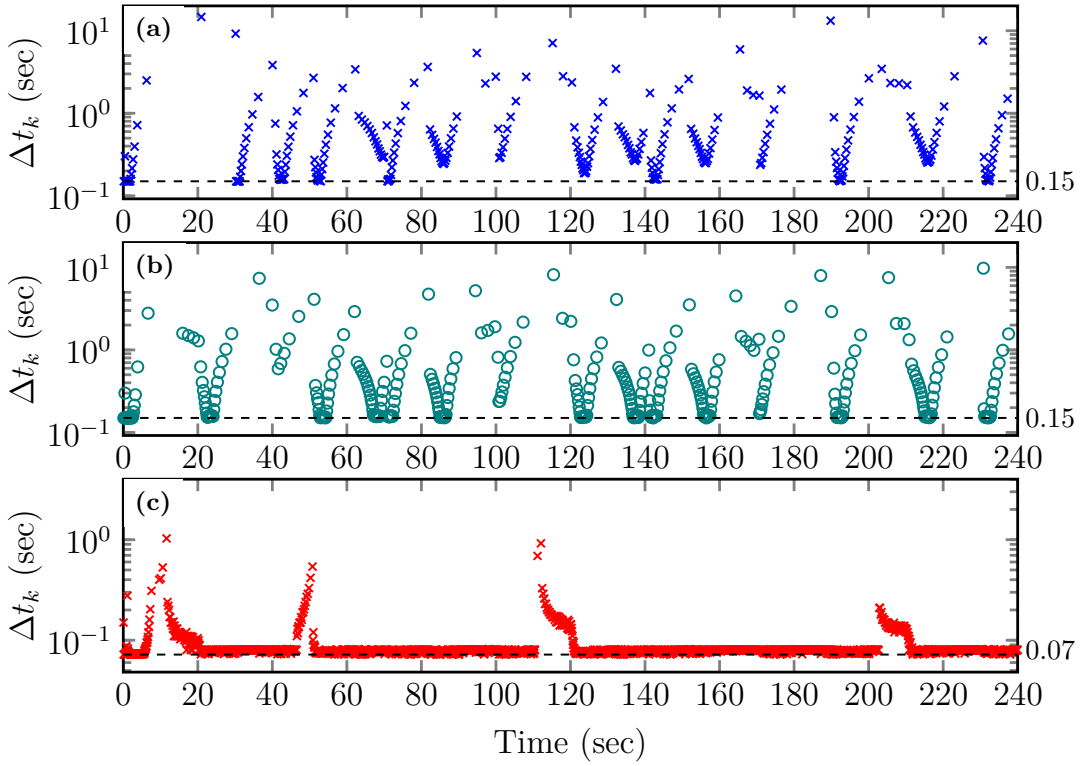

Figure 4.11 – Co-design – Test 2. Inter-event times obtained using the three ETCs. (a) Proposed dynamic ETC, (b) Static ETC, (c) Dynamic ETC of (DOLK *et al.*, 2017).

Table 4.7 – Average time between events during the transient phase T_{avg}, number of events N_{event}, obtained with three ETC schemes.

ETC	Indicator	Vehicle			
		1	2	3	4
Dynamic	T_{avg} (sec)	0.92	0.93	0.93	0.92
	N_{event}	256	255	254	257
Static	T_{avg} (sec)	0.61	0.62	0.61	0.61
	N_{event}	384	379	383	386
Dynamic (DOLK *et al.*, 2017)	T_{avg} (sec)	0.08	0.09	0.08	0.08
	N_{event}	2849	2830	2875	2894

4.8 Conclusion

Considering the control communication between vehicles in the predecessor-follower flow topology, a switched dynamic ETC method has been proposed for heterogeneous platoons. To counteract the uncertainties within the platooning system, a DOB-based uncertainty estimation is incorporated into the feedback linearization control law. The communication between vehicles is established based on a dynamic event-triggering condition with a minimum time to ensure Zeno-free behavior accounting for the transmission delays. For platooning control design, we model the system with dynamic ETC as a switching interconnected system, representing the interaction between adjacent vehicles. Subsequently, using a Lyapunov-Krasovskii functional time delay relaxation technique, sufficient LMI conditions are derived to ensure $\mathcal{L}_2$ stability between consecutive vehicles, as well as $\mathcal{L}_2$ string stability. Through simulations and comparisons, we demonstrate that the proposed DOB-based event-triggered platooning control method can ensure string stability despite the modeling uncertainties. Furthermore, the dynamic switched ETC can significantly reduce the amount of communication compared to other ETM conditions.

5 ETC feedback linearization

5.1 Introduction

As explored in Chapter 3 and Chapter 4, feedback linearization is an useful control technique that can be used in several applications such as, robot manipulators (BAGHERI *et al.*, 2019), planar collective motion (SEPULCHRE *et al.*, 2007), marine vehicles (PALIOTTA *et al.*, 2019), maglev positioning system (NIELSEN *et al.*, 2010) and double rotors (CHANG *et al.*, 2019).

For the classical feedback linearization approach, the state measurement and the control law must be continuously updated (KHALIL, 2002; ISIDORI, 1995). For example, in the platoon application in the previous chapters, the states necessary for computing the linearizing control law were assumed to be available in real time. However, it can appear that, the information used to compute, the feedback linearizing control law is issued from a sampling process (GOEBEL *et al.*, 2009). Since the control action is computed with sampled signals, the system nonlinearities can no longer be perfectly canceled via feedback linearization between samples. This gives rise to the presence of nonlinear mismatch terms in the expression of the closed-loop system, leading to a new challenge for the control design (MAITY; BARAS, 2015; STÖCKER; LUNZE, 2011).

In the context of event-triggered control via feedback linearization the same phenomena occurs, due to the sample and hold nature of the event-triggering conditions. In addition, the event-triggering condition has to be designed together with the feedback gain to guarantee closed-loop stability. The authors in (STÖCKER; LUNZE, 2011) address an event-based feedback linearization problem, where a reference model is considered to compute the control law and the event-triggering condition. Specifically, the control signal is continuously computed in real-time using a reference model and the system state is updated whenever the event-triggering condition holds. Based on a Lyapunov function, both the controller and the event-triggering condition are proposed for affine nonlinear systems in (MAITY; BARAS, 2015). When the controlled plant is not completely known, the system unknown nonlinearities have been approximated using neural networks (SAHOO *et al.*, 2016; GAO *et al.*, 2020; CHEN *et al.*, 2021) or online Gaussian learning process (UMLAUFT; HIRCHE, 2020) for event-based control design. Both static and dynamic event-triggering conditions are considered for the control results in (XU *et al.*, 2020). However, the nonlinear mismatches, caused by the use of sampled state measurements for the computation of nonlinear control laws, are not considered in the previous event-triggered control approaches. This can lead to instability of the closed-loop systems as illustrated in this Chapter.

Motivated by the above theoretical and practical issues, we propose conditions to co-design feedback linearization controllers and event-triggered mechanisms for nonlinear MIMO systems. Based on Lyapunov stability theory, the design conditions, to guarantee the closed-loop asymptotic stability while minimizing the inter event time (IET), are reformulated as optimization problems under linear matrix inequality (LMI) constraints. Both *full* and *partial* feedback linearization cases are considered for the event-triggered control design. In particular, applying the fundamental theorem of calculus and a polytopic approach, some nonlinear mismatches between continuous and sampled nonlinearities are *explicitly* taken into account in the LMI-based control design instead of being incorporated in the event-triggering conditions, allowing conditions to be extrapolated to other triggering mechanisms. Moreover, under some assumptions on Lipschitzian properties of the system nonlinearities, the ETM is able to ensure Zeno-free behavior (DONKERS; HEEMELS, 2012) in closed-loop.

The main contributions presented in this Chapter can be summarized as follows.

- We propose sufficient conditions to co-design feedback controllers and event-triggered mechanisms for feedback linearizable MIMO systems
- The mismatches between continuous and sampled nonlinearities are explicitly considered in the co-design to prevent instability. The co-design conditions are recast as LMI-based optimization problems to minimize IET.
- A lower bound for IET can be guaranteed for systems with Lipschitzian nonlinearities to avoid Zeno behavior.

5.2 Preliminaries

In this section we present preliminaries on feedback linearization control of MIMO systems required throughout this chapter.

5.2.1 Feedback linearization

Consider a nonlinear MIMO system affine in the control given by

$$\begin{aligned} \dot{x} &= f(x) + g(x)u \\ y &= h(x), \quad x \in \mathcal{X} \end{aligned} \tag{5.1}$$

where $x \in \mathbb{R}^{n_x}$, $u \in \mathbb{R}^{n_u}$ and $y \in \mathbb{R}^{n_y}$ are respectively the system states, control input and system output. The set $\mathcal{X} \subset \mathbb{R}^{n_x}$ is a compact set that contains the origin, which can represent either the set of interest or a set where the linearization is valid. The nonlinear vector valued functions $f(x)$, $g(x)$, $h(x)$ are smooth functions such that $f : \mathbb{R}^{n_x} \to \mathbb{R}^{n_x}$,

$g : \mathbb{R}^{n_x} \to \mathbb{R}^{n_u}$ and $h : \mathbb{R}^{n_x} \to \mathbb{R}^{n_y}$. We assume that in the set of interest, $x = 0$ is the unique equilibrium point, i.e., $f(0) = 0$ and $f(x) \neq 0$ for all $x \in \mathcal{X} - \{0\}$.

Definition 5.1. *System* (5.1) *is called linearizable if there is a diffeomorphism* $T : \mathcal{X} \to \mathcal{Z}$ *which maps* $z = T(x)$ *and leads system* (5.1) *into*

$$\dot{z} = Az + B[\alpha(x) + \gamma(x)u] \tag{5.2}$$

with the pair (A, B) *controllable and* $\gamma : \mathcal{X} \to \mathbb{R}^{n_y \times n_u}$ *nonsingular for all* $x \in \mathcal{X}$ *(ISIDORI, 1995).*

For MIMO systems, one possible methodology to achieve this transformation is to take the time derivative of each output until the input signal appears (ISIDORI, 1995). To ensure the linearization of system (5.1) we assume the following

Assumption 5.1. We assume that $f(x)$ and $g(x)$ satisfies the involutive condition (KHALIL, 2002) for $x \in \mathcal{X}$.

Remark 5.1. Although Assumption 5.1 is restrictive, it is fundamental to ensure the existence of a static feedback linearizing control law. Some relaxations are discussed in the literature, however these are only applicable to systems with particular structures. Addressing the problem considering these structures is beyond the scope of this work and we consider only the cases of systems that can be feedback linearized with static conditions.

Following the procedure as described in (ISIDORI, 1995), we chose the output $y_i = h_i(x)$, with $i \in \{1, 2, \ldots, n_y\}$. Taking the first time derivative results in

$$\begin{aligned} \dot{y}_i = \frac{dh_i(x)}{dt} &= \frac{\partial h_i}{\partial x} f(x) + \frac{\partial h_i}{\partial x} g(x)u \\ &= \mathcal{L}_f h_i(x) + \mathcal{L}_g h_i(x)u \end{aligned} \tag{5.3}$$

where $\mathcal{L}_g h_i(x)u = \sum_{i=1}^{n_u} \mathcal{L}_{g_j} h_i(x)u_j$ and $\mathcal{L}_{g_j} h_i(x)$ is the Lie derivative along the j-th column of $g(x)$. Assume that $\mathcal{L}_g h_i(x) = 0$, for $\forall x \in \mathcal{X}$, the derivative of y_i is taken until the control input appears, leading to $y_i^{(r_i)} = \mathcal{L}_f^{(r_i)} h_i(x) + \mathcal{L}_g \mathcal{L}_f^{(r_i-1)} h_i(x)u$, where $\mathcal{L}_g \mathcal{L}_f^{(r_i-1)} h_i(x) \neq 0$ and $y_i^{(r_i)}$ is the r_i-th time derivative of y_i. Repeating the outlined procedure to all outputs, we can group all equations in the form

$$\begin{bmatrix} y_1^{(r_1)} \\ y_2^{(r_2)} \\ \vdots \\ y_{n_y}^{(r_{n_y})} \end{bmatrix} = \begin{bmatrix} \mathcal{L}_f^{(r_1)} h_1(x) \\ \mathcal{L}_f^{(r_2)} h_2(x) \\ \vdots \\ \mathcal{L}_f^{(r_{n_y})} h_{n_y}(x) \end{bmatrix} + \begin{bmatrix} \mathcal{L}_g \mathcal{L}_f^{(r_1-1)} h_1(x) \\ \mathcal{L}_g \mathcal{L}_f^{(r_2-1)} h_2(x) \\ \vdots \\ \mathcal{L}_g \mathcal{L}_f^{(r_{n_y}-1)} h_{n_y}(x) \end{bmatrix} u, \tag{5.4}$$

defining $\alpha_i(x) = \mathcal{L}_f^{(r_i)}$ and $\gamma_i = \mathcal{L}_g\mathcal{L}_f^{(r_i-1)}$ we rewrite (5.4) as

$$\begin{bmatrix} y_1^{(r_1)} \\ y_2^{(r_2)} \\ \vdots \\ y_{n_y}^{(r_{n_y})} \end{bmatrix} = \begin{bmatrix} \alpha_1(x) + \gamma_1(x)u \\ \alpha_2(x) + \gamma_2(x)u \\ \vdots \\ \alpha_{n_y}(x) + \gamma_{n_y}(x)u \end{bmatrix} = \alpha(x) + \gamma(x)u. \tag{5.5}$$

The number of derivatives r_{n_i}, required for the control input to appear for the first time in $y_i^{n_i}$ is called the relative degree of the output y_i. The sum of all relative degrees will define the relative degree of the system and will be important to find the diffeomorphism $T(x)$ from Definition 5.1. Moreover, as a requirement to perform the linearization, we assume the following regarding $\gamma(x)$

Assumption 5.2. The matrix $\gamma(x)$ is assumed to be non-singular for all $x \in \mathcal{X}$

Remark 5.2. This assumption can be relaxed assuming that $\gamma(0)$ is non singular. Since $\gamma(x)$ is continuous, there exists a neighborhood of the origin $\mathcal{X}_0$ that is a subset of $\mathcal{X}$ such that $\gamma(x)$ is non-singular for all $x \in \mathcal{X}_0$. In this case the linearization is only valid in $\mathcal{X}_0$.

Before the next step we present a simple example to illustrate the procedure so far.

Illustrative example part 1 – System and derivatives

Consider the following nonlinear MIMO system

$$\begin{cases} \dot{x}_1 = x_2 \\ \dot{x}_2 = x_1^2 + x_2^2 + u_1 + x_2u_2 \\ \dot{x}_3 = -x_1 + \sin(x_3) + u_2 \\ y_1 = x_1 \\ y_2 = x_3. \end{cases} \tag{5.6}$$

In this case, the approach is straightforward as the system is already in the feedback linearized form. To verify, we take the time derivative of y_1 and y_2, which results in

$$\begin{aligned} \dot{y}_1 &= \dot{x}_1 = x_2 \\ \dot{y}_2 &= \dot{x}_3 = -x_1 + \sin(x_3) + u_2 \end{aligned}. \tag{5.7}$$

Notice the control input u_2 already appeared in the first derivative of y_2, thus $r_2 = 1$ (the relative degree of output y_2). For y_1, differentiating it once more give us

$$\ddot{y}_1 = \dot{x}_2 = x_1^2 + x_2^2 + u_1 + x_2u_2 \tag{5.8}$$

where both control inputs u_1 and u_2 appear. Since the procedure stopped at the second derivative of y_1, then $r_1 = 2$ (the relative degree of output y_1). As the control input is

achieved for both outputs, the procedure is finished and we have that

$$\begin{bmatrix}\ddot{y}_1\\ \dot{y}_2\end{bmatrix} = \underbrace{\begin{bmatrix}x_1^2+x_2^2\\ -x_1+\sin(x_3)\end{bmatrix}}_{\alpha(x)} + \underbrace{\begin{bmatrix}1 & x_2\\ 0 & 1\end{bmatrix}}_{\gamma(x)}\begin{bmatrix}u_1\\ u_2\end{bmatrix} \tag{5.9}$$

This example will be recalled in subsequent steps of the feedback linearization procedure

The next step is to find a diffeomorphism $T(x)$ that maps the nonlinear system (5.1) into the linear system (5.2), i.e., find $T(x)$ such that

$$\dot{x} = f(x) + g(x)u \quad \overset{T(x)}{\Longleftrightarrow} \quad \dot{z} = Az + B[\alpha(x) + \gamma(x)u], \tag{5.10}$$

Considering each output and its derivatives, a transformation can be achieved by considering $y_i^{(j)}$ for $j = 0, \ldots, r_i - 1$ as states of the transformed system, thus, we can write

$$z_i = \psi_i(x) = \begin{bmatrix} y_i \\ \dot{y}_i \\ \vdots \\ y_i^{(r_i-1)}\end{bmatrix}, \tag{5.11}$$

with $z_i = \text{col}\{z_{i,1},\ z_{i,2},\ \ldots,\ z_{i,r_{n_i}}\}$ the linearized states. Differentiating z_i with respect to the time, it follows from (5.5) and (5.11) that

$$\dot{z}_i = \begin{bmatrix}\dot{y}_i\\ \ddot{y}_i\\ \vdots\\ y_i^{(r_i)}\end{bmatrix} = \begin{bmatrix} z_{i,2}\\ z_{i,3}\\ \vdots\\ \alpha_i(x)+\gamma_i(x)u\end{bmatrix}. \tag{5.12}$$

which can finally be written as

$$\begin{aligned}\dot{z}_i &= A_i z_i + B_i[\alpha_i(x) + \gamma_i(x)u]\\ y_i &= C_i z_i\end{aligned} \tag{5.13}$$

where

$$A_i = \begin{bmatrix}0 & 1 & 0 & \ldots & 0\\ \vdots & \vdots & \vdots & \ddots & \vdots\\ 0 & 0 & 0 & \ldots & 1\\ 0 & 0 & 0 & \ldots & 0\end{bmatrix},\quad B_i = \begin{bmatrix}0\\ \vdots\\ 0\\ 1\end{bmatrix},\quad C_i = \begin{bmatrix}1 & 0 & \ldots & 0\end{bmatrix}. \tag{5.14}$$

Illustrative example part 2 – Transformation

Recalling (5.8) in the illustrative example, the first and second derivatives of y_1 are

$$\begin{aligned} \dot{y}_1 &= x_2 \\ \ddot{y}_1 &= x_1^2 + x_2^2 + u_1 + x_2 u_2 \end{aligned} \tag{5.15}$$

thus, the transformation regarding output y_1 is

$$z_1 = \psi_i(x) = \begin{bmatrix} y_1 \\ \dot{y}_1 \end{bmatrix} = \begin{bmatrix} x_1 \\ x_2 \end{bmatrix} \tag{5.16}$$

that is $\psi_i(x) = x$. Hence, for y_1 and its derivative we can write

$$\dot{z}_1 = \underbrace{\begin{bmatrix} 0 & 1 \\ 0 & 0 \end{bmatrix}}_{A_1} z_1 + \underbrace{\begin{bmatrix} 0 \\ 1 \end{bmatrix}}_{B_1} \Big(\underbrace{(x_1^2 + x_2^2)}_{\alpha_1(x)} + \underbrace{\begin{bmatrix} 1 & x_1 \end{bmatrix}}_{\gamma_1(x)} u \Big) \tag{5.17}$$

repeating the same steps for output y_2 gives

$$z_2 = \underbrace{-x_1 + \sin(x_3)}_{\alpha_2(x)} + \underbrace{\begin{bmatrix} 0 & 1 \end{bmatrix}}_{\gamma_2(x)} u \tag{5.18}$$

where $A_2 = 0$ and $B_2 = 1$.

As previously commented the system relative degree is given by $r = \sum_{i=1}^{n_y} r_i$ where r_i is the relative degree of each output. Depending of its value, two cases can be distinguished for control design: i) full feedback linearization ($r = n_x$), and ii) partial feedback linearization ($r < n_x$).

Case 1: If $r = n_x$, then system (5.1) is fully feedback linearizable and the transformation can be defined as $z = \psi(x)$ where $z = \text{col}\{z_1, z_2, \ldots, z_{n_y}\}$ represents the states of the linearized dynamics. Thus the transformed system can be defined from (5.13) as

$$\begin{aligned} \dot{z} &= Az + B[\alpha(x) + \gamma(x)u] \\ y &= Cz \end{aligned} \tag{5.19}$$

with matrices $A = \text{diag}(A_1,\ A_2,\ \ldots,\ A_{n_y})$, $B = \text{diag}(B_1,\ B_2,\ \ldots,\ B_{n_y})$ and $C = \text{diag}(C_1,\ C_2,\ \ldots,\ C_{n_y})$.

Illustrative example part 3

For the illustrative example the output relative degrees are $r_1 = 2$ and $r_2 = 1$ hence the system relative degree is $r = 3$, which is equal to the number of states, therefore the system is fully feedback linearizable. From (5.17) and (5.18) we have

that the diffeomorphism is $T(x) = x$ and

$$A = \left[\begin{array}{c|c} A_1 & 0 \\ \hline 0 & A_2 \end{array}\right] = \left[\begin{array}{cc|c} 0 & 1 & 0 \\ 0 & 0 & 1 \\ \hline 0 & 0 & 0 \end{array}\right], \quad B = \left[\begin{array}{c|c} B_1 & 0 \\ \hline 0 & B_2 \end{array}\right] = \left[\begin{array}{c|c} 0 & 0 \\ 1 & 0 \\ \hline 0 & 1 \end{array}\right] \tag{5.20}$$
$$\alpha(x) = \begin{bmatrix} \alpha_1(x) \\ \alpha_2(x) \end{bmatrix} = \begin{bmatrix} x_1^2 + x_2^2 \\ -x_1 + \sin(x_3) \end{bmatrix}, \quad \gamma(x) = \begin{bmatrix} \gamma_1(x) \\ \gamma_2(x) \end{bmatrix} = \begin{bmatrix} 1 & x_2 \\ 0 & 1 \end{bmatrix}$$

Case 2: If $r < n_x$, then the system (5.1) is partially feedback linearizable. In this case an extended transformation $T : \mathcal{X} \to S$ can be defined as

$$s = \left[\begin{array}{c} \eta \\ \hdashline z \end{array}\right] = T(x) = \left[\begin{array}{c} \phi(x) \\ \hdashline \psi(x) \end{array}\right] = \left[\begin{array}{c} \phi_1(x) \\ \vdots \\ \phi_{n_x - r}(x) \\ \hdashline \psi_1(x) \\ \vdots \\ \psi_{n_y}(x) \end{array}\right], \tag{5.21}$$

where $\mathcal{S}$ is a compact set . The functions $\phi_i(x)$ for $i \in \{1, 2, \ldots, n_x - r\}$ are selected such that $T(x)$ is a diffeomorphism and

$$\frac{\partial \phi_i}{\partial x} g(x) = 0. \tag{5.22}$$

Then, the nonlinear system (5.1) can be transformed as

$$\begin{aligned} \dot{\eta} &= f_0(\eta, z) \\ \dot{z} &= Az + B[\alpha(x) + \gamma(x)u] \\ y &= Cz \end{aligned} \tag{5.23}$$

where $f_0(\eta, z)$ and η, represents the system internal dynamic and internal dynamics states (KHALIL, 2002). For event-triggered control design purposes this non-observable dynamic is assumed to be exponentially stable.

Remark 5.3. As stated in (ISIDORI, 1995), due to Assumption (5.1) (involutive assumption), it is possible to find functions ϕ_i for $i \in \{1, 2, \ldots, n_x - r\}$ such that $T(x)$ is a diffeomorphism and the conditions $\frac{\partial \phi_i}{\partial x} g(x) = 0$ hold.

5.2.2 Event-triggered feedback linearization control

For the transformed systems (5.19) and (5.23), the event-triggered feedback control law is defined as

$$u_k = u(x_k) = \gamma(x_k)^{-1}[Kz_k - \alpha(x_k)], \ \forall t \in [t_k, t_{k+1}), \ k \in \mathbb{N}, \tag{5.24}$$

where z_k and x_k are time samples of z and x at sampling instants t_k that are held constant until the next sampling. The feedback gain K is a matrix of appropriate dimension to be determined.

Illustrative example part 4 – Linearizing control input

Considering the expression (5.24) the linearizing control law for system (5.6) is

$$u_k = \underbrace{\begin{bmatrix} 1 & -x_{2,k} \\ 0 & 1 \end{bmatrix}}_{\gamma(x_k)^{-1}} \left(Kz_k - \underbrace{\begin{bmatrix} x_{1,k}^2 + x_{2,k}^2 \\ -x_{1,k} - \sin(x_{3,k}) \end{bmatrix}}_{\alpha(x_k)} \right) \tag{5.25}$$

Applying the control law (5.24), the closed-loop linearized dynamics in (5.19) and (5.23) are defined as

$$\dot{z} = Az + B[\alpha(x) + \gamma(x)\gamma(x_k)^{-1}(Kz_k - \alpha(x_k))], \tag{5.26}$$

which, by adding a null term, can be written in the form

$$\begin{aligned} \dot{z} &= Az + B[\alpha(x) + \gamma(x)\gamma(x_k)^{-1}(Kz_k - \alpha(x_k)) \\ &\quad + \gamma(x_k)\gamma(x_k)^{-1}(Kz_k - \alpha(x_k)) - \gamma(x_k)\gamma(x_k)^{-1}(Kz_k - \alpha(x_k))] \\ &= Az + BKz_k + B(\alpha(x) - \alpha(x_k)) + B(\gamma(x) - \gamma(x_k))\gamma(x_k)^{-1}(Kz_k - \alpha(x_k)). \end{aligned} \tag{5.27}$$

Finally, defining the mismatch terms $\Delta\alpha(x) = \alpha(x) - \alpha(x_k)$, $\Delta\gamma(x) = \gamma(x) - \gamma(x_k)$ and the error $e_z = z - z_k$, system (5.27) can be rewritten as

$$\dot{z} = (A + BK)z - BKe_z + B\Delta\alpha(x) + B\Delta\gamma(x)u_k. \tag{5.28}$$

For the case of partial feedback linearization (i.e., $r < n_x$), since the transformation $T(\cdot)$ defined in (5.21) is a diffeomorphism, there is an inverse $T^{-1} : \mathcal{S} \to \mathcal{X}$ with $x = T^{-1}(s)$. As a result, the system nonlinearites $\alpha(x)$ and $\gamma(x)$ can be rewritten as $F(s) = \alpha(T^{-1}(s))$ and $G(s) = \gamma(T^{-1}(s))$. Hence, the closed-loop system (5.28) can be represented as

$$\dot{z} = (A + BK)z - BKe_z + B\Delta F(s) + B\Delta G(s)u_k, \tag{5.29}$$

where $\Delta F(s) = F(s) - F(s_k)$ and $\Delta G(s) = G(s) - G(s_k)$. Note that for this case (partial feedback linearization), the mismatches depend on both internal and linearized dynamics of system (5.23). Also, system (5.29) can be easily adapted for the case of fully feedback linearization (i.e., $r = n_x$) by making $s = z$.

5.3 Problem formulation

This section first presents a method to convexly rewrite the nonlinear mismatch term $\Delta F(s)$ in a polytopic representation. Next an event-triggered condition is proposed con-

sidering the effect of $\Delta G(s)u_k$. Finally the event-triggered design control problem is formulated.

5.3.1 Polytopic representation of $\Delta F(s)$

As a result of the smoothness of functions $f(x)$, $g(x)$ and $h(x)$ and considering that $T(s)$ is a diffeomorphism, the function $F(s)$ is continuously differentiable for $s \in \mathcal{S}$. Let $J_F(\cdot)$ be the Jacobian matrix of $F(\cdot)$ and let us define $e_s = s - s_k$. From the fundamental theorem of calculus, it follows that

$$\begin{aligned}
\Delta F(s) = F(s) - F(s_k) &= -\int_0^1 \frac{dF(s-\tau e_s)}{d\tau} d\tau \\
&= -\int_0^1 J_F(s-\tau e_s)\frac{d(s-\tau e_s)}{d\tau} d\tau \\
&= -\int_0^1 J_F(s-\tau e_s)(-e_s) d\tau \\
&= \left(\int_0^1 J_F(s-\tau e_s) d\tau\right) e_s \\
&= \underbrace{\left(\int_0^1 J_F(s-\tau(s-s_k)) d\tau\right)}_{\mathcal{A}(s,s_k)} e_s.
\end{aligned} \tag{5.30}$$

where $\tau \in [0,1]$ and the integral is element-wise. Notice that $\mathcal{A}(s,s_k)e_s$ only requires computing an integral that can be done by a symbolic software. For the purpose of achieving the polytopic form of $\Delta F(s)$ we consider the following assumption for $J_F(\cdot)$.

Assumption 5.3. Let $\mathcal{S} = T(\mathcal{X})$ be the set of interest after transformation and let $\bar{\mathcal{S}}$ be a given convex set that contains $\mathcal{S}$ ($\mathcal{S} \subseteq \bar{\mathcal{S}}$). The Jacobian matrix $J_F(\cdot)$ can be represented in the polytopic form

$$J_F(s) = \sum_{i=1}^{m} \upsilon_i(s) M_i \tag{5.31}$$

where $s \in \bar{\mathcal{S}}$ and $\upsilon_m(s) \in \Upsilon_m$ with Υ_m a unit simplex with m vertices is denoted as

$$\Upsilon_m = \left\{ \upsilon \in \mathbb{R}^n : \sum_{i=1}^{m} \upsilon_i = 1, \quad \upsilon_i \geq 0, \quad i = 1, \ldots, n \right\}. \tag{5.32}$$

.

Remark 5.4. Due to the compactness assumption of $\mathcal{X} \subset \mathbb{R}^{n_x}$, the polytopic representation (5.31) can be obtained for a large class of systems. Since $\mathcal{X}$ is compact and $T(x)$ is a diffeomorphism, the set $\mathcal{S}$ is also compact. Hence, $\mathcal{S}$ can be always contained in a convex set. Moreover the polytopic representation (5.31) can be determined using the sector nonlinearity approach (TANAKA; WANG, 2001).

To exemplify the procedure of achieving a convex representation via sector nonlinearity, we recall to the illustrative example.

Illustrative example part 5 – Jacobian Convex representation

Let us consider the set of interest $\mathcal{X} = \{x \mid |x_i| \leq 2, i = 1, 2, 3\}$. As previously defined, the diffeomorphism for system (5.6) is $T(x) = x$ (i.e., $T^{-1}(s) = s$), therefore $\mathcal{X} = \mathcal{S}$ and $F(s) = \alpha(T^{-1}(s)) = \alpha(s)$. Moreover, since the system is fully feedback linearizable it implies that $z = s$ (no internal dynamics). As $\mathcal{X}$ is already convex (and consequently $\mathcal{S}$), we can choose the convex set $\bar{\mathcal{S}}$ equal to $\mathcal{S}$.
From (5.20) we have that

$$F(z) = \alpha(x) = \begin{bmatrix} z_1^2 + z_2^2 \\ -z_1 + \sin(z_3) \end{bmatrix}, \tag{5.33}$$

and its Jacobian matrix is

$$J_F(z) = \begin{bmatrix} 2z_1 & 2z_2 & 0 \\ -1 & 0 & \cos(z_3) \end{bmatrix}. \tag{5.34}$$

Considering the sector nonlinearity approach explained in Chapter 2 Section 2.5, the functions are $2z_1$, $2z_2$ and $\cos(z_3)$. In the set $\|z_i\| \leq 2$ for $i = 1, 2, 3$ (set $\bar{\mathcal{S}}$) we have that

$$-4 \leq 2z_1 \leq 4, \quad -4 \leq 2z_2 \leq 4, \quad \cos(2) \leq \cos(z_3) \leq 1. \tag{5.35}$$

Following the procedure described in Section 2.5 we can write those functions as

$$\begin{aligned} 2z_i &= \underbrace{\left(\frac{4 - 2z_i}{8}\right)}_{v_1^i(z)}(-4) + \underbrace{\left(\frac{2z_i + 4}{8}\right)}_{v_2^i(z)}(4) \quad i = 1, 2 \\ \cos(z_3) &= \underbrace{\left(\frac{1 - \cos(z_3)}{1 - \cos(2)}\right)}_{v_1^3(z)}(\cos(2)) + \underbrace{\left(\frac{\cos(z_3) - \cos(2)}{1 - \cos(2)}\right)}_{v_2^3(z)}(1) \end{aligned} \tag{5.36}$$

To write $F(z)$ in a convex representation (5.31) we need to find the vertices M_i and v_i. For this purpose we evaluate $J_F(z)$ for all possible combinations of maximum and minimum values of $2z_1$, $2z_2$ and $\cos(z_3)$ for $\|z_i\| \leq 2$, which results in

$M_1 = \begin{bmatrix} -4 & -4 & 0 \\ -1 & 0 & \cos(2) \end{bmatrix}$, $\upsilon_1 = \upsilon_1^1\upsilon_1^2\upsilon_1^3$	$M_2 = \begin{bmatrix} 4 & -4 & 0 \\ -1 & 0 & \cos(2) \end{bmatrix}$, $\upsilon_2 = \upsilon_2^1\upsilon_1^2\upsilon_1^3$
$M_3 = \begin{bmatrix} -4 & 4 & 0 \\ -1 & 0 & \cos(2) \end{bmatrix}$, $\upsilon_3 = \upsilon_1^1\upsilon_2^2\upsilon_1^3$	$M_4 = \begin{bmatrix} 4 & 4 & 0 \\ -1 & 0 & \cos(2) \end{bmatrix}$, $\upsilon_4 = \upsilon_2^2\upsilon_2^2\upsilon_1^3$
$M_5 = \begin{bmatrix} -4 & -4 & 0 \\ -1 & 0 & 1 \end{bmatrix}$, $\upsilon_5 = \upsilon_1^1\upsilon_1^2\upsilon_2^3$	$M_6 = \begin{bmatrix} 4 & -4 & 0 \\ -1 & 0 & 1 \end{bmatrix}$, $\upsilon_6 = \upsilon_2^2\upsilon_1^2\upsilon_2^3$
$M_7 = \begin{bmatrix} -4 & 4 & 0 \\ -1 & 0 & 1 \end{bmatrix}$, $\upsilon_7 = \upsilon_1^1\upsilon_2^2\upsilon_2^3$	$M_8 = \begin{bmatrix} 4 & 4 & 0 \\ -1 & 0 & 1 \end{bmatrix}$. $\upsilon_8 = \upsilon_2^2\upsilon_2^2\upsilon_2^3$

(5.37)

Under Assumption 5.3, with $\bar{\mathcal{S}}$ a chosen convex set such that $\mathcal{S} \subseteq \bar{\mathcal{S}}$ where (5.30) holds, the following lemma is important to rewrite the mismatch $\Delta F(s)$ in a convex representation.

Lemma 5.1. *Consider a convex set $\bar{\mathcal{S}}$. Let $M(s)$, be a matrix that can be represented in a polytopic form*

$$M(s) = \sum_{i=1}^{m} \upsilon_i(s) M_i, \quad \upsilon(s) \in \Upsilon_m, \tag{5.38}$$

for $s \in \bar{\mathcal{S}}$, where M_i are known vertices. Take

$$\epsilon_i(s, e_s) = \int_0^1 \upsilon_i(s - \tau e_s) d\tau \tag{5.39}$$

for $i = 1, 2, \ldots m$, then, it follows that

$$\int_0^1 M(s - \tau e_s) d\tau = \sum_{i=1}^{m} \epsilon_i(s, e_s) M_i, \tag{5.40}$$

and $\epsilon(s, e_s)$ belongs to the unit simplex (i.e., $\epsilon(s, e_s) \in \Upsilon_m$).

Proof. It follows from the polytopic representation (5.38), by integrating both sides, that

$$\begin{aligned} \int_0^1 M(s - \tau e_s) d\tau &= \int_0^1 \left(\sum_{i=1}^{m} \upsilon_i(s - \tau e_s) M_i \right) d\tau = \sum_{i=1}^{m} \int_0^1 \upsilon_i(s - \tau e_s) d\tau M_i \\ &= \sum_{i=1}^{m} \epsilon_l(s, e_s) M_i. \end{aligned} \tag{5.41}$$

It remains to prove that $\epsilon(s, e_s) \in \Upsilon_m$. To this end it is required to prove that $\epsilon_l(s, e_s) \geq 0$ for $l = 1, \ldots, m$ and that $\sum_{i=1}^{m} \epsilon_l(s, e_s) = 1$.

1. Proof that $\epsilon_l(s, e_s) \geq 0$: Since $\bar{\mathcal{S}}$ is a convex set, then $(s - \tau e)$, which is the line segment from s to s_k, also belongs to $\bar{\mathcal{S}}$. Since $\upsilon(s) \in \Upsilon_m$ (belongs to a unity simplex) for any $s \in \bar{\mathcal{S}}$, then $\upsilon_l(s - \tau e_s) \geq 0$, which implies that

$$\int_0^1 \upsilon_l(s - \tau e_s) d\tau \geq 0. \tag{5.42}$$

2. Proof that $\sum_{i=1}^m \epsilon_l(s, e_s) = 1$: Since $\xi(\upsilon) \in \Upsilon_m$, then it follows that

$$\sum_{i=1}^m \upsilon_l(s - \tau e_s) = 1. \tag{5.43}$$

Integrating both sides of (5.43) for $\tau \in [0, 1]$, one has

$$\begin{aligned} \int_0^1 \sum_{i=1}^m \upsilon_l(s - \tau e_s) d\tau &= \int_0^1 1 d\tau \\ \sum_{i=1}^m \int_0^1 \upsilon_l(s - \tau e_s) d\tau &= \tau \Big|_0^1 \\ \sum_{i=1}^m \epsilon_l(s, e_s) d\tau &= 1. \end{aligned} \tag{5.44}$$

concluding the proof □

Remark 5.5. Notice that, for SISO systems, Lemma 5.1 is equivalent to the mean value theorem.

Applying Lemma 5.1 to $\Delta F(s)$ under Assumption 5.3, it follows that

$$\Delta F(s) = M(\epsilon) e_s = \sum_{i=1}^m \epsilon_i(s, e_s) M_i e_s \tag{5.45}$$

with $\epsilon(s, e_s) \in \Upsilon_m$, allowing us to write (5.28) as

$$\dot{z} = (A + BK)z - BKe_z + BM(\epsilon)e_s + B\Delta G(s)u_k, \tag{5.46}$$

moreover, by decomposing $M(\epsilon) = [M_\eta(\epsilon),\ M_z(\epsilon)]$, we can rewrite (5.46) as

$$\dot{z} = (A + BK)z + B(M_z(\epsilon) - K)e_z + BM_\eta(\epsilon)e_\eta + B\Delta G(s)u_k. \tag{5.47}$$

with $e_\eta = \eta - \eta_k$. Note that in (5.47) the errors e_z and e_η are decoupled. As will be shown later, this property allows us to define a proper event triggering condition that can compensate for the effect of e_η caused by the internal dynamics.

5.3.2 Event-triggering mechanism

To compensate for both e_z and e_η and the mismatch $\Delta G(s)u_k$, the following event-triggering mechanism is proposed

$$\begin{aligned} t_0 &= 0 \\ t_{k+1} &= \inf\{t > t_k \ :\ \Gamma_0(s, e_s) > 0\} \end{aligned} \tag{5.48}$$

with

$$\Gamma_0(s, e_s) = -z^T R_1 z - \bar{\theta}\eta^T\eta + e_z^T Q_1 e_z + \gamma e_\eta^T e_\eta + u_k^T \Delta G(s)^T Q_2 \Delta G(s) u_k \tag{5.49}$$

where Q_1, Q_2, R_1 are positive definite matrices of appropriate dimensions and γ, $\bar{\theta}$ positive scalars to be designed.

5.3.3 Problem statement

We consider the following event-triggered control problem.

Problem 5.1. Considering the nonlinear MIMO system (5.1), design an event-triggered control law (5.24) and event-triggering mechanism (5.48) such that the closed-loop system (5.47) is asymptotically stable.

The following lemma is required for the proof of the main theorems presented in Section 5.4.

Lemma 5.2 (Converse Theorem (KHALIL, 2002))**.** *Consider the internal dynamics $\dot{\eta} = f_0(\eta, z)$ in (5.23). If the zero dynamics $f_0(\eta, 0)$ is exponentially stable, then there is a continuously differentiable Lyapunov function $V_\eta(\eta)$ and positive scalars a_1 and a_2 such that the following conditions hold:*

$$\frac{\partial V_\eta}{\partial \eta} f_0(\eta, 0) \leq -a_1\|\eta\|^2 \tag{5.50}$$

$$\left\|\frac{\partial V_\eta}{\partial \eta}\right\| \leq a_2\|\eta\| \tag{5.51}$$

in some neighborhood of $\eta = 0$.

5.4 Results

First we introduce the theorem for event-triggered control design for the general case of partial feedback linearization. Then conditions that ensure the existence of a lower bound for IET are established. Finally, particular cases of fully feedback linearization and constant $\gamma(x)$ are discussed.

5.4.1 General case: Partial feedback linearization

The following theorem presents sufficient conditions to ensure the asymptotic stability of system (5.29).

Theorem 5.1. *Let $\mathcal{E}$ and $\mathcal{Z}$ be compact neighborhoods of $\eta = 0$ and $z = 0$, respectively, with $\mathcal{E} \times \mathcal{Z} \subseteq \mathcal{S}$. Consider system (5.23), where $f_0(\eta, 0)$ is exponentially stable for all*

$\eta \in \mathcal{E}$. If there exist a positive definite function $V_z(z)$ for system (5.23)*, and a positive scalar $\bar{\rho}$ such that*

$$\dot{V}_z(z) - \Gamma_1(s, e_s) < -\bar{\rho} z^T z, \tag{5.52}$$

holds for all $s \in \mathcal{E} \times \mathcal{Z}$, where $\Gamma_1 = \Gamma_0 + \bar{\theta}\eta^T\eta$, with Γ_0 defined in (5.49)*, or equivalently,*

$$\Gamma_1(s, e_s) = -z^T R_1 z + e_z^T Q_1 e_z + \gamma e_\eta^T e_\eta + u_k^T \Delta G(s)^T Q_2 \Delta G(s) u_k, \tag{5.53}$$

then the closed-loop system (5.29) *is asymptotically stable under control law* (5.24) *and event-triggering mechanism* (5.48)*, where*

$$\bar{\theta} = \frac{a_1}{\sigma}\theta \tag{5.54}$$

$$\sigma > \frac{a_2^2 L_f^2}{4a_1(1-\theta)\bar{\rho}}, \tag{5.55}$$

with θ a positive scalar in the range $(0, 1)$, and L_f being a Lipschitz constant for $f_0(\eta, \cdot)$.

Proof. For simplicity of notation, throughout this proof, we will write simply V_η, V_z, Γ_0 and Γ_1 when no confusion can arise. Let us define $V_s = V(\eta, z) = V_\eta + \sigma V_z$, where the Lyapunov function V_η satisfies the conditions from Lemma 5.2. Taking the time derivative of V_s yields

$$\dot{V}_s = \frac{\partial V_\eta}{\partial \eta} f_0(\eta, z) + \sigma \dot{V}_z \tag{5.56}$$

$$= \frac{\partial V_\eta}{\partial \eta} f_0(\eta, 0) + \frac{\partial V_\eta}{\partial \eta}(f_0(\eta, z) - f_0(\eta, 0)) + \sigma \dot{V}_z \tag{5.57}$$

$$\leq -a_1\|\eta\|^2 + L_f a_2 \|\eta\|\|z\| + \sigma \dot{V}_z \tag{5.58}$$

where (5.58) is attained from conditions (5.50), (5.51) and Lipschitz condition.

It follows from (5.58), the definitions of Γ_0 in (5.49) and Γ_1 in (5.53), and $\bar{\theta}$ in (5.54) that

$$\begin{aligned}
\dot{V}_s - \sigma\Gamma_0 &\leq -a_1\|\eta\|^2 + L_f a_2\|\eta\|\|z\| + \sigma\dot{V}_z - \sigma\Gamma_0 \\
&= -a_1\|\eta\|^2 + L_f a_2\|\eta\|\|z\| + \sigma\bar{\theta}\eta^T\eta + \sigma(\dot{V}_z - \Gamma_1) \\
&< -a_1\left(1 - \frac{\sigma}{a_1}\bar{\theta}\right)\|\eta\|^2 + L_f a_2\|\eta\|\|z\| - \sigma\bar{\rho}\|z\|^2 \\
&= -a_1(1-\theta)\|\eta\|^2 + L_f a_2\|\eta\|\|z\| - \sigma\bar{\rho}\|z\|^2
\end{aligned} \tag{5.59}$$

with θ defined in (5.54). Completing the squares on the right-hand side of (5.59), it follows that

$$\dot{V}_s - \sigma\Gamma_0 < -\left(\sqrt{a_1(1-\theta)}\|\eta\| - \sqrt{\sigma\bar{\rho}}\|z\|\right)^2 - \left(2\sqrt{a_1(1-\theta)}\sqrt{\sigma\bar{\rho}} - L_f a_2\right)\|\eta\|\|z\| \tag{5.60}$$

Choosing σ such in (5.55), we have $2\sqrt{a_1(1-\theta)}\sqrt{\sigma\bar{\rho}} - L_f a_2 > 0$. Combining with (5.60) we conclude that

$$\dot{V}(\eta, z) - \sigma\Gamma_0 < 0. \tag{5.61}$$

Since condition (5.61) holds for all $(\eta, z) \in \mathcal{E} \times \mathcal{Z}$, it follows from (5.61) that $\dot{V}(\eta, z) < 0$ whenever $\Gamma_0 < 0$. The proof is concluded. □

Based on the results in Theorem 5.1, the next theorem provides an LMI-based optimization problem to design the parameters K in (5.24), and Q_1, Q_2, R_2, γ from event-triggering mechanism (5.48).

Theorem 5.2. *Consider the partially feedback linearized dynamics* (5.23)*, where* $f_0(\eta, 0)$ *is exponentially stable, and the event-triggered controller* (5.24)*. For given positive scalars* δ*,* ρ *and vertices* $M_i = [M_{\eta,i}, M_{z,i}]$ *of* $J_F(\cdot)$ *as defined in* (5.38)*, if there exist a matrix* Y*, positive definite matrices* P*,* $\bar{Q}_1$*,* Q_2 *and* $\bar{R}_1$ *of appropriate dimensions, and a positive scalar* γ*, solutions to the optimization problem*

$$\min \ \operatorname{Tr}(\bar{Q}_1) + \operatorname{Tr}(Q_2) \tag{5.62}$$

s.t.

$$\begin{bmatrix} \operatorname{He}\{AP + BY\} + \bar{R}_1 + \rho P & B(M_{z,i}P - Y) & B & BM_{\eta,i} \\ * & -\bar{Q}_1 & 0 & 0 \\ * & * & -Q_2 & 0 \\ * & * & * & -\gamma I \end{bmatrix} \prec 0, \tag{5.63}$$

$$\bar{R}_1 - \delta I \succ 0, \tag{5.64}$$

for $i = 1, \ldots, m$ *then the closed-loop system* (5.29) *is asymptotically stable under the event-triggered control law* (5.24) *and feedback gain* $K = YP^{-1}$*, i.e., condition* (5.52) *is satisfied with*

$$V_z(z) = z^T P^{-1} z, \ Q_1 = P^{-1}\bar{Q}_1 P^{-1}, \ R_1 = P^{-1}\bar{R}_1 P^{-1}. \tag{5.65}$$

.

Proof. Let us choose a Lyapunov function $V_z(z) = z^T P^{-1} z$, where P is a positive definite matrix. From the closed-loop equation (5.47), the condition (5.52) (i.e., $\dot{V}_z - \Gamma_1 < 0$) and the definition of $\Gamma_1(s, e_s)$ in (5.53), it follows that

$$\begin{aligned} \dot{V}_z(z) - \Gamma_1(s, e_s) = &\left((A + BK)z - (M_z(\epsilon) - K)e_z + BM_\eta(\epsilon)e_\eta + B\Delta G(s)u_k\right)^T P^{-1} z \\ &+ z^T P^{-1} \left((A + BK)z - (M_z(\epsilon) - K)e_z + BM_\eta(\epsilon)e_\eta + B\Delta G(s)u_k\right) \\ &+ z^T R_1 z - e_z^T Q_1 e_z - \gamma e_\eta^T e_\eta - (\Delta G(s)u_k)^T Q_2 (\Delta G(s)u_k) < -\bar{\rho} z^T z \end{aligned} \tag{5.66}$$

for $s \neq 0$. Notice that making $\dot{V}_z(z) - \Gamma_1(s, e_s) < -\rho z^T P^{-1} z^T$ implies in condition (5.52) with $\bar{\rho} = \rho \lambda_{\min}(P^{-1})$. Moreover, following LMI condition

$$\begin{bmatrix} \operatorname{He}(P^{-1}(A + BK)) + R_1 + \rho P^{-1} & P^{-1}BM_z(\epsilon) - P^{-1}BK & P^{-1}B & P^{-1}BM_\eta(\epsilon) \\ * & -Q_1 & 0 & 0 \\ * & * & -Q_2 & 0 \\ * & * & * & -\gamma I \end{bmatrix} \prec 0. \tag{5.67}$$

is sufficient to ensure $\dot{V}_z(z) - \Gamma_1(s, e_s) < -\rho z^T P^{-1} z^T$. Multiplying (5.67) on the right and on the left by $\text{diag}(P, P, I, I)$ leads to

$$\begin{bmatrix} \text{He}((A+BK)P) + PR_1P + \rho P & BM_z(\epsilon)P - BKP & BP & BM_\eta(\epsilon) \\ * & -PQ_1P & 0 & 0 \\ * & * & -Q_2 & 0 \\ * & * & * & -\gamma I \end{bmatrix} \prec 0 \tag{5.68}$$

Hence, by defining $Y = KP$, $\bar{Q}_1 = PQ_1P$, $\bar{R}_1 = PR_1P$ and from the convex property of the polytopic representation of $M_z(z)$ and $M_\eta(\eta)$, it is sufficient that

$$\begin{bmatrix} \text{He}(AP + BY) + \bar{R}_1 + \bar{\rho}P & BM_{z,i}P - BY & BP & BM_{\eta,i} \\ * & -\bar{Q}_1 & 0 & 0 \\ * & * & -Q_2 & 0 \\ * & * & * & -\gamma I \end{bmatrix} \prec 0 \tag{5.69}$$

for all $i = 1, \ldots, m$ to ensure (5.68).

The proof is then concluded. □

Remark 5.6. Condition (5.63) and the selected cost function $\text{Tr}(\bar{Q}_1)+\text{Tr}(\bar{Q}_2)$ in (5.62) are used for IET maximization. Looking at the event triggering condition (5.49), to maximize the inter event time, the magnitude of R_1 should be large whereas the magnitudes of Q_1 and Q_2 should be small.

5.4.2 Particular cases: Full feedback linearization

The case of full feedback linearization can be seen as a particular case of partial feedback linearization where $f_0(\eta, z) = 0$ in (5.23) and system relative degree $r = n_x$. Then, system (5.23) reduces to (5.19) and the closed-loop system (5.47) is reduced to

$$\dot{z} = (A + BK)z - BKe_z + BM_z(\epsilon)e_z + B\Delta G(z)u_k. \tag{5.70}$$

For system (5.70), e_η and η are not required for the event-triggering mechanism, which can be redefined as

$$t_{k+1} = \inf\{t > t_k \ : \ -z^T R_1 z + e_z^T Q_1 e_z + u_k^T \Delta G(s)^T Q_2 \Delta G(s) u_k > 0\}. \tag{5.71}$$

From the results of Theorem 5.1 and Theorem 5.2, the following corollary provides sufficient conditions to guarantee the asymptotic stability of system (5.70).

Corollary 5.1. *Consider the fully feedback linearized dynamics* (5.19)*, and the event-triggered control law* (5.24) *with triggering condition* (5.71)*. For given positive scalars* δ*,* ρ *and matrices* $M_i = M_{z,i}$ *of* $J_F(\cdot)$ *as in* (5.31)*, if there exist a matrix* Y*, positive matrices* W*,* $\bar{Q}_1$*,* Q_2 *and* $\bar{R}_1$ *of appropriate dimensions, solution to the optimization problem*

$$\min \ \text{Tr}(\bar{Q}_1) + \text{Tr}(Q_2) \tag{5.72}$$

such that (5.64) *and*

$$\begin{bmatrix} \mathrm{He}\{AP+BY\}+\bar{R}_1+\rho P & B(M_{z,i}P-Y) & B \\ * & -\bar{Q}_1 & 0 \\ * & * & -Q_2 \end{bmatrix} \prec 0 \tag{5.73}$$

for $i=1,\ldots,m$ *then the closed-loop system* (5.70) *is asymptotically stable under the event-triggering mechanism* (5.71) *with* $Q_1=P^{-1}\bar{Q}_1P^{-1}$, $R_1=P^{-1}\bar{R}_1P^{-1}$. *Moreover, the feedback gain is defined as* $K=YP^{-1}$.

Further assuming that $\gamma(x)$ is constant, then the fully feedback linearized dynamics (5.19) reduces to

$$\dot{z}=(A+BK)-BKe_z+BM_z(\epsilon)e_z. \tag{5.74}$$

Moreover, the event-triggering mechanism corresponding to system (5.74) is defined as

$$t_{k+1}=\inf\{t>t_k \ : \ -z^TR_1z+e_z^TQ_1e_z>0\}. \tag{5.75}$$

Therefore, the following result can be derived from Corollary 5.1 to guarantee the asymptotic stability of system (5.74).

Corollary 5.2. *Consider the fully feedback linearized dynamics* (5.19)*, with* $\gamma(x)$ *constant, and the event-triggered controller* (5.24)*. For given positive scalar* δ, ρ *and vertices* $M_i=M_{z,i}$ *of* $J_F(\cdot)$ *as in* (5.31)*, if there exist a matrix* Y *and positive matrices* W, $\bar{Q}_1$ *and* $\bar{R}_1$ *of appropriate dimensions, solution to the optimization problem.*

$$\min \ \ Tr(\bar{Q}_1) \tag{5.76}$$

such that (5.64) *and*

$$\begin{bmatrix} He(AP+BY)+\bar{R}_1+\rho P & B(M_{z,i}P-Y) \\ * & -\bar{Q}_1 \end{bmatrix} \prec 0, \ \ i=1,\ldots,m \tag{5.77}$$

$$\tag{5.78}$$

for $i=1,\ldots,m$ *then the closed-loop system* (5.74) *is asymptotically stable under the event-triggering mechanism* (5.75) *with* $Q_1=P^{-1}\bar{Q}_1P^{-1}$, $R_1=P^{-1}\bar{R}_1P^{-1}$. *Moreover, the feedback gain is defined as* $K=YP^{-1}$.

Remark 5.7. Minimizing the IETs via LMI-based optimization may lead to a feedback gain K with an excessively large magnitude. To prevent this numerical issue, an additional LMI constraint can be included in the optimization problems

$$\begin{bmatrix} \kappa^2 I & Y \\ * & P \end{bmatrix} \succ 0 \tag{5.79}$$

for some given $\kappa > 0$. Indeed, by Schur's complement (Lemma 2.10, Section 2.7), condition (5.79) is equivalent to

$$YP^{-1}Y^T - \kappa^2 I \prec 0. \tag{5.80}$$

Substituting $Y = KP$, it follows from inequality (5.80) that

$$KPK^T \prec \kappa^2 I \tag{5.81}$$

which leads to

$$\|K\| < \frac{\kappa}{\sqrt{\|P\|}} \tag{5.82}$$

Hence, LMI (5.79) guarantees an upper bound on the feedback gain magnitude.

5.4.3 Existence of a lower bound for the inter-event time (IET)

The design conditions in Theorem 5.1 guarantee asymptotic stability of the closed-loop system (5.29) under event-triggering mechanism (5.48). However, those conditions do not ensure the absence of Zeno behavior. Therefore, the following theorem provides sufficient conditions to guarantee a minimum positive inter-event time.

Theorem 5.3. *If the linearized system* (5.23) *is stabilizable by control law* (5.24) *with event triggering condition* (5.48) *and* $\gamma(x)$ *and* $\alpha(x)$ *are Lipschitz for all* $x \in \mathcal{X}$ *then there is a positive lower bound for IET.*

Proof. First, since system (5.29) is assumed to be stable under controller (5.24) and event-triggering mechanism (5.48), then states are bounded. Additionally, since $\mathcal{X}$ is compact, then $T(x)$ and its inverse $T^{-1}(s)$ verify the Lipschitz property on $\mathcal{X}$ and $\mathcal{S}$, respectively. Hence $\gamma(T^{-1}(s)) = G(s)$ and $\alpha(T^{-1}(s)) = F(s)$ are Lipschitz on compact sets and $u = u(x)$ is bounded.

From the event-triggering mechanism (5.48) and the definition of $\Gamma_0(s, e_s)$ in (5.49), we have that $\Gamma_0(s, e_s) < 0$ which implies

$$e_z^T Q_1 e_z + \gamma e_\eta^T e_\eta + u_k^T \Delta G(s)^T Q_2 \Delta G(s) u_k < z^T R_1 z + \bar{\theta}\eta^T \eta \tag{5.83}$$

Then, considering the left hand side of (5.83) we can define an upper bound as

$$\begin{aligned} & e_z^T Q_1 e_z + \gamma e_\eta^T e_\eta + u_k^T \Delta G(s)^T Q_2 \Delta G(s) u_k \\ & \quad \leq \|e_z^T Q_1 e_z + \gamma e_\eta^T e_\eta + u_k^T \Delta G(s)^T Q_2 \Delta G(s) u_k\| \\ & \quad \leq \|e_z^T Q_1 e_z\| + \|\gamma e_\eta^T e_\eta\| + \|u_k^T \Delta G(s)^T Q_2 \Delta G(s) u_k\| \\ & \quad \leq \lambda_{\max}(Q_1)\|e_z\|^2 + \gamma\|e_\eta\|^2 + u_{\sup}^2 L_G^2 \lambda_{\max}(Q_2)\|e_s\|^2 \end{aligned} \tag{5.84}$$

where L_G is the Lipschitz constant for $G(s)$ (i.e., L_G is a constant such that $\|G(s_k) - G(s)\| \leq L_G\|s - s_k\|$), and $u_{\sup} = \sup_{x_k \in \mathcal{X}}\{\|u(x_k)\|\}$. Notice that $\|u(x_k)\|$ is bounded since

the closed-loop system is stable, and the solutions, between events, belong to a compact set. Moreover, since $e_s = \text{col}\{e_z, e_\eta\}$, note that $\|e_s\|^2 = \|e_z\|^2 + \|e_\eta\|^2 \geq \|e_z\|^2$, hence $\|e_s\| \leq \|e_z\|$ and $\|e_s\| \leq \|e_\eta\|$; therefore, from (5.84), it follows that

$$\begin{aligned} & e_z^T Q_1 e_z + \gamma e_\eta^T e_\eta + u_k^T \Delta G(s)^T Q_2 \Delta G(s) u_k \\ & \quad \leq \lambda_{\max}(Q_1)\|e_s\|^2 + \gamma\|e_s\|^2 + u_{\sup}^2 L_G^2 \lambda_{\max}(Q_2)\|e_s\|^2 \\ & \quad = \sigma_1 \|e_s\|^2 \end{aligned} \tag{5.85}$$

with $\sigma_1 = \lambda_{\max}(Q_1) + u_{\sup}^2 L_G^2 \lambda_{\max}(Q_2) + \gamma$. Performing a similar procedure to the right hand side of (5.83), we can define a lower bound as

$$z^T R_1 z + \bar{\theta}\eta^T \eta \geq \lambda_{\min}(R_1)\|z\|^2 + \bar{\theta}\|\eta\|^2 \geq \sigma_2(\|z\|^2 + \|\eta\|^2) = \sigma_2\|s\|^2 \tag{5.86}$$

where $\sigma_2 = \min\{\lambda_{\min}(R_1),\ \bar{\theta}\}$. From (5.85) and (5.86) a new event-triggering mechanism is defined as

$$t_{k+1} = \inf\{t > t_k \ :\ \|e_s\| - \sigma_s\|s\| > 0\} \tag{5.87}$$

with $\sigma_s = \sqrt{\sigma_2/\sigma_1}$. Note that condition (5.87) is more conservative than (5.48), i.e., it takes less time to be fulfilled than (5.48) (shorter inter event time). This condition is used to prove the existence of a lower bound for IET. Since this condition takes less time to trigger, a lower bound for it is also a lower bound for (5.48). Thus, taking the time derivative of the error $e_z = z - z_k$, for the time interval between events, it follows that $\dot{e}_z = \dot{z}$, which, from (5.29), give us

$$\begin{aligned} \dot{e}_z &= (A + BK)z - BKe_z + B[\Delta F(s) + \Delta G(s)u_k] \\ &= (A + BK)z_k + Ae_z + B[\Delta F(s) + \Delta G(s)u_k] \\ &= \begin{bmatrix} 0 & A + BK \end{bmatrix} s_k + \begin{bmatrix} 0 & A \end{bmatrix} e_s + B[\Delta F(s) + \Delta G(s)u_k] \end{aligned} \tag{5.88}$$

By considering the norm of e_z it follows from (5.88) that

$$\begin{aligned} \|\dot{e}_z\| &= \left\| \begin{bmatrix} 0 & A + BK \end{bmatrix} s_k + \begin{bmatrix} 0 & A \end{bmatrix} e_s + B[\Delta F(s) + \Delta G(s)u_k] \right\| \\ &\leq \left\| \begin{bmatrix} 0 & A + BK \end{bmatrix} s_k \right\| + \left\| \begin{bmatrix} 0 & A \end{bmatrix} e_s \right\| + \|B\Delta F(s)\| + \|B\Delta G(s)u_k\| \\ &\leq \|A + BK\|\|s_k\| + \|A\|\|e_s\| + \|B\|L_F\|e_s\| + \|B\|L_G u_{\sup}\|e_s\| \\ &= L_k\|s_k\| + L_z\|e_s\| \end{aligned} \tag{5.89}$$

with $L_k = \|A + BK\|$, $L_z = \|A\| + \|B\|(L_F + L_G u_{\sup})$ and L_F is the Lipschitz constant for $F(s)$ (i.e., L_F is a constant such that $\|F(s) - F(s_k)\| \leq L_f\|s - s_k\|$). Following similar steps for $e_\eta = \eta - \eta_k$, leads to $\dot{e}_\eta = \dot{\eta} = f_0(\eta, z)$, and

$$\|\dot{e}_\eta\| \leq L_{f_0}\|s\| \leq L_{f_0}\|s_k| + L_{f_0}\|e_s\|, \tag{5.90}$$

where L_{f_0} is the Lipschitz constant for $f_0(\eta, z)$. Combining (5.89) and (5.90), an upper bound for the time derivative of $e_s = s - s_k$ can be defined as

$$\|\dot{e}_s\| \leq \|\dot{e}_z\| + \|\dot{e}_\eta\| \leq L_s\|s_k\| + L_e\|e_s\| \tag{5.91}$$

with $L_s = L_{f_0} + L_k$ and $L_e = L_{f_0} + L_z$. From the fundamental theorem of calculus, one has $e_s = \int_{t_k}^{t} \dot{e}_s d\tau$. Then, it follows from condition (5.91) that

$$\begin{aligned} \|e_s\| &\leq \int_{t_k}^{t} \|\dot{e}_s\| d\tau \\ &\leq \int_{t_k}^{t} L_s \|s_k\| d\tau + \int_{t_k}^{t} L_e \|e_s\| d\tau \\ &\leq (t - t_k) L_s \|s_k\| + \int_{t_k}^{t} L_e \|e_s\| d\tau \end{aligned} \tag{5.92}$$

Applying the Grönwall inequality (Lemma 2.3.2, Section 2.2) to (5.92) yields

$$\begin{aligned} \|e_s\| &\leq (t - t_k) L_s \mathrm{e}^{L_e (t - t_k)} \|s_k\| \\ &= (t - t_k) L_s \mathrm{e}^{L_e (t - t_k)} \|s - e_s\| \\ &\leq (t - t_k) L_s \mathrm{e}^{L_e (t - t_k)} (\|s\| + \|e_s\|) \end{aligned} \tag{5.93}$$

From the event-triggering mechanism (5.87), we have that between events $\|e_s\| \leq \sigma_s \|s\|$. Then, until a new event happens, there is a positive constant $\sigma_l > \sigma_s$ such that $\|e_s\| \leq \sigma_l \|s\|$. Therefore, from (5.93), between events, the following inequality holds:

$$\|e_s\| \leq L_s (t - t_k) \mathrm{e}^{L_e (t - t_k)} (1 + \sigma_l) \|s\| \tag{5.94}$$

To estimate a lower bound for the time between events, two cases can be addressed.

Case 1: $(t - t_k) L_e \geq 1$. This implies that $(t - t_k) \geq 1/L_e > 0$, in other words, there is a positive lower bound for IET.

Case 2: $(t - t_k) L_e < 1$. Using the inequality $\mathrm{e}^x < 1/(1 - x)$ for all $x < 1$, it follows from (5.94) that

$$\|e_s\| \leq L_s (1 + \sigma_l) \frac{(t - t_k)}{1 - L_e (t - t_k)} \|s\| \tag{5.95}$$

A lower bound for the inter event time can be found by determining the minimum time $\Delta t = t_{k+1} - t_k$ such that the right hand side of (5.95) equals to $\sigma_s \|s\|$, thus

$$L_s (1 + \sigma_l) \frac{\Delta t}{1 - L_e \Delta t} \|s\| = \sigma_s \|s\| \tag{5.96}$$

From equation (5.96) follows that

$$\Delta t = \sigma_s \frac{\sigma_s}{L_e \sigma_s + L_s (1 + \sigma_l)} > 0 \tag{5.97}$$

which guarantees that there is a positive lower bound for the interval between events.

The proof can be now concluded.

□

5.5 Examples

This section provides numerical examples to illustrate the effectiveness of the proposed event-triggered control design. All related optimization problems are solved using YALMIP toolbox (LÖFBERG, 2004) with MOSEK solver (APS, 2019). For all examples, we assume that $x \in \mathcal{X}$ with a predefined compact set $\mathcal{X}$ to compute the vertices of $J_F(\cdot)$ for its polytopic representation (5.31). Moreover, for comparison purposes, all simulations corresponding to the results in (XU *et al.*, 2020) are performed using the design parameters reported in their work.

Example 5.1. Consider the nonlinar MIMO system

$$\begin{cases} \dot{x}_1 = x_2 \\ \dot{x}_2 = x_1^2 + x_2^2 + u_1 + x_2 u_2 \\ \dot{x}_3 = -x_1 + \sin(x_3) + u_2 \\ y_1 = x_1 \\ y_2 = x_2 \end{cases} \tag{5.98}$$

where $-2 \leq x_i \leq 2$, for $i = 1, 2, 3$. Note that this nonlinear system is fully feedback linearizable, i.e., there is no internal dynamics. The transformation is given by $T(x) = x$. Hence, we can obtain

$$F(z) = \begin{bmatrix} z_1^2 + z_2^2 \\ -z_1 + \sin(z_3) \end{bmatrix} \quad G(z) = \begin{bmatrix} 1 & z_2 \\ 0 & 1 \end{bmatrix}. \tag{5.99}$$

The polytopic representation of the Jacobian matrix $J_F(\cdot)$ and was derived in the steps of the illustrative example. The control law (5.24) and the event-triggering condition (5.71) are designed using Corollary 5.1 with $\delta = 1$ and $\rho = 1.5$. The corresponding solution is given by

$$P = \begin{bmatrix} 0.85 & 0.32 & -0.01 \\ 0.32 & 0.31 & 0.02 \\ -0.01 & 0.02 & 1.0 \end{bmatrix}. \quad Q_1 = \begin{bmatrix} 6.49 & 4.68 & -0.66 \\ 4.68 & 5.13 & 0.34 \\ -0.66 & 0.34 & 5.66 \end{bmatrix}, \quad K = \begin{bmatrix} -15.26 & 0.23 \\ -13.92 & 0.06 \\ -2.34 & -5.25 \end{bmatrix}^T$$
$$R_1 = \begin{bmatrix} 0.83 & 0.37 & -0.01 \\ 0.37 & 0.20 & 0.02 \\ -0.01 & 0.02 & 0.1 \end{bmatrix}, \quad Q_2 = \begin{bmatrix} 0.99 & 0.01 \\ 0.01 & 0.94 \end{bmatrix}, \tag{5.100}$$

The response of the closed-loop system corresponding to the initial condition $x(0) = [-1,\ 1,\ 1]^T$ is shown in Figure 5.1. Observe that the trajectories converge to the origin with reasonable magnitudes of the control inputs.

Figure 5.2 shows the IETs, where the stems positions on the x-axis indicate the triggering time, and their amplitudes correspond to the elapsed time Δt since the last event.

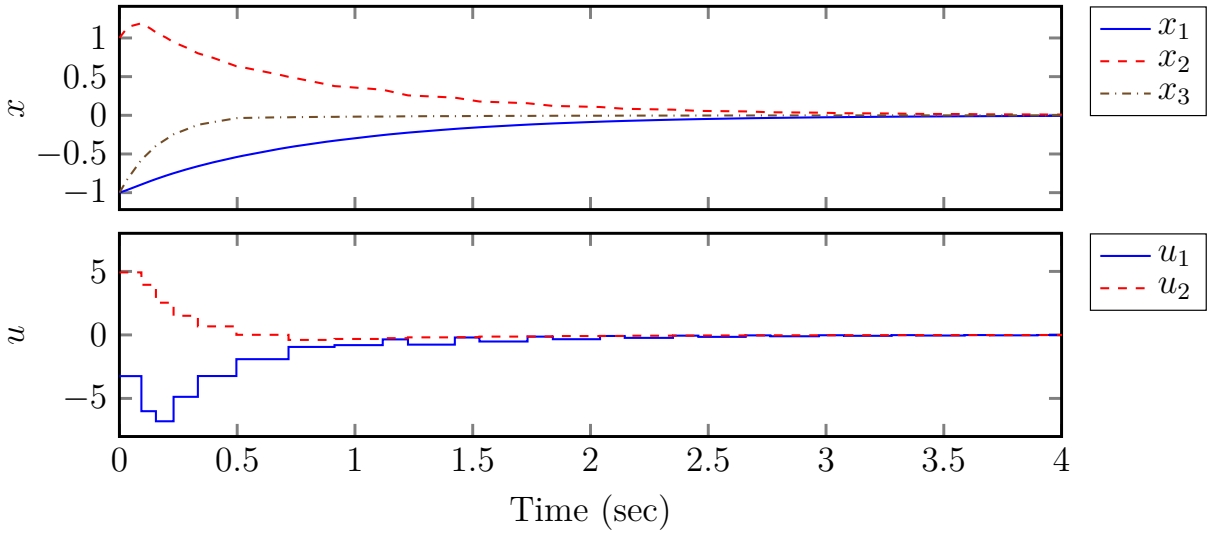

Figure 5.1 – Time response and control inputs applied to the closed-loop system (5.98) with the control design in Corollary 5.1.

To better evaluate the number of events, during simulations, the same experiment was repeated 1000 times, starting from random initial conditions. Over a ten-second simulation duration, the average number of events was about 70.89.

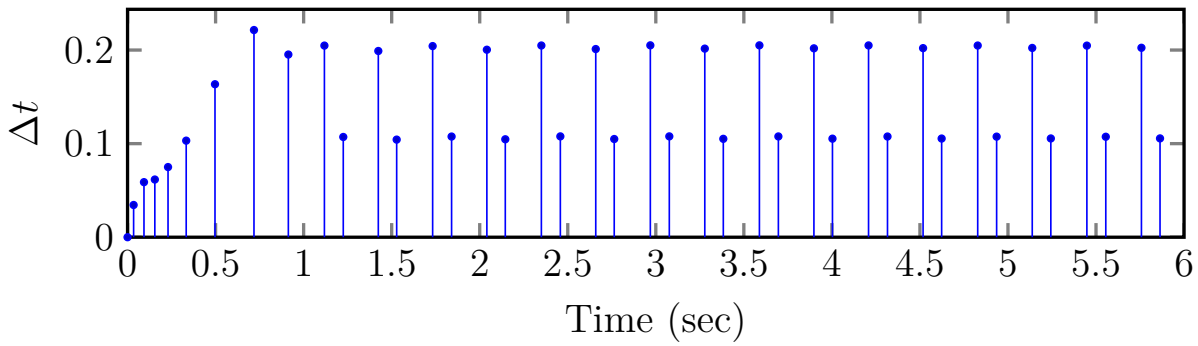

Figure 5.2 – Inter event times for system (5.98) with the control law (5.24) and the event-triggering condition (5.71) designed from Corollary 5.1.

Example 5.2. Consider the following pendulum system borrowed from (KHALIL, 2002)

$$\begin{cases} \dot{x}_1 = x_2 \\ \dot{x}_2 = -10\left(\sin\left(x_1 + \pi/4\right) - 1/\sqrt{2}\right) - 10u \\ y = x_1 \end{cases} \tag{5.101}$$

where x_1 is the angular position, x_2 is the angular velocity, u is the applied torque, and $-\pi \leq x_1 \leq \pi$ and $-5 \leq x_2 \leq 5$. The transformation is defined as $T(x) = x$, and the

nolinearities and Jacobian matrix are deduced as

$$\begin{aligned} F(z) &= -10\left(\sin\left(z_1 + \pi/4\right) - 1/\sqrt{2}\right), \quad G(z) = -10, \\ J_F(z) &= \begin{bmatrix} -10\cos(z_1 + \pi/4) \\ 0 \end{bmatrix} \end{aligned} \tag{5.102}$$

Both control law (5.24) and the event-triggering condition (5.75) are co-designed using Corollary (5.2) with $\delta = 0.2$ and $\rho = 0$. The corresponding control solution is given by

$$\begin{aligned} Q_1 &= \begin{bmatrix} 4.83 & 1.82 \\ 1.82 & 0.68 \end{bmatrix}, \quad R_1 = \begin{bmatrix} 0.17 & 0.06 \\ 0.06 & 0.02 \end{bmatrix}, \\ K &= \begin{bmatrix} -7.60 & -5.52 \end{bmatrix}, \end{aligned} \tag{5.103}$$

and it is compared with the results in (XU *et al.*, 2020). Figure 5.3 presents the closed-loop responses and the control signals of system (5.101) for initial condition $x(0) = [\pi,\ 0]^T$. The trajectories relative to the proposed approach converge faster and more smoothly to the origin. For the control signals, they might indicate that both approaches have similar control efforts. However, when evaluating the number of events and IET, Figure 5.4, it is clear that the proposed control design leads to fewer events than the approach in (XU *et al.*, 2020). This can be verified by checking the zoomed area in Figure 5.4, which shows a high number of events in a short time period.

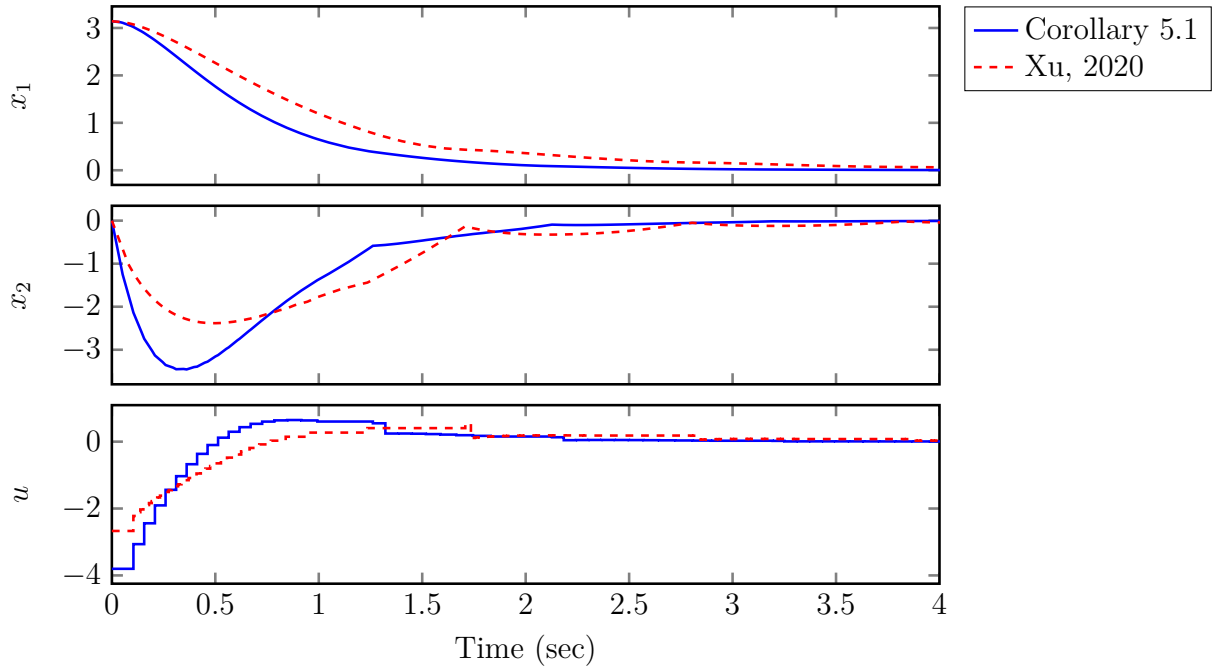

Figure 5.3 – Comparison of time responses and control signals applied to the closed-loop system (5.101) between the control design from Corollary 5.2 and the approach in (XU *et al.*, 2020).

For a better comparison in terms of the number of events, 1000 numerical simulations with both control approaches were performed for 1000 times starting from random initial

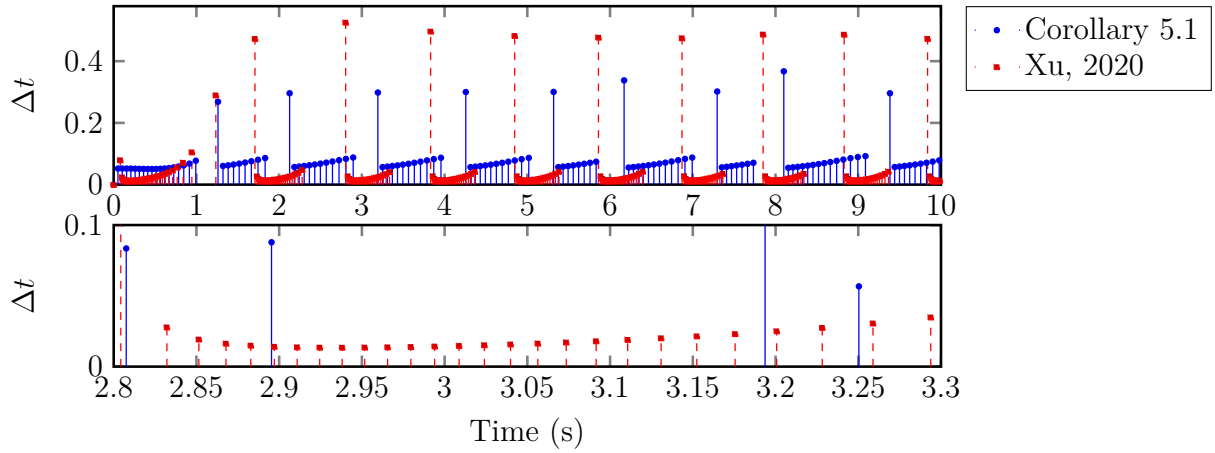

Figure 5.4 – Comparison of IETs obtained with the closed-loop system (5.101) between the control design from Corollary 5.2 and the approach in (XU *et al.*, 2020).

conditions. The event-triggered controller designed with Corollary 5.2 leads to 119.35 events on average, while the control approach in (XU *et al.*, 2020) leads to 276.69 events.

Example 5.3. We consider the following nonlinear system adapted from (XU *et al.*, 2020):

$$\begin{cases} \dot{x}_1 = x_1^3 + x_2 \\ \dot{x}_2 = -3x_1^2 x_2 + 10u \\ y = x_1, \quad x \in \mathcal{X} \end{cases} \tag{5.104}$$

where $\mathcal{X} = \{x \in \mathbb{R}^2 \ : \ |x_i| \leq 1.5, \quad i = 1, 2\}$. Note that (5.104) is fully feedback linearizable. Differentiating the output y, the transformation can be defined as $z_1 = x_1$ and $z_2 = x_1^3 + x_2$. Then, we can obtain

$$F(z) = 3z_1^5, \quad G(z) = 10, \quad J_F(z) = \begin{bmatrix} 15z_1^4 \\ 0 \end{bmatrix}. \tag{5.105}$$

Solving the design conditions in Corollary 5.2 with $\delta = 0.2$ and $\rho = 1$, the following control solution is attained:

$$\begin{aligned} Q_1 &= \begin{bmatrix} 51.75 & 8.39 \\ 8.39 & 2.48 \end{bmatrix}, \quad R_1 = \begin{bmatrix} 0.197 & 0.025 \\ 0.025 & 0.009 \end{bmatrix}, \\ K &= \begin{bmatrix} -13.91 & -15.32 \end{bmatrix}. \end{aligned} \tag{5.106}$$

To evaluate the importance of an explicit consideration of the nonlinearity mismatches in the event-triggered control design, system (5.104) is simulated, starting from different initial conditions using the controllers designed from Corollary 5.2 and the approach in (XU *et al.*, 2020) with the same design parameters reported therein. In Figure 5.5 we compare the initial conditions that lead to stable behavior of the closed-loop system (5.104) for both event-triggered controllers. Remark that the proposed controller can

ensure the asymptotic stability for the system (5.104) starting from any initial condition inside $\mathcal{X}$. However, without taking into account the nonlinearity mismatches, the controller proposed by (XU *et al.*, 2020) cannot ensure the stability for many initial conditions even with its feedback linearization being valid globally.

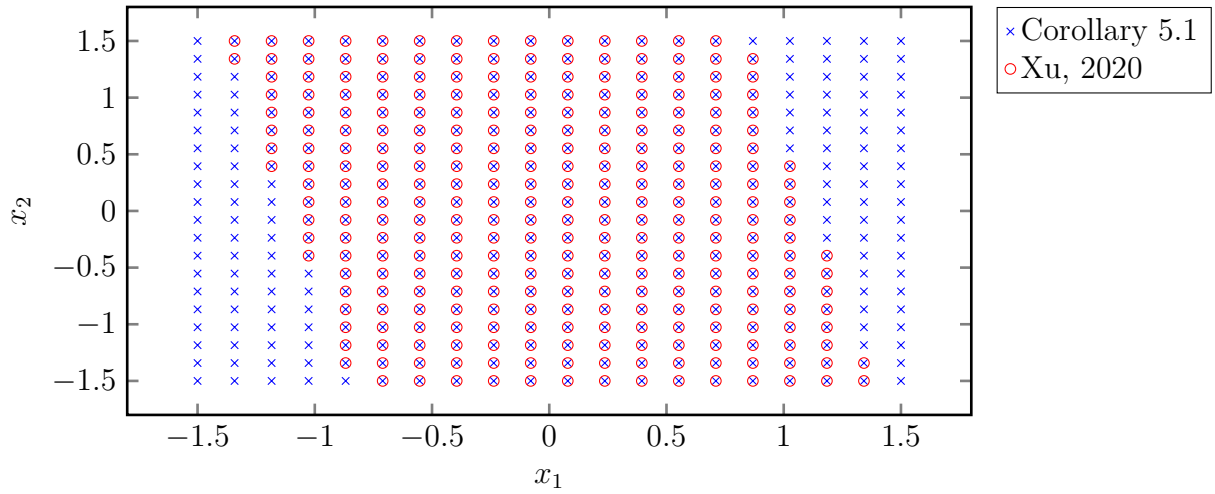

Figure 5.5 – Comparison of stable initial conditions for system (5.104) between the control design from Corollary 5.2 and the approach in (XU *et al.*, 2020).

For further illustration, we consider the initial condition $x(0) = [-1.1,\ -0.1]^T$. The corresponding closed-loop response obtained with both control methods are presented in Figure 5.6. The proposed approach provides much smoother state convergence and smaller control input signal magnitude. From the inter event times in Figure 5.7 we can see that the proposed approach yields an almost periodic triggering behavior. However, the approach in (XU *et al.*, 2020) can have a significant number of events for some intervals as shown in the corresponding zoom of Figure 5.7. Performing 1000 simulations with random initial conditions, on average the control result in (XU *et al.*, 2020) yields 354.22 events, whereas the proposed approach yields 164.19 events in a 10 seconds simulation.

Example 5.4. Consider the nonlinear system taken from (XU *et al.*, 2020)

$$\begin{cases} \dot{x}_1 = -x_1 + \dfrac{2 + x_3^2}{1 + x_3^2} u \\ \dot{x}_2 = x_3 \\ \dot{x}_3 = x_1 x_3 + u \\ y = x_2 \end{cases} \tag{5.107}$$

where $|x_i| \leq 3$ for $i = 1, 2, 3$. Note that system (5.107) is partially feedback linearizable with a relative degree $r = 2$. Following the same procedure in (XU *et al.*, 2020), we define

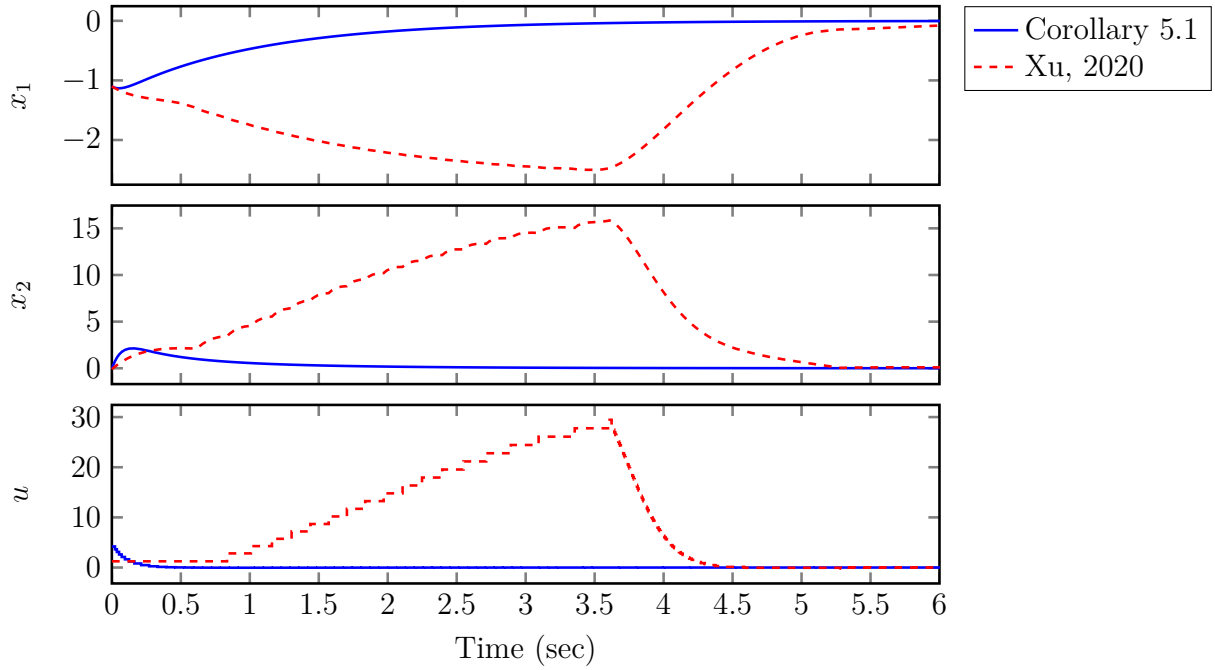

Figure 5.6 – Comparison of trajectories and control input signals applied to system (5.104) between the control design from Corollary 5.2 and the approach in (XU *et al.*, 2020).

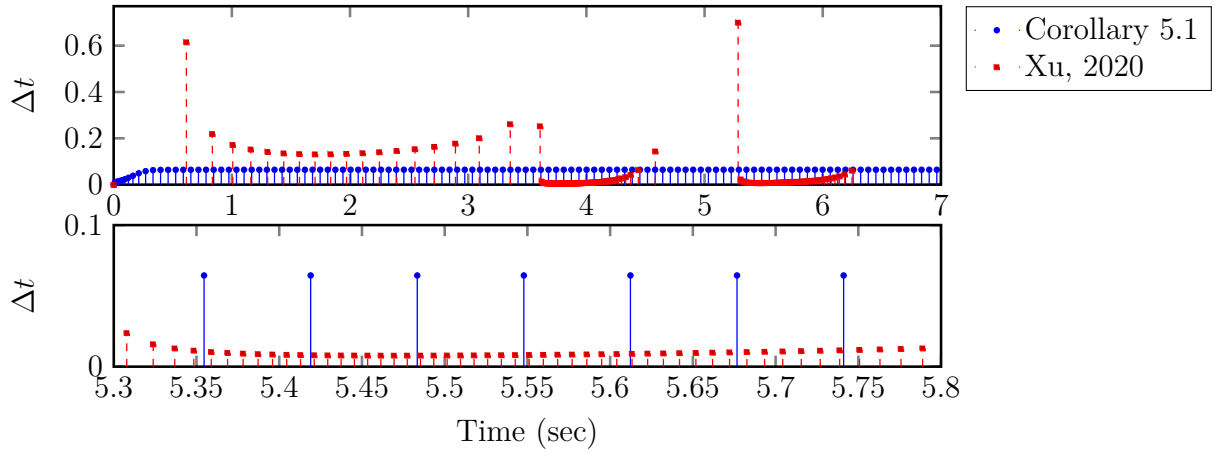

Figure 5.7 – Comparison of IETs obtained with system (5.104) between the control design from Corollary 5.2 and the approach in (XU *et al.*, 2020).

the transformation as

$$\begin{bmatrix} z_1 \\ z_2 \\ \eta \end{bmatrix} = T(x) = \begin{bmatrix} x_2 \\ x_3 \\ -x_1 + x_3 + \tan^{-1}(x_3) \end{bmatrix}, \tag{5.108}$$

which leads to the following transformed system:

$$\begin{cases} \dot{z}_1 = z_2 \\ \dot{z}_2 = \left(-\eta + z_2 + \tan^{-1}(z_2)\right) z_2 + u \\ \dot{\eta} = \left(-\eta + z_2 + \tan^{-1}(z_2)\right) \left(1 + \dfrac{2 + z_2^2}{1 + z_2^2} z_2\right) \end{cases} \tag{5.109}$$

Note that if $z = \text{col}\{z_1, z_2\} = 0$, then the zero dynamics in (5.109) becomes $\dot{\eta} = -\eta$. Since the zero dynamics is exponentially stable, Theorem 5.1 can be applied for the event-triggered control design of system (5.109). With the transformation (5.108), we can also define

$$\begin{aligned} F(z) &= \left(-\eta + z_2 + \tan^{-1}(z_2)\right) z_2, \quad G(z) = 1 \\ J_F(z) &= \begin{bmatrix} 0 \\ -\eta + z_2 + \tan^{-1}(z_2) + \left(1 + \dfrac{1}{1 - z_2^2}\right) z_2 \\ -z_2 \end{bmatrix} \end{aligned} \tag{5.110}$$

From the zero dynamics, selecting $V_\eta = \eta^T \eta$, the constants from Lemma 5.2 can be determined as $a_1 = 1$ and $a_2 = 1$. A Lipschitz constant for $f_0(\cdot, z)$ can be computed as approximately $L_f = 12$. Moreover, the event-trigger parameter is selected from (5.54) as $\bar{\theta} = 0.0002$. Solving the optimization problem in Theorem 5.2 with $[\delta, \rho, \gamma] = [1, 1.5, 1]$, the following feedback gain is obtained:

$$K^* = \begin{bmatrix} -19.7164 & -19.8374 \end{bmatrix} \tag{5.111}$$

The resulting gain K^* is large, which may lead to some numerical issues, *e.g.*, a large magnitude of control input. Hence, we redesign the feedback gain by including the additional constraint (5.79) with $\kappa = 10$ to limit the magnitude of the feedback gain, as explained in Remark 5.7. Then, the following control results are obtained:

$$\begin{aligned} Q_1 &= \begin{bmatrix} 11.24 & 10.15 \\ 10.15 & 13.74 \end{bmatrix}, \quad R_1 = \begin{bmatrix} 0.77 & 0.41 \\ 0.41 & 0.25 \end{bmatrix}, \\ K &= \begin{bmatrix} -6.61 & -5.96 \end{bmatrix}. \end{aligned} \tag{5.112}$$

Note that the additional constraint (5.79) significantly reduces the feedback gain magnitude, yet achieving a decent control performance as shown in Figure 5.8. Observe also that the approach in (XU *et al.*, 2020) provides a similar closed-loop behavior. However, concerning the inter event times, we can see from Figure 5.9 that the proposed approach triggers fewer times than the control result from (XU *et al.*, 2020). This is corroborated by performing, over 1000 simulations with random initial conditions, for both designed controllers. On average the approach in (XU *et al.*, 2020) leads to 341.33 triggered events, while the new proposed approach leads to 229.85 events.

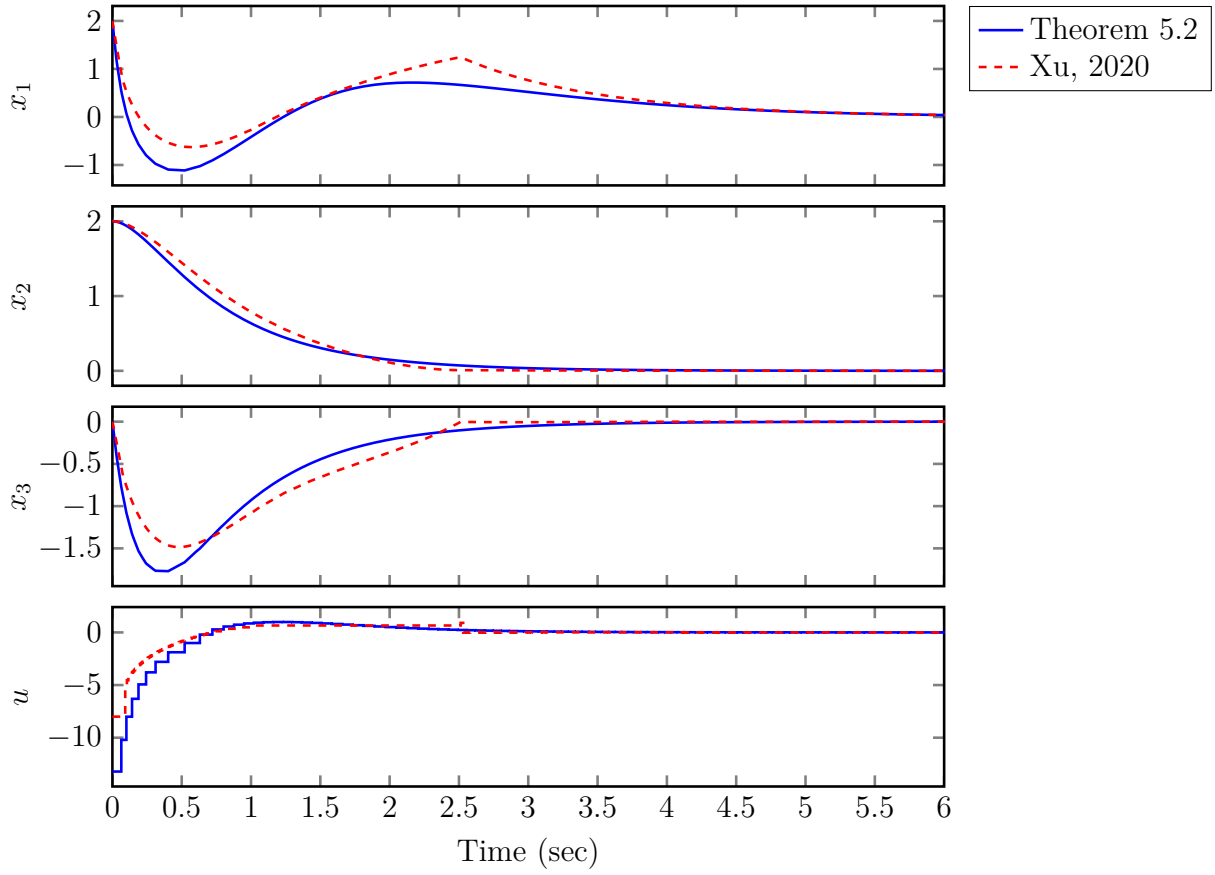

Figure 5.8 – Comparison of time responses and control input applied to system (5.107) between the control design from Theorem 5.2 and the approach in (XU *et al.*, 2020).

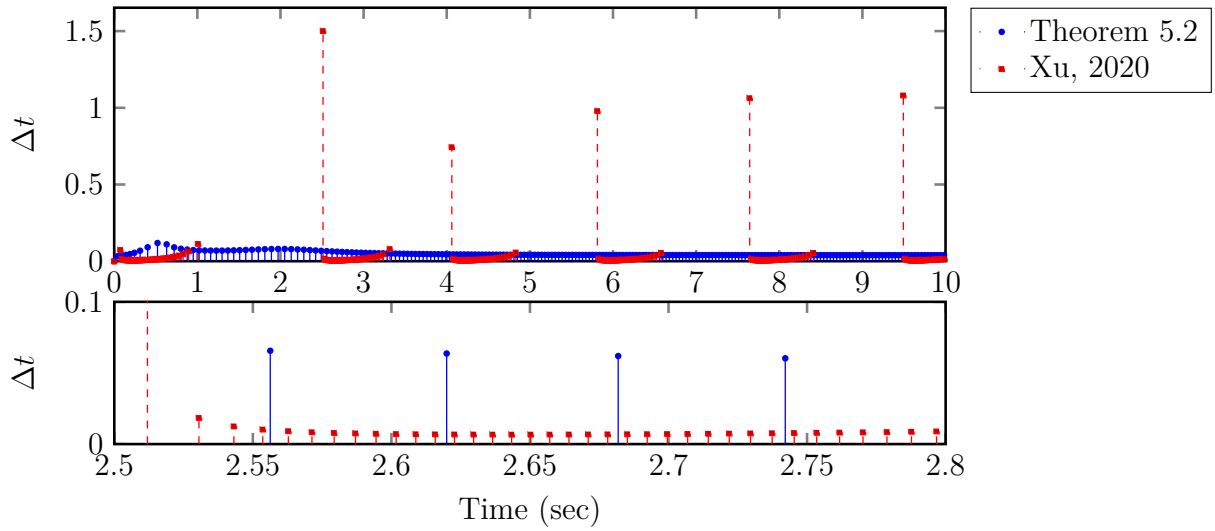

Figure 5.9 – Comparison of IETs obtained with system (5.107) between the control design from Theorem 5.2 and the approach in (XU *et al.*, 2020).

5.6 Conclusion

Using the feedback linearization approach, an event-triggered control design has been proposed for nonlinear MIMO systems. Sufficient conditions are provided to co-design the event-triggering conditions and the feedback controllers for both cases of full feedback linearization and partial feedback linearization with exponentially stable zero dynamics. By Lyapunov stability theory, the event-triggered control co-design is reformulated as optimization problems under LMI constraints. Moreover, using a polytopic approach and the fundamental theorem of calculus, some nonlinear mismatch terms can be explicitly incorporated to LMI-based design conditions, instead of being included in the event-triggering conditions, to reduce the number of control events. In particular, under some assumptions on Lipschitzian properties of the system nonlinearities, the proof for the existence of a lower bound for inter event time is given. The performance superiority of the proposed control approach over the related literature, mainly in terms of reducing the number of triggered events for the feedback controllers, is illustrated via several numerical examples.

6 Conclusion and perspectives

In this thesis the problem of designing event-triggering control laws for nonlinear systems has been addressed, focusing on vehicle platoon applications.

Chapter 3 has addressed the problem of control designing for longitudinal platoons equipped with cooperative adaptive cruise control. In this chapter the vehicles model has been assumed as uncertain, resulting in mismatches in the feedback linearization, which, as illustrated via simulation, can affect vehicles safety distance. A disturbance observer compensation has been proposed to estimate the combined effect of uncertainties and exogenous inputs. The estimated disturbance has been incorporated into the feedback linearizing control law and it shows to effectively compensate for the disturbances, thus resulting in acceptable safe distance error.

To account for the uncertainties and the disturbance compensations in the designing conditions an extension to $\mathcal{L}_2$ string stability conditions have been proposed in Chapter 3. Considering two procedures to model the vehicles interactions, design conditions have been derived to ensure both individual and string stability in the presence of uncertainties. Throughout simulation, the two models have been compared with both being able to achieve a platoon formation with safe distance even when starting from a platoon without correct positioning. In Chapter 3 we show that an important feature of the proposed conditions is scalability. Taking advantage of the vehicle communication topology and the feedback linearization procedure, designing conditions have been achieved, which are independent of the number of vehicles.

Chapter 4 has focused on the problem of efficient communication. Considering the models derived in Chapter 3 an event triggered communication has been introduced. To ensure Zeno free behavior a minimum waiting time has been enforced between consecutive transmission and a switching approach has been introduced for model the system under event triggered communication. A dynamic switching mechanism has been proposed and designing conditions have been attained considering scenarios with and without communication delays. Simulations have illustrated that, under the scenarios in study, the proposed method is able to improve communication efficiency compared with other methodologies in the literature.

In Chapter 5 the feedback linearization procedure utilized in Chapter 3 and Chapter 4 has been detailed, however, considering an event-based linearization procedure. In the previous chapter, signals necessary for feedback linearization were assumed to be measured continuously. In Chapter 5 the feedback linearization procedure has been detailed assuming that the signals necessary for the linearization procedures are updated according to a event condition. Assuming that feedback linearization is possible, designing conditi-

ons for both controller and event-triggering mechanism have been proposed for multiple input multiple output nonlinear systems. Examples have been provided to illustrate the effectiveness of the method, comparing against other existing methodologies.

The results achieved in this thesis are promising for longitudinal vehicle platooning. The proposed disturbance compensation can handle the effects of uncertainty and ensure safe distance between vehicles. Moreover, the proposed designing conditions account for uncertainties in string stability analysis while ensuring scalability of the conditions unlike most related methods in literature. The method can also reduce communication while maintaining performance utilizing the proposed ETM even in the presence of delays.

Although the method is effective, important considerations are required before real implementation. Some of them are still challenging from a theoretical point-of-view (saturation with feedback linearization, reconfiguration of the platoon...); others are important steps before real application (saturation, noise, measurements, denial of service...). Some of these aspects are shortly described in the next section.

6.1 Research perspectives

From a theoretical point of view, many works propose solutions to saturation of the control input for LPV systems, generally adding LMI constraints to the initial problem. Nevertheless, few works address the saturation problem for feedback linearization.

Saturation issue

To illustrate the issue, consider again the platooning problem. In this work, even in a scenario free of disturbance, it was assumed that the vehicles have unsaturated signals; they can achieve any speed required and produce any torque without limitations. Including saturations for the signals can be challenging. For example, if they are introduced on the control input, the signal required for linearization might not be achievable. Moreover, when adding uncertainties, noise... the problem is still open. Let us consider an input saturation in the feedback linearization scheme of vehicle Σ_i, Figure 6.1.

With the saturation the vehicles dynamics is described by:

$$\begin{aligned} \dot{p}_i &= v_i \\ \dot{v}_i &= \frac{1}{\boldsymbol{W}_i}\left(\boldsymbol{R}_{h,i}T_i - \boldsymbol{m}_i\mathbf{g}F_{r,i} - \boldsymbol{B}_i v_i - \boldsymbol{C}_i v_i^2\right) \\ \dot{T}_i &= -\frac{1}{\rho_i}T_i + \frac{1}{\rho_i}\mathrm{sat}(u_{e,i}) \end{aligned} \tag{6.1}$$

where $\mathrm{sat}(\cdot)$ denotes the saturation. The following tests illustrate the challenges that can appear due to saturation.

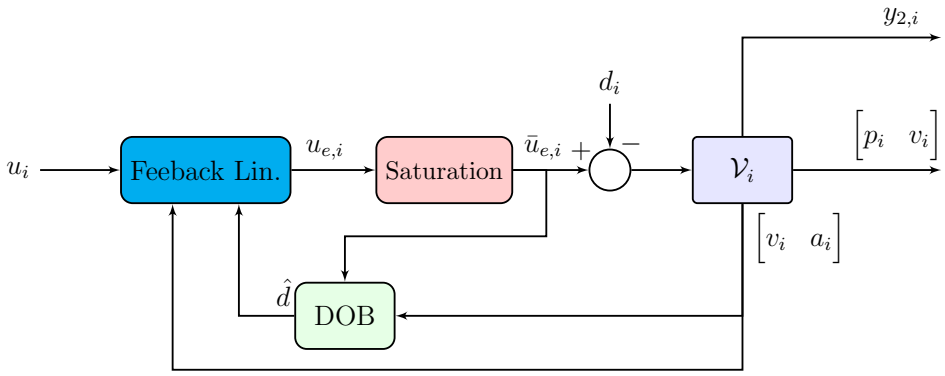

Figure 6.1 – Feeback linearization loop with DOB compensation and control input saturation.

Test 1 - Saturation without uncertainty

Consider an example with one vehicle following the leader without uncertainties and a saturation, Figure 6.1, on the control input of Σ_1. The platoon configuration is set as $\mathbb{J} = 0, 2$ with based values given in Table 6.1. Moreover, for this test, the DOB is removed. The saturation has been fixed to 75% of the maximum torque. The test corresponds to an acceleration and a braking, Figure 6.2 top left, the result without saturation is in black (dotted). Figure 6.2 shows the velocity (top left), the distance policy error (top right) along with the torque applied to the vehicle (bottom). As can be noticed even in this ideal scenario, the saturation affects the tracking performance, leading to larger values of error (up to 5 meters) and a velocity overshoot.

Table 6.1 – Nominal values for the vehicle parameters (Σ_i columns) and respective values used for simulation ($\tilde{\Sigma}_i$).

Vehicle	r	$\boldsymbol{m}$	$\boldsymbol{h}_w$	$\boldsymbol{J}_r$	$\boldsymbol{J}_e$	$\boldsymbol{R}_g$	$\boldsymbol{B}$	$\boldsymbol{C}$	ρ
Σ_0^b		1724	0.28	0.75	0.14	0.10	7.35	0.05	0.05
$\tilde{\Sigma}_0^b$		1724	0.25	1.05	0.14	0.13	8.09	0.06	0.08
Σ_2^b	2.5	2930	0.41	1.57	0.27	0.20	11.02	0.08	0.08
$\tilde{\Sigma}_2^b$		2637	0.33	1.26	0.40	0.30	8.82	0.05	0.06

Test 2 - Saturation with uncertainty and DOB compensation

When uncertainties are considered and disturbance compensation is introduced, the effects of saturation can be detrimental. With DOB compensation, the estimated disturbance is added to the linearizing input:

$$u_{e,i} = \text{sat}\left(\frac{1}{b_i}\left(-\frac{1}{\rho_d}a_i - f_i(v_i, a_i) + \frac{1}{\rho_d}u_i\right) + \frac{1}{b_i}\hat{d}_i\right) \tag{6.2}$$

which can make the input saturate faster. Moreover, the saturation also affects the DOB dynamics, which is given by:

$$\begin{aligned} \dot{\omega}_i &= \frac{\partial L_i(a_i)}{\partial a_i}(f_i(v_i, a_i) + b_i \text{sat}(u_{e,i}) - \hat{d}_i) \\ \hat{d}_i &= \omega_i - L_i(a_i). \end{aligned} \tag{6.3}$$

For illustration let us consider a scenario with the same platoon configuration as in Test 1, including uncertainties and disturbances. Figure 3 shows the velocity (top left), distance policy error (top right), the torque applied to the vehicle (bottom left) and disturbance estimation (bottom right). Indeed, in this scenario, the saturation affects the disturbance estimation that makes the results worse. The distance policy error is higher (up to 10 meters) and the velocity has a larger overshoot.

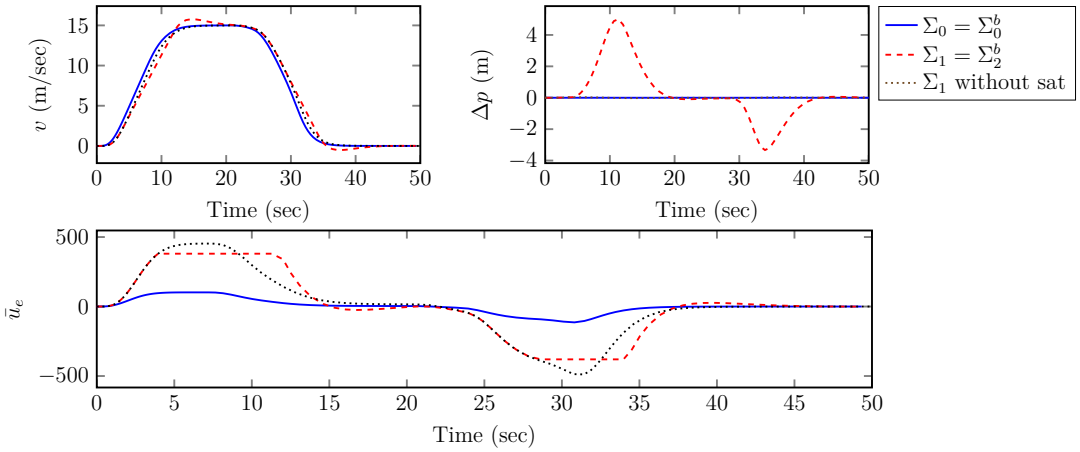

Figure 6.2 – Test 1: Platoon $\mathbb{J} = \{0, 2\}$. Velocity (top left), distance policy error (top right) and torque input (bottom) for nominal case with saturation.

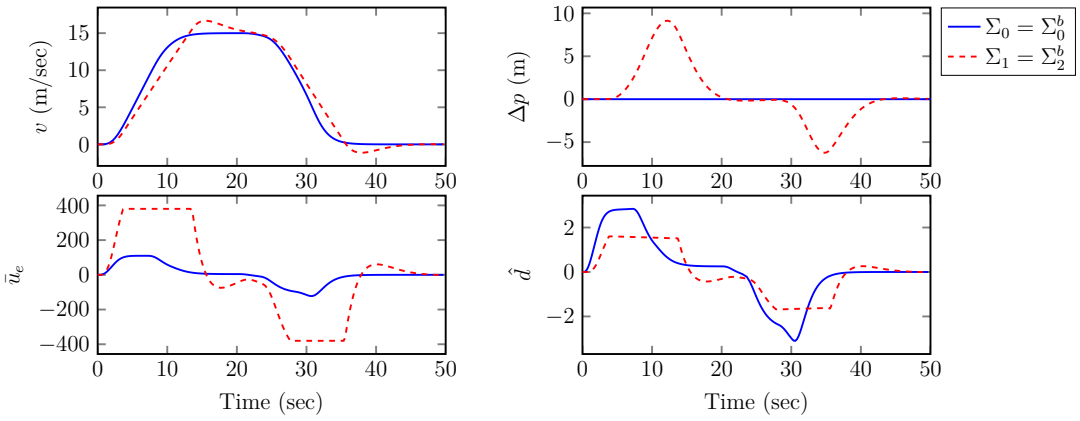

Figure 6.3 – Test 2: Platoon $\mathbb{J} = \{0, 2\}$. Velocity (top left), distance policy error (top right), torque input (bottom) and and disturbance estimation (bottom right) for the uncertain case with saturation.

A straightforward option to tackle this issue is to design the controller without considering the saturation and verifying via simulation that the control law will not saturate. This strategy cannot be used safely, especially because for emergency situations, fast actions will be required that may force the control input to saturate. Alternatively, a safe solution must include the saturation into the nonlinear systems equations and provide designing conditions and appropriate solutions. However, this approach is not trivial due to the feedback linearization procedure as the signal required for linearization might not be achievable.

Of course, many other challenges can be considered, amongst them, problems regarding communication quality are crucial.

Communication quality

Communication was assumed to be affected only by delays, however other phenomena like faults, attacks, or denial of service can occur. Many works already address those aspects under various methodologies (PEIXOTO *et al.*, 2023; PESSIM *et al.*, 2021; WANG *et al.*, 2022b; MA *et al.*, 2020). A part of the adaptation can be, at first sight, straightforward, for example if the faults do not affect the feedback linearization (WANG *et al.*, 2022b; MA *et al.*, 2020), even though, the effects need to be evaluated theoretically and in practice. On the contrary, the problem is not trivial.

There are also a lot of improvements that can be thought of for the application of platooning, especially if we consider reconfiguration and communications topology.

Platoon reconfiguration

In platooning, vehicles can leave the platoon formation because of technical problems or because it is addressed for those vehicles to leave the formation. This is a particular case of platoon reconfiguration, where the other vehicles need to compensate for the vehicles leaving the formation. This situation must be considered. For example, considering the scenario described in Figure 6.4, with one leader and 4 followers. At some moment, vehicle 1 and vehicle 2 leave the formation and a gap remains between vehicle 3 and the leader. One problem that can occur during the reconfiguration is that the sensor will lose range (i.e., vehicle 3 cannot measure its distance from the leader).

To handle this class of problems, assumptions about communication must be set. For example, in the scenario, Figure 6.4, we can assume that when vehicle 1 and vehicle 2 leave the platoon they stop communication. One supplementary assumption has to be set for the leader. If we take the assumption that the leader is able to communicate with vehicle 3, then one approach is to predefine the maximum range for the sensor. Therefore, we can consider the vehicles leave as a “saturation” problem. In this example, during the time that vehicle 3 is not able to measure the distance to the leader, the distance is set as

its maximum. If the communication with the leader is lost, vehicle 3 has to become the new leader.

These aspects are strongly related to the topology of the platoon.

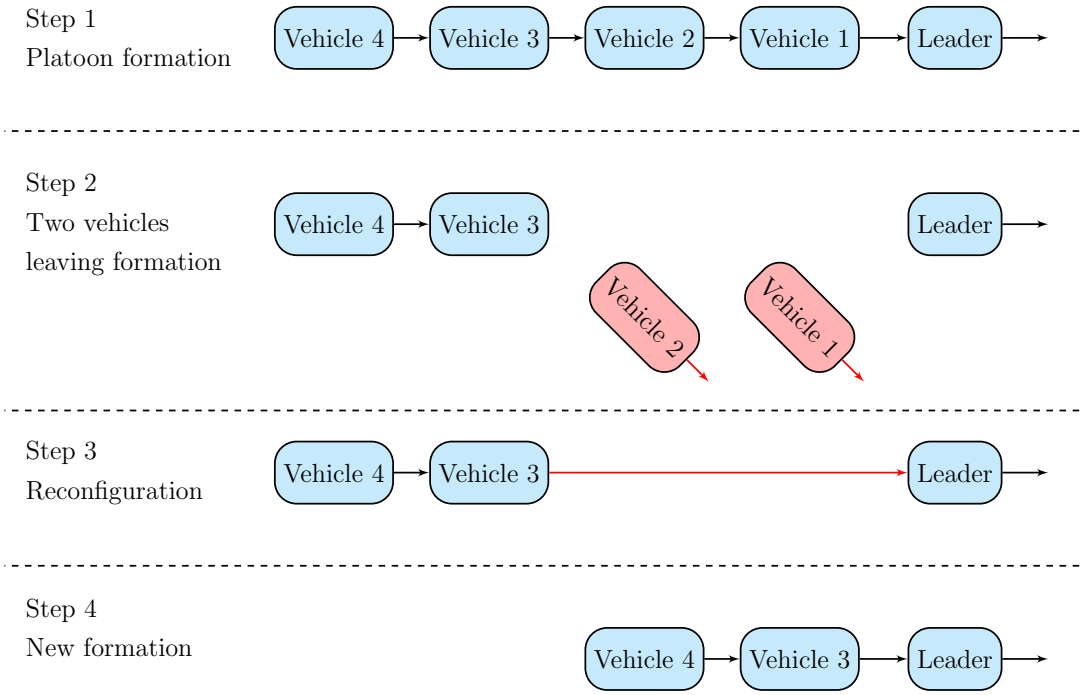

Figure 6.4 – Vehicle platoon reconfiguration with two vehicles leaving formation.

Different topologies

The main topology considered in this work is the predecessor follower topology, where communication only occurs between adjacent vehicles and information only flows from vehicle i to vehicle $i+1$. We took advantage of this topology specification to achieve design conditions that do not depend on the number of vehicles (scalability). For other topologies, adaptations are necessary especially if scalability is desired. In Figure 6.5 we show a topology of two predecessor followers, with bidirectional communication. In this case it is necessary to account for the interaction between 2 vehicles and the effects of the bidirectional communication.

Moreover, it is assumed that vehicle i only measures $\hat{p}_i$ and Δv_i from vehicle $i-1$. In Figure 6.5, indicated by the red arrows, we consider a case where the vehicle i can also measure $\hat{p}_{i+1}$ and Δv_{i+1}. This approach can be useful, for example in platoon reconfiguration where one or more vehicles are not able to follow the formation. This topology can also allow platoon formation to adjust not only according to the leader reference, but according to both the leader and the follower(s). For example, if the vehicle i is not able to follow vehicle $i-1$ (for example, because of a slowest acceleration) vehicle i can decelerate. Therefore, an issue will be how to design the control strategy of vehicle i

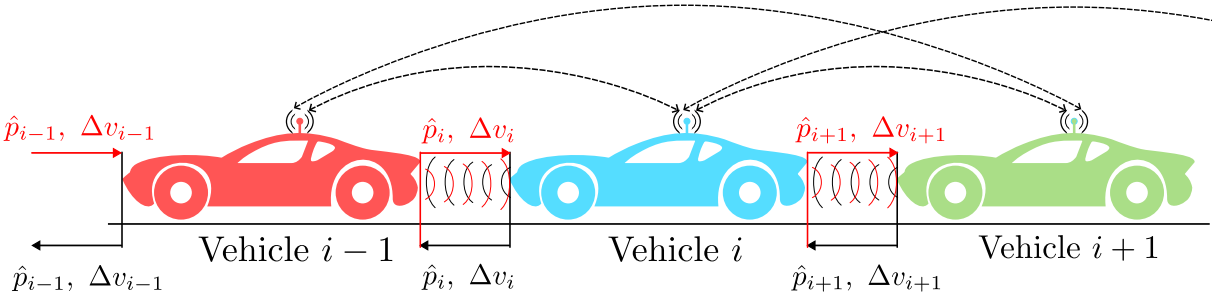

Figure 6.5 – Vehicle platoon with bidirectional communication and two predecessor follower topology.

as a tradeoff between the desired distance policy between vehicles $i-1$, vehicles i and vehicles $i+1$, keeping good performances and safety.

Regarding the platoon problem, other aspects can interfere with the platoon performance: road conditions, weather conditions... can affect the vehicles behavior and consequently the platoon.

Environment adjustments

In rainy situations, foggy, and specially ice roads, additional care is needed. Foggy can affect sensors while rain and especially ice roads affect tire adherence. A possible approach to account for these changes in the environment is to adjust the distance policy according to the scenario. In the distance policy:

$$\Delta p_{d,i} = r_i + hv_i \tag{6.4}$$

the standstill distance r_i and the constant time distance h, can be chosen as time varying variables, that change according to the environment conditions. The design of the controller(s), must take into account these changes. Methodologies such as LPV and/or switching systems can be thought to have controllers that appropriately change according to those conditions.

This work only considered longitudinal motion. Including lateral motion is crucial for completeness of the platoon problem.

Longitudinal and Lateral

A challenging aspect for platooning is combining both the longitudinal and lateral motions. Few works in literature consider string stability analysis with lateral dynamics (MAHFOUZ *et al.*, 2023). Lateral motion introduces more challenges as lateral velocity is not measured and there are additional disturbances (LI *et al.*, 2020; LI *et al.*, 2019; MAHFOUZ *et al.*, 2023; NGUYEN *et al.*, 2023). The disturbance compensation proposed cannot be adapted directly for the lateral case as it requires lateral speed measurement.

An alternative is to design an output-based disturbance observer or utilize an observer to estimate the necessary states for the DOB.

Moreover, feedback linearization can be applied for the longitudinal dynamics, but not for the lateral one. Although some nonlinearities can be canceled, full linearization (via feedback linearization) is not possible. In this case the problem can be addressed using an LPV-modeling of the system. Although, ensuring string stability can be challenging when combining with lateral dynamics.

References

ABDELRAHIM, M.; POSTOYAN, R.; DAAFOUZ, J.; NESIC, D. Stabilization of nonlinear systems using event-triggered output feedback controllers. *IEEE Transactions on Automatic Control*, Institute of Electrical and Electronics Engineers (IEEE), v. 61, n. 9, p. 2682–2687, sep 2016.

ABDELRAHIM, M.; POSTOYAN, R.; DAAFOUZ, J.; NEŠIĆ, D. Robust event-triggered output feedback controllers for nonlinear systems. *Automatica*, Elsevier BV, v. 75, p. 96–108, jan 2017.

APS, M. *The MOSEK optimization toolbox for MATLAB manual. Version 9.0.* [S.l.], 2019. Disponível em: <http://docs.mosek.com/9.0/toolbox/index.html>.

ASADI, B.; VAHIDI, A. Predictive cruise control: Utilizing upcoming traffic signal information for improving fuel economy and reducing trip time. *IEEE Transactions on Control Systems Technology*, Institute of Electrical and Electronics Engineers (IEEE), v. 19, n. 3, p. 707–714, maio 2011. ISSN 1558-0865.

BAGHERI, M.; NASERADINMOUSAVI, P.; KRSTIĆ, M. Feedback linearization based predictor for time delay control of a high-DOF robot manipulator. *Automatica*, Elsevier BV, v. 108, p. 108485, oct 2019.

BAI, T.; JOHANSSON, A.; JOHANSSON, K. H.; MÅRTENSSON, J. Large-scale multi-fleet platoon coordination: A dynamic programming approach. *IEEE Trans. Intell. Transp. Syst.*, Institute of Electrical and Electronics Engineers (IEEE), v. 24, n. 12, p. 4427–4442, 2023.

BELLMAN, R. The stability of solutions of linear differential equations. *Duke Mathematical Journal*, Duke University Press, v. 10, n. 4, dec 1943.

BIAN, Y.; ZHENG, Y.; REN, W.; LI, S.-E.; WANG, J.; LI, K. Reducing time headway for platooning of connected vehicles via V2V communication. *Transp. Res. Part C Emerg. Technol.*, Elsevier, v. 102, p. 87–105, 2019.

BORGERS, D. P.; HEEMELS, W. P. M. H. Event-separation properties of event-triggered control systems. *IEEE Transactions on Automatic Control*, Institute of Electrical and Electronics Engineers (IEEE), v. 59, n. 10, p. 2644–2656, out. 2014.

BOYD, S.; El Ghaoui, L.; FERON, E.; BALAKRISHNAN, V. *Linear Matrix Inequalities in System and Control Theory*. Philadelphia, PA: SIAM, 1994. v. 15. ISBN 0-89871-334-X.

CARNEVALE, D.; TEEL, A. R.; NESIC, D. A Lyapunov proof of an improved maximum allowable transfer interval for networked control systems. *IEEE Transactions on Automatic Control*, Institute of Electrical and Electronics Engineers (IEEE), v. 52, n. 5, p. 892–897, may 2007.

CHANG, P.-F.; CHEN, C.-C.; CHANG, J.-R. Observer-based feedback linearization control of multi-input multi-output nonlinear system and application to double rotor system. *Advances in Mechanical Engineering*, SAGE Publications, v. 11, n. 4, p. 168781401984546, apr 2019.

CHEN, J.; WEI, H.; ZHANG, H.; SHI, Y. Asynchronous self-triggered stochastic distributed MPC for cooperative vehicle platooning over vehicular ad-hoc networks. *IEEE Trans. Veh. Technol.*, v. 72, n. 11, p. 14061–14073, 2023.

CHEN, Z.; NIU, B.; ZHAO, X.; ZHANG, L.; XU, N. Model-based adaptive event-triggered control of nonlinear continuous-time systems. *Applied Mathematics and Computation*, Elsevier BV, v. 408, p. 126330, nov 2021.

DARBHA, S.; KONDURI, S.; PAGILLA, P. R. Benefits of V2V communication for autonomous and connected vehicles. *IEEE Transactions on Intelligent Transportation Systems*, Institute of Electrical and Electronics Engineers (IEEE), v. 20, n. 5, p. 1954–1963, maio 2019.

DEY, K. C.; YAN, L.; WANG, X.; WANG, Y.; SHEN, H.; CHOWDHURY, M.; YU, L.; QIU, C.; SOUNDARARAJ, V. A review of communication, driver characteristics, and controls aspects of cooperative adaptive cruise control (CACC). *IEEE Transactions on Intelligent Transportation Systems*, Institute of Electrical and Electronics Engineers (IEEE), v. 17, n. 2, p. 491–509, fev. 2016.

DOLK, V.; PLOEG, J.; HEEMELS, M. Event-triggered control for string-stable vehicle platooning. *IEEE Trans. Intell. Transp. Syst.*, v. 18, n. 12, p. 3486–3500, 2017.

DONKERS, M. C. F.; HEEMELS, W. P. M. H. Output-based event-triggered control with guaranteed $\mathcal{L}_\infty$-gain and improved and decentralized event-triggering. *IEEE Transactions on Automatic Control*, Institute of Electrical and Electronics Engineers (IEEE), v. 57, n. 6, p. 1362–1376, jun 2012.

FENG, S.; ZHANG, Y.; LI, S. E.; CAO, Z.; LIU, H. X.; LI, L. String stability for vehicular platoon control: Definitions and analysis methods. *Annu. Rev. Control.*, Elsevier BV, v. 47, p. 81–97, 2019.

FRIDMAN, E. Tutorial on Lyapunov-based methods for time-delay systems. *European Journal of Control*, Elsevier BV, v. 20, n. 6, p. 271–283, nov 2014.

GAO, F.; LI, S. E.; ZHENG, Y.; KUM, D. Robust control of heterogeneous vehicular platoon with uncertain dynamics and communication delay. *IET Intell. Transp. Syst.*, Institution of Engineering and Technology (IET), v. 10, n. 7, p. 503–513, set. 2016.

GAO, H.; SONG, Y.; WEN, C. Event-triggered adaptive neural network controller for uncertain nonlinear system. *Information Sciences*, Elsevier BV, v. 506, p. 148–160, jan 2020.

GE, X.; HAN, Q.; ZHANG, X.; DING, D. Communication resource-efficient vehicle platooning control with various spacing policies. *IEEE/CAA Journal of Automatica Sinica*, Institute of Electrical and Electronics Engineers (IEEE), v. 11, n. 2, p. 362–376, fev. 2024.

GE, X.; HAN, Q.-L.; DING, L.; WANG, Y.-L.; ZHANG, X.-M. Dynamic event-triggered distributed coordination control and its applications: A survey of trends and techniques. *IEEE Transactions on Systems, Man, and Cybernetics: Systems*, Institute of Electrical and Electronics Engineers (IEEE), v. 50, n. 9, p. 3112–3125, set. 2020. ISSN 2168-2232.

GIRARD, A. Dynamic triggering mechanisms for event-triggered control. *IEEE Trans. Autom. Control*, v. 60, n. 7, p. 1992–1997, 2015.

GOEBEL, R.; SANFELICE, R. G.; TEEL, A. R. Hybrid dynamical systems. *IEEE Control Systems*, Institute of Electrical and Electronics Engineers (IEEE), v. 29, n. 2, p. 28–93, apr 2009.

GU, K.; KHARITONOV, V.; CHEN, J. *Stability of time-delay systems*. [S.l.]: Birkhäuser Boston, 2003.

GU, K.; NICULESCU, S.-I. Survey on recent results in the stability and control of time-delay systems∗. *Journal of Dynamic Systems, Measurement, and Control*, ASME International, v. 125, n. 2, p. 158–165, jun 2003.

GUANETTI, J.; KIM, Y.; BORRELLI, F. Control of connected and automated vehicles: State of the art and future challenges. *Annu. Rev. Control.*, Elsevier BV, v. 45, p. 18–40, 2018. ISSN 1367-5788.

GUO, X.; WANG, J.; LIAO, F.; TEO, R. Distributed adaptive integrated-sliding-mode controller synthesis for string stability of vehicle platoons. *IEEE Trans. Intell. Transp. Syst.*, Institute of Electrical and Electronics Engineers (IEEE), v. 17, n. 9, p. 2419–2429, 2016.

HEEMELS, W. P. M. H.; DONKERS, M. C. F.; TEEL, A. R. Periodic event-triggered control based on state feedback. In: *IEEE Conference on Decision and Control and European Control Conference*. Orlando, USA: IEEE, 2011.

HEEMELS, W. P. M. H.; JOHANSSON, K. H.; TABUADA, P. An introduction to event-triggered and self-triggered control. In: *2012 IEEE 51st IEEE Conference on Decision and Control (CDC)*. Maui, USA: IEEE, 2012.

HUANG, C.; KARIMI, H. Non-fragile $\mathcal{H}_\infty$ control for LPV-based CACC systems subject to denial-of-service attacks. *IET Control. Theory Appl.*, Institution of Engineering and Technology (IET), v. 15, n. 9, p. 1246–1256, 2021.

ISIDORI, A. *Nonlinear control systems*. 3. ed. [S.l.]: Springer London, 1995.

JIA, D.; LU, K.; WANG, J.; ZHANG, X.; SHEN, X. A survey on platoon-based vehicular cyber-physical systems. *IEEE Commun. Surv. Tutor.*, Institute of Electrical and Electronics Engineers (IEEE), v. 18, n. 1, p. 263–284, 2016.

JOHANSSON, A.; BAI, T.; JOHANSSON, K. H.; MÅRTENSSON, J. Platoon cooperation across carriers: From system architecture to coordination. *IEEE Intell. Transp. Syst. Mag.*, Institute of Electrical and Electronics Engineers (IEEE), v. 15, n. 3, p. 132–144, 2023.

JU, Z.; ZHANG, H.; LI, X.; CHEN, X.; HAN, J.; YANG, M. A survey on attack detection and resilience for connected and automated vehicles: From vehicle dynamics and control perspective. *IEEE Trans. Intell. Veh.*, v. 7, n. 4, p. 815–837, 2022.

JU, Z.; ZHANG, H.; TAN, Y. Distributed stochastic MPC for heterogeneous vehicle platoons subject to modeling uncertainties. *IEEE Intell. Transp. Syst. Mag.*, v. 14, n. 2, p. 25–40, 2022.

KHALIL, K. *Nonlinear Systems*. [S.l.]: Prentice Hall, 2002.

LESCH, V.; BREITBACH, M.; SEGATA, M.; BECKER, C.; KOUNEV, S.; KRUPITZER, C. An overview on approaches for coordination of platoons. *IEEE Transactions on Intelligent Transportation Systems*, Institute of Electrical and Electronics Engineers (IEEE), v. 23, n. 8, p. 10049–10065, ago. 2022.

LI, H.; CHEN, Z.; FU, B.; WU, Z.; JI, X.; SUN, M. Event-triggered vehicle platoon control under random communication noises. *IEEE Access*, v. 9, p. 51722–51733, 2021.

LI, L.; NOVEL, B. d'Andrea; THOREL, S. New online estimation algorithm of lateral tire-road coefficients based on inertial navigation system. In: *2019 IEEE Intelligent Transportation Systems Conference (ITSC)*. [S.l.]: IEEE, 2019.

LI, L.; NOVEL, B. d'Andréa; QUADRAT, A. Longitudinal and lateral control for four wheel steering vehicles. *IFAC-PapersOnLine*, Elsevier BV, v. 53, n. 2, p. 15713–15718, 2020. ISSN 2405-8963.

LI, Z.; HU, B.; LI, M.; LUO, G. String stability analysis for vehicle platooning under unreliable communication links with event-triggered strategy. *IEEE Trans. Veh. Technol.*, v. 68, n. 3, p. 2152–2164, 2019.

LIN, Y.-C.; NGUYEN, H. L. T. Adaptive neuro-fuzzy predictor-based control for cooperative adaptive cruise control system. *IEEE Transactions on Intelligent Transportation Systems*, Institute of Electrical and Electronics Engineers (IEEE), v. 21, n. 3, p. 1054–1063, mar. 2020. ISSN 1558-0016.

LINSENMAYER, S.; DIMAROGONAS, D. V. Event-triggered control for vehicle platooning. In: *2015 American Control Conference (ACC)*. Chicago, USA: IEEE, 2015.

LIU, K.; SELIVANOV, A.; FRIDMAN, E. Survey on time-delay approach to networked control. *Annual Reviews in Control*, Elsevier BV, v. 48, p. 57–79, nov. 2019.

LIU, X.; GOLDSMITH, A.; MAHAL, S.; HEDRICK, J. Effects of communication delay on string stability in vehicle platoons. In: *ITSC 2001. 2001 IEEE Intelligent Transportation Systems. Proceedings (Cat. No.01TH8585)*. [S.l.]: IEEE, 2001. (ITSC-01).

LÖFBERG, J. YALMIP : A toolbox for modeling and optimization in MATLAB. In: *In Proceedings of the CACSD Conference*. Taipei, Taiwan: [s.n.], 2004.

LUO, Q.; NGUYEN, A.-T.; FLEMING, J.; ZHANG, H. Unknown input observer based approach for distributed tube-based model predictive control of heterogeneous vehicle platoons. *IEEE Trans. Veh. Technol.*, v. 70, n. 4, p. 2930–2944, 2021.

MA, F.; WANG, J.; ZHU, S.; GELBAL, S. Y.; YANG, Y.; AKSUN-GUVENC, B.; GUVENC, L. Distributed control of cooperative vehicular platoon with nonideal communication condition. *IEEE Transactions on Vehicular Technology*, Institute of Electrical and Electronics Engineers (IEEE), v. 69, n. 8, p. 8207–8220, ago. 2020. ISSN 1939-9359.

MAHFOUZ, D.; SHEHATA, O.; MORGAN, E. Development and evaluation of a unified integrated platoon control system architecture. *IEEE Trans. Intell. Transp. Syst.*, Institute of Electrical and Electronics Engineers (IEEE), v. 24, n. 6, p. 5685–5704, 2023.

MAITY, D.; BARAS, J. S. Event based control for control affine nonlinear systems: A Lyapunov function based approach. In: *2015 54th IEEE Conference on Decision and Control (CDC)*. Osaka, Japan: IEEE, 2015.

MENHOUR, L.; NOVEL, B. d'Andrea; FLIESS, M.; GRUYER, D.; MOUNIER, H. An efficient model-free setting for longitudinal and lateral vehicle control: Validation through the interconnected pro-sivic/rtmaps prototyping platform. *IEEE Transactions on Intelligent Transportation Systems*, Institute of Electrical and Electronics Engineers (IEEE), v. 19, n. 2, p. 461–475, fev. 2018. ISSN 1558-0016.

MILANES, V.; SHLADOVER, S. E.; SPRING, J.; NOWAKOWSKI, C.; KAWAZOE, H.; NAKAMURA, M. Cooperative adaptive cruise control in real traffic situations. *IEEE Transactions on Intelligent Transportation Systems*, Institute of Electrical and Electronics Engineers (IEEE), v. 15, n. 1, p. 296–305, fev. 2014.

MOREIRA, L. G.; GROFF, L. B.; SILVA, J. M. G. da. Event-triggered state-feedback control for continuous-time plants subject to input saturation. *Journal of Control, Automation and Electrical Systems*, Springer Science and Business Media LLC, v. 27, n. 5, p. 473–484, aug 2016.

MOSER, D.; SCHMIED, R.; WASCHL, H.; RE, L. del. Flexible spacing adaptive cruise control using stochastic model predictive control. *IEEE Transactions on Control Systems Technology*, Institute of Electrical and Electronics Engineers (IEEE), v. 26, n. 1, p. 114–127, jan. 2018. ISSN 1558-0865.

NARANJO, J.; GONZALEZ, C.; REVIEJO, J.; GARCIA, R.; PEDRO, T. de. Adaptive fuzzy control for inter-vehicle gap keeping. *IEEE Transactions on Intelligent Transportation Systems*, Institute of Electrical and Electronics Engineers (IEEE), v. 4, n. 3, p. 132–142, set. 2003. ISSN 1524-9050.

NGUYEN, C. M.; NGUYEN, A.-T.; DELPRAT, S. Neural-network-based fuzzy observer with data-driven uncertainty identification for vehicle dynamics estimation under extreme driving conditions: Theory and experimental results. *IEEE Transactions on Vehicular Technology*, Institute of Electrical and Electronics Engineers (IEEE), v. 72, n. 7, p. 8686–8696, jul. 2023. ISSN 1939-9359.

NIELSEN, C.; FULFORD, C.; MAGGIORE, M. Path following using transverse feedback linearization: Application to a maglev positioning system. *Automatica*, Elsevier BV, v. 46, n. 3, p. 585–590, mar 2010.

NUNEN, E. van; REINDERS, J.; SEMSAR-KAZEROONI, E.; WOUW, N. van de. String stable model predictive cooperative adaptive cruise control for heterogeneous platoons. *IEEE Trans. Intell. Veh.*, v. 4, n. 2, p. 186–196, 2019.

OHTAKE, H.; TANAKA, K.; WANG, H. O. Fuzzy modeling via sector nonlinearity concept. *Integrated Computer-Aided Engineering*, IOS Press, v. 10, n. 4, p. 333–341, set. 2003.

OLIVEIRA, M. C. de; SKELTON, R. E. Stability tests for constrained linear systems. In: _____. *Lecture Notes in Control and Information Sciences*. [S.l.]: Springer London, 2001. p. 241–257. ISBN 9781846285769.

ONCU, S.; PLOEG, J.; WOUW, N. van de; NIJMEIJER, H. Cooperative adaptive cruise control: Network-aware analysis of string stability. *IEEE Trans. Intell. Transp. Syst.*, Institute of Electrical and Electronics Engineers (IEEE), v. 15, n. 4, p. 1527–1537, 2014.

PACHPATTE, B. G. *Inequalities for differential and integral equations*. [S.l.]: Elsevier Science & Technology Books, 1997. ISBN 9780080534640.

PALIOTTA, C.; LEFEBER, E.; PETTERSEN, E. E.; PINTO, J.; COSTA, M.; SOUSA, J. T. F. B. Trajectory tracking and path following for underactuated marine vehicles. *IEEE Transactions on Control Systems Technology*, Institute of Electrical and Electronics Engineers (IEEE), v. 27, n. 4, p. 1423–1437, jul 2019.

PANANURAK, W.; THANOK, S.; PARNICHKUN, M. Adaptive cruise control for an intelligent vehicle. In: *2008 IEEE International Conference on Robotics and Biomimetics*. [S.l.]: IEEE, 2009.

PEIXOTO, M. L. C.; COUTINHO, P. H. S.; BESSA, I.; PESSIM, P. S. P.; PALHARES, R. M. Event-triggered control of Takagi-Sugeno fuzzy systems under deception attacks. *International Journal of Robust and Nonlinear Control*, Wiley, v. 33, n. 13, p. 7471–7487, maio 2023. ISSN 1099-1239.

PENG, C.; LI, F. A survey on recent advances in event-triggered communication and control. *Inf. Sci.*, v. 457–458, p. 113–125, 2018.

PESSIM, P. S.; PEIXOTO, M. L.; PALHARES, R. M.; LACERDA, M. J. Static output-feedback control for cyber-physical LPV systems under DoS attacks. *Information Sciences*, Elsevier BV, v. 563, p. 241–255, jul. 2021. ISSN 0020-0255.

PLOEG, J.; SCHEEPERS, B.; van Nunen, E.; van de Wouw, N.; NIJMEIJER, H. Design and experimental evaluation of perative adaptive cruise control. In: *14th Int. IEEE Conf. Intell. Transp. Syst.* Washington, DC, USA: [s.n.], 2011. p. 260–265. ISBN 978-1-4577-2197-7 978-1-4577-2198-4 978-1-4577-2196-0.

PLOEG, J.; van de Wouw, N.; NIJMEIJER, H. $\mathcal{L}_p$ string stability of cascaded systems: Application to vehicle platooning. *IEEE Trans. Control Syst. Technol.*, v. 22, n. 2, p. 786–793, 2014.

POLACK, P.; NOVEL, B. d'Andréa; FLIESS, M.; FORTELLE, A. de L.; MENHOUR, L. Finite-time stabilization of longitudinal control for autonomous vehicles via a model-free approach * *this work was supported by the international chair mines paris-tech - peugeot-citroën - safran - valeo on ground vehicle automation and the anr project 15 ce23 0007 (project finite4sos). *IFAC-PapersOnLine*, Elsevier BV, v. 50, n. 1, p. 12533–12538, jul. 2017. ISSN 2405-8963.

PROTTER, M. H.; MORREY, C. B. *Intermediate Calculus*. [S.l.]: Springer New York, 1985. ISSN 0172-6056. ISBN 9781461210863.

RAJAMANI, R. *Vehicle Dynamics and Control*. Boston, MA: Springer US, 2012.

SAHOO, A.; XU, H.; JAGANNATHAN, S. Neural network-based event-triggered state feedback control of nonlinear continuous-time systems. *IEEE Transactions on Neural Networks and Learning Systems*, Institute of Electrical and Electronics Engineers (IEEE), v. 27, n. 3, p. 497–509, mar 2016.

SAMII, A.; BEKIARIS-LIBERIS, N. Simultaneous compensation of actuation and communication delays for heterogeneous platoons via predictor-feedback CACC with integral action. *IEEE Trans. Intell. Veh.*, p. 1–13, 2024.

SAWANT, J.; CHASKAR, U.; GINOYA, D. Robust control of cooperative adaptive cruise control in the absence of information about preceding vehicle acceleration. *IEEE Transactions on Intelligent Transportation Systems*, Institute of Electrical and Electronics Engineers (IEEE), v. 22, n. 9, p. 5589–5598, set. 2021. ISSN 1558-0016.

SELIVANOV, A.; FRIDMAN, E. Event-triggered $\mathcal{H}_\infty$ control: A switching approach. *IEEE Trans. Autom. Control*, v. 61, n. 10, p. 3221–3226, 2016.

SEPULCHRE, R.; PALEY, D. A.; LEONARD, N. R. Stabilization of planar collective motion: All-to-all communication. *IEEE Transactions on Automatic Control*, Institute of Electrical and Electronics Engineers (IEEE), v. 52, n. 5, p. 811–824, may 2007.

SEURET, A.; GOUAISBAUT, F. Stability of linear systems with time-varying delays using Bessel–Legendre inequalities. *IEEE Transactions on Automatic Control*, Institute of Electrical and Electronics Engineers (IEEE), v. 63, n. 1, p. 225–232, jan. 2018.

SONTAG, E. D.; WANG, Y. New characterizations of input-to-state stability. *IEEE Transactions on Automatic Control*, Institute of Electrical and Electronics Engineers (IEEE), v. 41, n. 9, p. 1283–1294, set. 1996.

STÖCKER, C.; LUNZE, J. Event-based control of input-output linearizable systems. *IFAC Proceedings Volumes*, Elsevier BV, v. 44, n. 1, p. 10062–10067, jan 2011.

SU, Y.; YANG, X.; SHI, P.; WEN, G.; XU, Z. Consensus-based vehicle platoon control under periodic event-triggered strategy. *IEEE Trans. Syst., Man, Cybern.: Syst.*, Institute of Electrical and Electronics Engineers (IEEE), v. 54, n. 1, p. 533–542, 2024. ISSN 2168-2232.

SWAROOP, D.; HEDRICK, K.; CHIEN, C.; IOANNOU, P. A comparision of spacing and headway control laws for automatically controlled vehicles. *Veh. Syst. Dyn.*, Taylor & Francis, v. 23, n. 1, p. 597–625, 1994.

TABUADA, P. Event-triggered real-time scheduling of stabilizing control tasks. *IEEE Trans. Autom. Control*, v. 52, n. 9, p. 1680–1685, 2007.

TANAKA, K.; WANG, H. O. *Fuzzy control systems design and analysis: A linear matrix inequality approach*. [S.l.]: John Wiley & Sons, Inc., 2001.

TOULOTTE, P. F.; DELPRAT, S.; GUERRA, T. M.; BOONAERT, J. Vehicle spacing control using robust fuzzy control with pole placement in LMI region. *Engineering Applications of Artificial Intelligence*, Elsevier BV, v. 21, n. 5, p. 756–768, ago. 2008.

UMLAUFT, J.; HIRCHE, S. Feedback linearization based on gaussian processes with event-triggered online learning. *IEEE Transactions on Automatic Control*, Institute of Electrical and Electronics Engineers (IEEE), v. 65, n. 10, p. 4154–4169, oct 2020.

VILCA, J.; ADOUANE, L.; MEZOUAR, Y. A novel safe and flexible control strategy based on target reaching for the navigation of urban vehicles. *Robotics and Autonomous Systems*, Elsevier BV, v. 70, p. 215–226, ago. 2015. ISSN 0921-8890.

WANG, B.; LUO, Y.; ZHONG, Z.; LI, K. Robust non-fragile fault tolerant control for ensuring the safety of the intended functionality of cooperative adaptive cruise control. *IEEE Trans. Intell. Transp. Syst.*, v. 23, n. 10, p. 18746–18760, 2022.

WANG, J.; MA, F.; YANG, Y.; NIE, J.; AKSUN-GUVENC, B.; GUVENC, L. Adaptive event-triggered platoon control under unreliable communication links. *IEEE Trans. Intell. Transp. Syst.*, Institute of Electrical and Electronics Engineers (IEEE), v. 23, n. 3, p. 1924–1935, 2022.

WANG, L.; HU, M.; BIAN, Y.; GUO, G.; LI, S.; CHEN, B.; ZHONG, Z. Periodic event-triggered fault detection for safe platooning control of intelligent and connected vehicles. *IEEE Trans. Veh. Technol.*, p. 1–14, 2023.

WANG, Z.; WU, G.; BARTH, M. J. A review on cooperative adaptive cruise control (CACC) systems: Architectures, controls, and applications. In: *2018 21st International Conference on Intelligent Transportation Systems (ITSC)*. Maui, USA: IEEE, 2018.

WEAVER, N. *Lipschitz algebras*. [S.l.]: WORLD SCIENTIFIC, 1999.

WEI, Y.; LIYUAN, W.; GE, G. Event-triggered platoon control of vehicles with time-varying delay and probabilistic faults. *Mech. Syst. Signal Process.*, Elsevier BV, v. 87, p. 96–117, 2017.

WU, G.; CHEN, G.; ZHANG, H.; HUANG, G. Fully distributed event-triggered vehicular platooning with actuator uncertainties. *IEEE Trans. Veh. Technol.*, Institute of Electrical and Electronics Engineers (IEEE), v. 70, n. 7, p. 6601–6612, 2021.

WU, Z.; SUN, J.; HONG, S. RBFNN-based adaptive event-triggered control for heterogeneous vehicle platoon consensus. *IEEE Trans. Intell. Transp. Syst.*, v. 23, n. 10, p. 18761–18773, 2022.

XIAO, L.; GAO, F. Practical string stability of platoon of adaptive cruise control vehicles. *IEEE Transactions on Intelligent Transportation Systems*, Institute of Electrical and Electronics Engineers (IEEE), v. 12, n. 4, p. 1184–1194, dez. 2011. ISSN 1524-9050.

XIAO, S.; GE, X.; HAN, Q.-L.; ZHANG, Y. Dynamic event-triggered platooning control of automated vehicles under random communication topologies and various spacing policies. *IEEE Trans. Cybern.*, Institute of Electrical and Electronics Engineers (IEEE), v. 52, n. 11, p. 11477–11490, 2022.

XU, B.; LIU, X.; WANG, H.; ZHOU, Y. Event-triggered control for nonlinear systems via feedback linearisation. *International Journal of Control*, Informa UK Limited, v. 94, n. 10, p. 2679–2689, feb 2020.

YAN, S.; SHEN, M.; NGUANG, S. K.; ZHANG, G.; ZHANG, L. A distributed delay method for event-triggered control of T-S fuzzy networked systems with transmission delay. *IEEE Transactions on Fuzzy Systems*, Institute of Electrical and Electronics Engineers (IEEE), v. 27, n. 10, p. 1963–1973, oct 2019.

YU, L.; WANG, R. Researches on adaptive cruise control system: A state of the art review. *Proceedings of the Institution of Mechanical Engineers, Part D: Journal of Automobile Engineering*, SAGE Publications, v. 236, n. 2–3, p. 211–240, maio 2021.

ZHANG, H.; LIU, J.; WANG, Z.; YAN, H.; ZHANG, C. Distributed adaptive event-triggered control and stability analysis for vehicular platoon. *IEEE Transactions on Intelligent Transportation Systems*, Institute of Electrical and Electronics Engineers (IEEE), v. 22, n. 3, p. 1627–1638, mar. 2021.

ZHENG, Y.; LI, S.; WANG, J.; CAO, D.; LI, K. Stability and scalability of homogeneous vehicular platoon: Study on the influence of information flow topologies. *IEEE Trans. Intell. Transp. Syst.*, Institute of Electrical and Electronics Engineers (IEEE), v. 17, n. 1, p. 14–26, 2016.

ZHU, Y.; HE, H.; ZHAO, P. LMI-based synthesis of string-stable controller for cooperative adaptive cruise control. *IEEE Trans. Intell. Transp. Syst.*, v. 21, n. 11, p. 4516–4525, 2020.